

REVIEW ARTICLES

Charge Transfer on the Nanoscale: Current Status

David M. Adams,[†] Louis Brus,[†] Christopher E. D. Chidsey,[‡] Stephen Creager,[§] Carol Creutz,^{*,||} Cherie R. Kagan,[⊥] Prashant V. Kamat,[⊗] Marya Lieberman,[○] Stuart Lindsay,[#] Rudolph A. Marcus,[∇] Robert M. Metzger,[◆] M. E. Michel-Beyerle,[△] John R. Miller,^{||} Marshall D. Newton,^{||} Debra R. Rolison,[×] Otto Sankey,[#] Kirk S. Schanze,[◇] James Yardley,⁺ and Xiaoyang Zhu[∞]

Department of Chemistry, Columbia University, 3000 Broadway, MC 3167, New York, New York 10027; Department of Chemistry and Stanford Synchrotron Research Laboratory, Stanford University, Stanford, California 94305-5080; Department of Chemistry, Clemson University, Clemson, South Carolina 29634; Chemistry Department, Brookhaven National Laboratory, Upton, New York 11973-5000; IBM T. J. Watson Research Center, Yorktown Heights, New York 10598; Radiation Laboratory, University of Notre Dame, Notre Dame, Indiana 46556; Department of Chemistry and Biochemistry, University of Notre Dame, Notre Dame, Indiana 46556; Department of Physics and Astronomy, Arizona State University, Tempe, Arizona 85287-1504; Caltech 127–72, Pasadena, California 91125; Department of Chemistry, The University of Alabama, Tuscaloosa, Alabama 35487-0336; Institut für Physikalische und Theoretische Chemie, Technische Universität München, Lichtenbergstr. 4, D-85748 Garching, Germany; Naval Research Laboratory, 4555 Overlook Avenue, SW, Washington, District of Columbia 20375-5342; Department of Chemistry, University of Florida, P.O. Box 117200, Gainesville, Florida 32611-7200; Columbia Radiation Laboratory, 1020 Schapiro Center (CEPSR), 530 West 120th Street, Mail code 8903, Columbia University, New York, New York 10027; and Department of Chemistry, University of Minnesota, Minneapolis, Minnesota 55455

Received: August 27, 2002; In Final Form: April 29, 2003

This is the report of a DOE-sponsored workshop organized to discuss the status of our understanding of charge-transfer processes on the nanoscale and to identify research and other needs for progress in nanoscience and nanotechnology. The current status of basic electron-transfer research, both theoretical and experimental, is addressed, with emphasis on the distance-dependent measurements, and we have attempted to integrate terminology and notation of solution electron-transfer kinetics with that of conductance analysis. The interface between molecules or nanoparticles and bulk metals is examined, and new research tools that advance description and understanding of the interface are presented. The present state-of-the-art in molecular electronics efforts is summarized along with future research needs. Finally, novel strategies that exploit nanoscale architectures are presented for enhancing the efficiencies of energy conversion based on photochemistry, catalysis, and electrocatalysis principles.

1. Introduction

Molecular and bulk level charge-transfer processes are now fairly well understood,^{1–4} while characterization of processes on the nanoscale (1 to 100 nm) is at its beginning.^{5–7} Recent

interest in the area has been driven by the exploration of the use of molecular units as elements of computer circuits, “moletronics”.^{8,9} Nanoscale charge transfer is important to both the frontier of fundamental science and to applications in molecular electronics including problems as diverse as sensors, photonics, electrocatalysis, and solar photoconversion. Progress in the area of nanoscale charge transfer requires interdisciplinary collaboration, combining a wide range of materials synthesis and characterization, a challenging range of experimental techniques to probe charge-transfer processes, as well as theory for their interpretation. Current interest ranges from the utilization of single or small groups of (usually organic) molecules as components in electronic devices to the exploitation of semiconductor and metal nanoparticles because of their high surface areas and other size-dependent properties. The nature of the attachment of such components to bulk metal and semiconductor surfaces and the control of their properties are

* Corresponding author.

[†] Department of Chemistry, Columbia University.

[‡] Stanford University.

[§] Clemson University.

^{||} Brookhaven National Laboratory.

[⊥] IBM T. J. Watson Research Center.

[⊗] Radiation Laboratory, University of Notre Dame.

[○] Department of Chemistry and Biochemistry, University of Notre Dame.

[#] Arizona State University.

[∇] Caltech.

[◆] The University of Alabama.

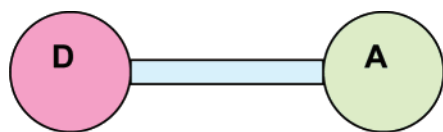
[△] Technische Universität München.

[×] Naval Research Laboratory.

[◇] University of Florida.

⁺ Columbia Radiation Laboratory, Columbia University.

[∞] University of Minnesota.

TABLE 1: Donor–Bridge–Acceptor Systems^{5,6}

	donor	acceptor	measurement
1	molecule ^a	molecule ^a	kinetics
2	molecule	electrode	kinetics SMS ^b
3	electrode	electrode	resistance
4	nanoparticle	molecule	kinetics
5	nanoparticle	electrode	kinetics SMS ^a
6	SPM tip ^c	electrode	current

^a “Molecule” can include complex enzyme system. ^b Single molecule spectroscopy; see section 3.2. ^c Scanning probe microscopy.

overarching concerns. The experimental measurements used to characterize nanoscale charge-transfer properties include rate constants, spectroscopy, and conductance/resistance measurements, depending on the nature of the system studied.

From the multidisciplinary nature of the research, difficulties naturally arise with language, terminology, and even conceptual approaches. The range of materials requires a very broad knowledge of their properties and leads to questions about how to connect one material to another and about what the nature of the contact between the materials is. The partial complementary nature of different types of physical measurements, specifically rate constant and conductance, raises the challenge of providing models that relate one quantity to another.

The donor–bridge–acceptor classification developed by Ratner⁵ provides a unifying framework for discussion of a broad range of nanoscale charge-transfer processes. Here it has been modified to explicitly incorporate nanospecies, and the distinction between “bridge” and “wire” is neglected. A bridge may function as a spacer or a wire and may comprise a molecule or a nanoparticle. (Here the term “molecular wire” will be used only in a specific sense. The ideal wire is a metallic nanoscale conductor, one with an electronic transmission of unity and a Landauer resistance of $h/2e^2$; only molecular interconnects that approach this transmission will be labeled “wires” here.)

Within this framework the electron transfer is viewed as proceeding from a donor (D) to an acceptor (A) via a bridge or a wire. The donor and/or acceptor may be a molecule or an electrode.

A metal or semiconductor nanoparticle (NP) may also serve as donor/acceptor or bridge, for example, NP-bridge-molecule,¹⁰ shown as 4 in Table 1. The detailed behavior of the nanoparticle systems involves the role of the finite size of the nanoparticle in determining its filled and unfilled energy levels. The nanoparticle may be a semiconductor or a metal, and there are, of course, significant differences between them in the theoretical treatment, as well as some similarities. Furthermore, increasingly systems of interest involve the tip of a scanning tunneling microscope (STM) as one electrode. Thus entry 6 in Table 1 includes an STM tip in place of a bulk electrode.^{11,12} The STM tip–bridge–bulk electrode has been studied, usually with nonbonded interactions between tip and molecule and nonbonded interactions between molecule and bulk electrode.^{13,14} The STM tip–bridge–nanoparticle combination has also been studied recently,^{15,16} typically with a bonded interaction between the nanoparticle and bridge, although a Coulombic bonding is also possible. Its description again entails the specific properties of the nanoparticle. The nanoparticle–electrode combination has been studied both with metal¹⁰ and with semiconductor¹⁷

nanoparticles. The nanoparticle–insulator situation includes studies where the nanoparticle is excited by light, and then the phenomenon of blinking can be observed.¹⁸ In a number of these studies the charge-transfer process is accompanied by a charging process and double-layer effects.¹⁹ A task for a combined effort in experiment and theory is to define what these many systems have in common and what problems are very specific to each.

The remainder of this paper is organized into four sections. In section 2, the current status of basic electron-transfer research, both theoretical and experimental, are addressed, with emphasis on the distance-dependent measurements. We have attempted to integrate terminology and notation of solution electron-transfer kinetics with that of conductance analysis. In section 3, the interface between molecules or nanoparticles and bulk metals is examined and new research tools that advance description and understanding of the interface are presented. In section 4, the present status of molecular electronics efforts is summarized and research needs are discussed. In the last section, section 5, examples of nanoscale architectures for energy conversion based on photochemistry, catalysis, and electrocatalysis are considered.

2. Electron Transport Theory and Experiment

In the past half century there have been extraordinary advances in our understanding of electron-transfer processes and in the theory and tools we bring to bear on this important process. Electron-transfer studies, begun with spectroscopic observations and experimental and theoretical studies of bimolecular reactions in solution, attained a high level of understanding of homogeneous solution processes, culminating with supermolecular species of known three-dimensional structure, which enabled a detailed examination of electronic pathways.^{20–22} Bridging groups in these supermolecules in which the rigidity of the bridge was a crucial element, included fused alkanes, polypeptides, aromatic hydrocarbons, and proteins. Knowledge of electron transfer between adsorbed molecules and a metal electrode was immensely advanced by introducing redox molecules into self-assembled monolayers (SAMs).²³ With a SAM, the three-dimensional structure itself imposes a three-dimensional order on the charge-transfer bridge so that even bridges containing normally “floppy” alkane chains can be studied at fixed donor–acceptor distance. Both the homogeneous and metal–adsorbate studies use kinetics, and very ingenious techniques have been devised to study charge-transfer rates in these systems. Very recently, it has become possible to determine the conductance of a bridge as a single molecule by measuring the current in a metal–bridge–metal assembly (in break junctions,²⁴ between mercury drops,²⁵ or other assemblies^{26,27}). The methodology that makes the strongest contact with the solution studies uses an STM or conducting AFM tip²⁸ to probe the current through a SAM such as those described above. Current is determined as a function of tip position and potential bias. While nuclear factors introduce an activation barrier to charge-transport kinetics, the conductance can be expected to be dominated by electronic overlaps. What is our current level of understanding of charge transport through molecules in solution, on electrodes, and between two electrodes and what are the barriers to further progress in these areas? These questions are addressed in this section.

To interpret and exploit the explosion of experimental data for charge transport on the nanoscale, based on chemical kinetics, conductance, and associated spectroscopic techniques, it is essential to have a unified theoretical framework which spans the broad range of structural, energetic, and dynamical

regimes underlying transport behavior, identifying the key controlling factors, and facilitating the efficient prediction guiding design of new systems and processes. In addition to basic intellectual understanding, the theory should be capable of yielding models of quantitative validity. The theory is also important in formulating and analyzing detailed numerical simulations, ideally at the molecular level.

A particular dynamical issue of central importance in charge transport is the role of tunneling of carriers between contacts and extended molecular spacers. A number of specialized, formal models for such tunneling are available in the chemistry and physics literature,^{7,8,29–33} but their applicability to realistic situations of chemical complexity requires specification of crucial energy (gaps) and electronic (transfer integrals) parameters. Such information is increasingly available from computer-intensive electronic structure calculations, although this can still be a daunting task in situations of extended nanostructures.

Time-dependent quantum mechanics yields generic expressions for rate constants or conductance, but the physical basis of the ingredients in these expressions may be fundamentally different in different transport regimes (e.g., vibronic Franck–Condon control in the case of polar media, in contrast to the analogous situation pertaining to electronic continua in the case of metal or other electrodes).^{29,30} Within the Born–Oppenheimer framework and associated Franck–Condon control common to the chemical kinetics approach to activated charge transport, carrier “tunneling” is addressed only indirectly, with no explicit reference to a “barrier” for the electron (or hole) to penetrate. On the other hand, many physical models are based explicitly on such barriers (defined with respect to an electronic coordinate).³³ In the latter “barrier” models, for example, the influence of applied potential bias on tunneling between metallic electrodes is relatively straightforward, whereas for the former case (e.g., Franck–Condon controlled charge transfer), the influence of such a bias is more indirect. A thermally activated electron-transfer process requires a fluctuation to bring the donor and acceptor sites into “resonance” (the transition state corresponding to the crossing of (vibronic) diabatic energy surfaces), irrespective of the overall driving force of the process. When the vibronic bath associated with Franck–Condon control is replaced by the electronic manifolds of the metal electrode in conductive junctions, off-resonance tunneling can occur within the band of energies lying between the Fermi energies of the two electrodes, which may be offset by some bias potential.^{7,30,34} New research effort is important in bridging such distinct methodological approaches for tunneling, and a common language is needed for capturing the essential features as they vary with the nature of the conductive junction.

2.1. Homogeneous Solution. Solution electron-transfer reactions can generally be regarded as occurring via assembly 1 (Table 1), a molecule–space/bridge–molecule assembly. For bimolecular reactions, one considers the first-order rate constant for electron transfer within the D–B–A assembly (“precursor complex”).³⁵ In the case of an outer-sphere reaction the so-called bridging material is simply the material between the redox centers—solvent molecules and, in the case of metal complexes, ligands surrounding the metal centers. Electron transfer between donor and acceptor sites connected by a molecular bridge is now fairly well understood.^{36–38} A detailed comparison of experimental and theoretical results for various donor–bridge–acceptor systems has been given.³⁸ In that work independent experimental data provided the donor-LUMO or donor-HOMO gap. A similar quantity is needed for any other bridge-assisted electron and hole transfers. The rates decrease with increasing

separation of the donor and acceptor and can generally be interpreted in terms of a first-order rate constant k_{et}

$$-d\{D\}/dt = k_{\text{et}}\{D\}$$

that is a function of a combination of electronic and nuclear factors:³⁸

$$k_{\text{et}} = \frac{2\pi H_{\text{DA}}^2}{h} \left[\frac{\pi}{\lambda k_{\text{B}} T} \right]^{1/2} \exp \left[-\frac{(\lambda + \Delta G^\circ)^2}{4\lambda k_{\text{B}} T} \right] \quad (2.1)$$

Here H_{DA} is the electronic coupling between the donor and acceptor sites, λ is the nuclear reorganization parameter, h is Planck’s constant, k_{B} is the Boltzmann constant, and ΔG° is the standard free-energy change for the electron transfer. (Symbols and conversion units are summarized in Appendix A.) For molecular species these parameters may be independently evaluated through spectroscopic studies of charge-transfer band intensities and energies (H_{DA} , λ), structural and vibrational frequency differences (λ), and electrochemical or other thermodynamic measurements (ΔG°).

2.1.1. Distance Dependence. The nature, magnitude, and energetics of the electronic interaction of the separated donor–acceptor sites has a major role in determining whether the electron-transfer (a) proceeds by a coherent tunneling process (superexchange,³⁹ with an exponential dependence on the separation distance), in which the electron or hole never resides on the bridge, or (b) involves thermally activated (or nonactivated) reduction or oxidation of the bridge.⁴⁰ Superexchange, which is the quantum tunneling through molecular orbitals with energies removed from that of the tunneling charge, is mediated by (virtual) states D^+B^-A or DB^+A^- (for electron and hole transfer, respectively), and these states are not populated in a superexchange mechanism. The exponential dependence of the superexchange rate constant k_{tunn} on separation distance d_{DA} is commonly expressed as

$$k_{\text{et}} = k_{\text{tunn}} = k_0 \exp(-\beta d_{\text{DA}}) \quad (2.2)$$

where it is assumed that k_{et} has been corrected for the distance dependence of the nuclear factor.⁴¹ Alternatively, the distance dependence may be expressed in terms of N , the number of repeated molecular units. Then the rate constant is

$$k_{\text{tunn}} = k_0 \exp(-\beta_N N) \quad (2.3)$$

In a superexchange model³⁹

$$\beta = -(2/a) \ln(H_{\text{BB}}/\Delta E_{\text{DB}}) \quad (2.4)$$

where H_{BB} is the internal coupling energy between the bridge units, a is the bridge-unit length, and ΔE_{DB} is the energy of the mediating state (D^+B^-A or DB^+A^-) above the ground state (assumed large relative to H_{BB}). For efficient long-range transfer, β should be small, which is favored by decreasing E_{DB} .

In the second mechanism the electron (or hole) actually resides on the bridge and may be delocalized over the entire bridge or diffuse by hopping between bridge sites. This is the so-called “chemical” mechanism. The states D^+B^-A or DB^+A^- are real rather than virtual. When diffusive hopping between bridge sites becomes rate limiting, the distance dependence of the electron transfer is Ohmic⁵ (inversely proportional to the D–A separation).

$$k_{\text{et}} = k_{\text{hop}} \propto 1/N \quad (2.5)$$

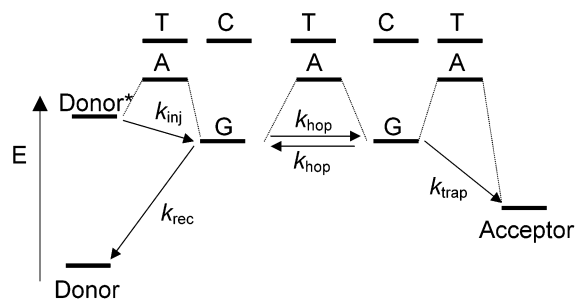


Figure 2.1. Guanine (G)-to-guanine hole hopping along DNA.

When ΔE_{DB} is positive, the rate depends on this energy gap.

$$k_{et} \propto 1/N \exp(-\Delta E_{DB}/RT) \quad (2.6)$$

In general, tunneling and hopping pathways operate in parallel.

$$k_{et} = k_{tun} + k_{hop} \quad (2.7)$$

When both contribute significantly to the rate, a region of distance independence of the rate may occur. The temperature dependences of the two pathways can be used to clarify the relative importance of each.

It is also possible for “resonant tunneling” to take place when the gap is zero, and little, if any, falloff with distance (wire length) is expected.⁶ Variable range hopping is also possible.^{42,43}

2.1.2. Experimental Results. The distance dependences of charge-transfer rates in a range of molecules in homogeneous solution have now been elucidated, spanning a range from $\beta \sim 0.2 \text{ \AA}^{-1}$ for unsaturated hydrocarbon bridges^{44,45} to $\sim 1.0 \text{ \AA}^{-1}$ for saturated hydrocarbon bridges.^{46,47} These β values can be attributed to the electronic matrix elements only if the distance dependence of the activation energy to β is small or if the correction for its distance dependence has been included.^{41,48} In cases where the ΔE_{DB} is small ($< 1 \text{ eV}$), as for hole transfer in DNA duplexes, the contribution of the distance-dependent solvent reorganization energy (λ_0) to β may apparently arise not only through the activation energy but also from the influence of λ on ΔE_{DB} ,^{4,49} since the relevant ΔE_{DB} for thermal electron transfer pertains to the transition state. Thus the analysis of β values inferred for DNA systems, which cover a very broad range (values between 0.1^{50} to $1.5^{51} \text{ \AA}^{-1}$ have been reported), still remains an open question to some extent, with much current attention focused on following the transition from superexchange coupling to the hopping regime.⁵² Recent work by Lewis et al.⁵³ (kinetics) and Giese et al.⁵⁴ (yields) has yielded $\beta \sim 0.6\text{--}0.8 \text{ \AA}^{-1}$ for hole transfer between guanine (G) donor and acceptor sites in DNA duplexes, consistent with superexchange tunneling. Recent studies of photoinitiated electron transfer through oligo phenylene vinylene bridges of variable length revealed a dramatic switch from exponentially decaying superexchange tunneling to sequential hopping as ΔE_{DB} becomes very small ($< 0.1 \text{ eV}$).⁵⁵ A series of X^+ -(9-amino-6-chloro-2-methoxy-acridine = X^+)-modified DNA duplexes with donor–acceptor distances varying from 4 to 11 \AA was characterized with femtosecond to nanosecond spectroscopic techniques used to measure forward and back charge-shift rate constants as a function of temperature. Increasing the separation between the acridine derivative and the guanine produced a significant increase in activation energy,⁵⁶ and λ , due to a dominant solvent contribution, was estimated to increase from 0.6 eV for 0.34 nm separation to 1.6 eV at 1.02 nm separation. This recent work thus reinforces the importance of considering the distance dependence of both nuclear and electronic factors.

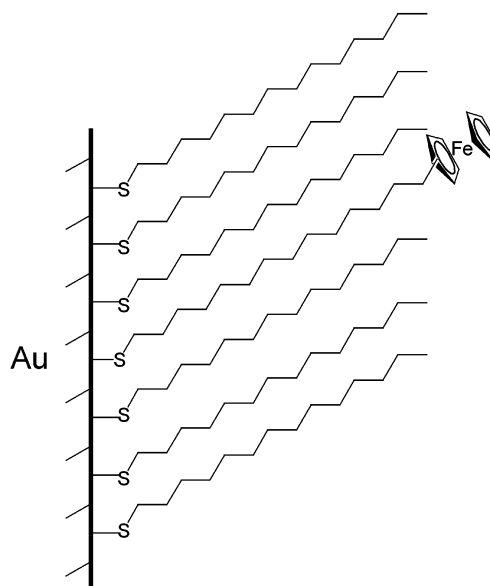


Figure 2.2. Self-assembled monolayer of ferrocene “doped” C13 thiol on a gold electrode.

2.2. Adsorbate–Metal Electrode. The rate constant for nonadiabatic interfacial electron transfer from a metal electrode to a bound redox group is:^{4,23,57–60}

$$k_f = \frac{2\pi\rho_M(E_F)}{h} \left[\frac{\pi}{\lambda k_B T} \right]^{1/2} \int_{-\infty}^{\infty} [H_{DA}(\epsilon)]^2 \times \exp \left[-\frac{(\lambda + (E_{app} - E^\circ)e - \epsilon)^2}{4\lambda k_B T} \right] f(\epsilon) d\epsilon \quad (2.8)$$

where $\rho_M(E_F)$ is the effective density of electronic states near the Fermi level (E_F) of the electrode (assumed independent of energy; 0.3 per eV for Au⁵⁸), E_{app} is the applied potential and E° is the reduction potential of the redox species, ϵ is the energy of a particular electrode level relative to the Fermi level ($E_F = -E_{app}e$), e is the elementary charge, and $f(\epsilon)$ is the Fermi–Dirac distribution of occupied states in the metal.

$$f(\epsilon) = \frac{1}{1 + \exp[\epsilon/k_B T]}$$

The product $\rho_M(H_{DA})^2$ is given as $|V(\epsilon)|^2$, an average over k states which is defined in eq 5 of ref 59. Equation 2.8 is analogous to eq 2.1. Both express the nonadiabatic, electron-transfer rate constant in terms of the reorganization barrier, the driving force (here $(E_{app} - E^\circ)e$), and the electronic factor.

Provided that the electronic coupling element H_{DA} is independent of energy, the standard electron-transfer rate constant under equilibrium conditions ($E_{app} = E^\circ$) is⁶¹

$$k^0 \cong k_{hop}^0 \gamma_M \quad (2.9)$$

where k_{hop}^0 is given by eq 2.1 when $\Delta G^\circ = 0$ and γ_M is a factor associated with the electronic density of states as will be exploited further in section 2.3.

$$\gamma_M = \pi k_B T \rho_M(E_F) \quad (2.10)$$

2.2.1. Self-Assembled Monolayers. Electrochemical measurements on self-assembled monolayers “doped” with redox-active species such as ferrocene (see Figure 2.2) have contributed powerfully to knowledge of nm-scale tunneling processes. The

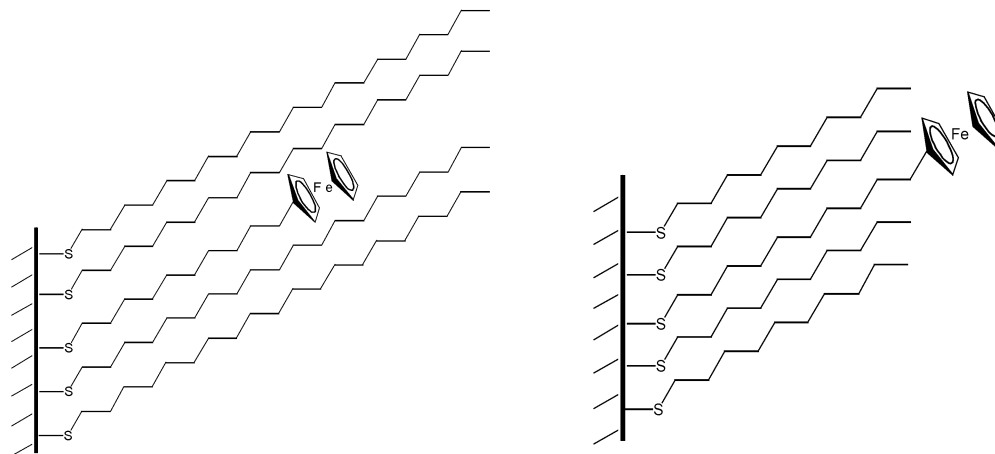


Figure 2.3. The standard electron-transfer rate constant for ferrocene oxidation/ferrocenium reduction in the structure at left is 200 s^{-1} , whereas that for the structure at right is $40,000 \text{ s}^{-1}$. The differences in rate for the two C_{13} thiols are closely correlated with the nature, particularly the size, of the electrolyte anions.

interfacial electron-transfer processes studied involve a metal electrode and a molecular unit (entry 2 in Table 1) in self-assembled monolayers, typically composed of thiols bound to gold. The exponential distance dependence of k_{et} has been demonstrated for organic thiols as a function of length and the nature of the bridge (e.g., alkane vs aromatic), yielding results similar to those inferred from homogeneous electron transfer (above). For alkanes, β lies in the range $0.9\text{--}1.3 \text{ per } \text{\AA}$.^{23,60,62} for oligophenylene, β is smaller, $0.4\text{--}0.5 \text{ per } \text{\AA}$.^{63–65} (Ref 27 reviews the recent literature.)

2.2.2. Localized Charge Generation and Ion Motion. Charge transfer in classical chemical systems involves motion of ionic charges, often via a combination of long-range electron transfer and counterion motion. The overall reaction driving force and rate in such systems are greatly affected by the electrostatic interactions of ions with their local environment and with each other. Charge balance is usually simple because no electrons or ions are added from external sources, and one can usually consider the system in isolation.

In electrochemical systems the situation can be more complex. Fixed charges are generated by electron transfer to/from an electrode, and charge-compensating counterions are generated at another electrode that is usually positioned far away. The important electrostatics are those associated with the electro-generated ion and its local environment, and with the charge-compensating counterion(s) that may or may not be present in the region near where the ion is generated. Generation of an ion in a place that is isolated from ions of opposite charge is energetically costly, and that cost affects the energy required to generate the ion.^{66,67} The energetic cost is diminished if counterion(s) can come close to the electrogenerated ion, but if that process is slow then it can limit the overall rate of charge transfer.

These ideas are illustrated in recent work by Sumner and co-workers (see Figure 2.3) involving an electrochemical system in which a redox molecule (ferrocene) is positioned in a self-assembled monolayer on a gold electrode in a microenvironment that does not permit access of counterions to the redox molecule.⁶⁸ Charge transfer between ferrocene and gold is dramatically slowed when the ferrocene is “buried” in a hydrophobic pocket into which anion access is inhibited. In contrast, direct exposure of the ferrocene to the contacting electrolyte increases the ferrocene oxidation/reduction rate by over 2 orders of magnitude, despite the fact that the molecular “bridge” connecting ferrocene to gold is the same in both cases.

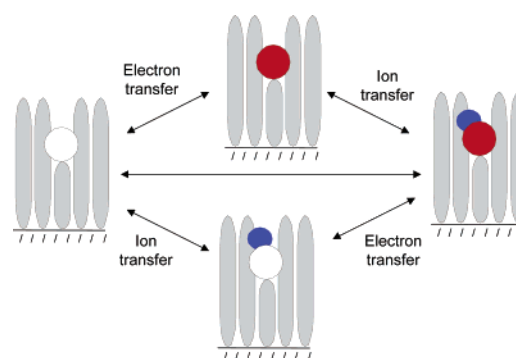


Figure 2.4. Mechanistic schemes for coupled electron/ion transfer in metal–bridge–redox molecule structures.

These results highlight the coupled nature of electron and ion transport in chemical systems on nanoscopic distance scales. Several microscopic mechanisms could be envisioned by which this coupled electron/ion transfer reaction could occur; some of them are illustrated in Figure 2.4. A critical question is whether one should consider the ion transport step as a coupled chemical reaction that occurs separately from electron transfer (i.e., a two-step process), or as one component of an overall reaction coordinate involving both electron and ion transfer (i.e., a concerted process).

Effects of counterions have also been seen on rates of long-range electron transfer in nonelectrochemical systems, and these have been modeled in several ways.⁶⁹ For example, Barnett and co-workers report that thermal motions of hydrated sodium counterions can strongly affect hole transport along DNA double helices in solution.⁷⁰ In their experiments, hole transport along native B DNA oligomers was compared with that along comparable oligomers that had been modified to incorporate Na^+ -starved regions into the double-helix region between the charge injection point and the GG site to which the injected holes ultimately migrate. The extent of hole migration was much less for the Na^+ -deficient oligonucleotides than for the native oligonucleotides, in agreement with simulations which suggest that hole transport is coupled to stochastic fluctuations in the counterion spatial configurations. This work and the work by Sumner et al. highlight the manner in which electron (hole) and ion dynamics can become coupled in systems where charge exists in localized states.

2.3. Metal/STM Tip–Molecule–Metal Electrode. In contrast to homogeneous and interfacial electron transfer, in which

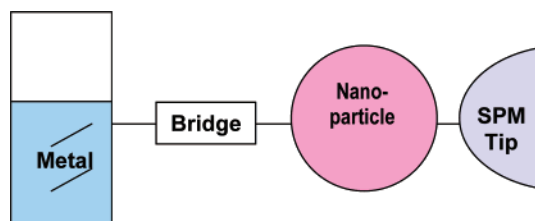


Figure 2.5. Configuration used for multiple conductance measurements. (Au–S–(CH₂)_N–S–Au–NP–Au) where Au–NP is a ligand-capped, gold nanoparticle.

a rate constant is the experimental quantity sought for motifs 3 and 6 in Table 1, resistance or conductance (reciprocal of the resistance) is the experimental parameter. The conductance is given by the Landauer⁷¹ formula, which relates the linear conductance g of a contact–(molecular bridge)–contact system to the electron transmission coefficient T :

$$g = \frac{2e^2}{h} T(E_F) \quad (2.11)$$

where E_F is the Fermi level of the contacts at zero voltage bias. For $T = 1$, $g = 2e^2/h = (12.9 \text{ k}\Omega)^{-1}$, the maximum conductance per molecule. In principle, the distance dependence of the conductance (like that for the rate constant) can be exponential

$$g = g_0 \exp(-\beta d_{DA}) \quad (2.12)$$

or “Ohmic”

$$g \propto 1/N \exp(-\Delta E_{DB}/RT) \quad (2.13)$$

where (as above) N is the number of repeated residues (e.g., CH₂, etc.).

2.3.1. Experimental Studies. Several types of “MIMs” (metal–insulator–metal) have been devised and studied, with the goal of characterizing the conductance of the (usually organic) molecule. In “break” junctions single molecules are trapped between metal electrodes.^{24,72} Self-assembled monolayers as described in section 2.2 are interrogated with scanning tunneling microscopy in dry N₂¹² or under a solvent. Self-assembled thiolate monolayers on gold were probed as a function of thiolate with the gold tip of a conducting AFM probe, and β factors of 0.42 Å⁻¹ and 0.96 Å⁻¹ were found for oligophenylene and alkane, respectively.²⁸ This distance dependence (measured in the presence of dry N₂) is similar to that found for the electrochemical solution measurements obtained for aqueous media (somewhat surprising, given the potentially large shift in energies on changing the surrounding environment). Wold and Frisbie found electronic transport across all-trans alkyl chains (in the absence of solvent) to depend critically on whether the chains are chemically bound to the electrodes or not in metal/molecule/p-type semiconductor junctions; tunneling of holes in these semiconductor-containing systems is more efficient than that of electrons; indeed, hole tunneling in σ -bonded chains appeared similar to electron tunneling through conjugated ones.⁷³

The configuration shown in Figure 2.5 has been used to make conductance measurements at more than 4000 “single-molecule” sites, where it is assumed that the alkanes are in the fully trans conformation.¹⁶ Dithiol bridges were introduced into thiol self-assembled monolayers and then topped with gold nanoparticles (“Au₁₀₁(PPh₃)₂₁Cl₅”⁷⁴) capped with triphenyl phosphine ligands. The assemblies (under toluene) were then probed with a

conducting AFM tip. The scans were stopped at nanoparticle junctions and the conductances of individual assemblies were probed as a function of bias voltage, and, in some cases, lateral force. Multiple measurements were obtained by probing different nanoparticle junction sites.

One remarkable aspect of the system’s behavior is the appearance of 1–5 “quanta” of current. These quanta are attributed to 1 to 5 dithiols linked to the tip by the intervening nanoparticle(s). Another potential issue is the exact role of the nanoparticle, since Coulomb blockade has been observed for gold nanoparticles in the 1.1 to 2.0 nm size range.^{15,75} Other aspects of the charge transport appear to be quite different from what is observed in alkanethiol monolayers (by, e.g., electrochemical or STM/AFM measurements). The absolute magnitude of the conductance (at low bias) of molecules in metal–molecule–metal junctions is close to what can be inferred from interfacial electron-transfer rate constants measured for related systems. (See section 2.4.) However, the electronic decay coefficient, β , is reduced below the value found for the case of contact to just one electrode. Corresponding to the small value of β at small (<50 mV) bias, β at high bias (up to ± 1 V) drops substantially with increasing bias. These observations are difficult to understand. Electronic structure calculations show that the gold Fermi level lies near the middle of the HOMO–LUMO gap,⁷⁶ so that the dithiol molecular orbitals are some 5 eV away from resonance. Under these conditions β should be about 1.0 (per methylene) and only very weakly dependent on bias. An implication of the observed distance dependence is that the dithiol energy levels have shifted dramatically with respect to the gold Fermi level. This raises the issue that the metal electrodes used to contact molecular conductors may play a dominant role in conduction of the overall system, a topic dealt with in the next subsection.

2.3.2. Role of Metals in Molecular Conduction. An important factor that affects the current–voltage characteristics of a metal–molecule–metal system is the energy of the metal Fermi level E_F relative to that of the HOMO and LUMO levels of the molecule. At equilibrium and with no applied voltage, the Fermi levels (chemical potentials) of the two metals will coincide at energy E_F . The alignment of E_F relative to the HOMO or LUMO affects how readily an applied bias can bring a molecular level into resonance with a metallic conduction state to produce an apparent large turn-on of the current. Before resonance the alignment of E_F affects the tunneling decay rate β , and this exponentially affects the magnitude of the current. While such sensitivity has been suggested for the conductance data,¹⁶ it should be noted that the analogous data for examining such sensitivity in the electrochemical kinetics²³ is not available.

Exactly where E_F lines up relative to the molecular levels does not have a simple “universal” answer. The situation is quite reminiscent of the metal/semiconductor interface, which produces the Schottky barrier ϕ . The barrier ϕ is the energy difference between the metal Fermi level E_F and the semiconductor conduction band E_c , $\phi = E_c - E_F$. This problem has been examined extensively,⁷⁷ and we briefly review it here to learn the general principles as well as the difficulties in obtaining a quantitative theory. The simplest estimate of ϕ is to set the vacuum levels of the metal and semiconductor equal. This estimate is $\phi = W - \chi$, where W is the metal work function and χ is the electron affinity of the semiconductor. This so-called “Schottky limit” seldom works because it neglects the charge transfer and rebonding at the interface, which produces interface dipoles. Another limit is the Bardeen limit in which E_F is “pinned” at the same level for a particular semiconductor

for all metals. In the Bardeen limit all metals produce the same barrier ϕ . This is observed in many semiconductor/metal systems. Tersoff⁷⁸ put forward a model of Fermi-level pinning for metal/semiconductors in which the alignment is controlled by the semiconductor and has little to do with the metal. The concept is that the metal states with energies within the semiconductor band gap tunnel into the semiconductor, and the tunneling behavior is controlled by the semiconductor. These metal-induced band gap states are filled up to the so-called "charge neutrality level" (CNL) of the semiconductor. The CNL is where the tunneling states change from valence-band to conduction-band character. This theory has been quite successful and qualitatively explains the data. But for some systems, it too fails.

A fully self-consistent electronic structure calculation is able, in principle, to determine the lineup of a metal/molecule system since it includes all charge redistribution effects. Xue et al.⁷⁹ have used a density functional technique to study phenyldithiolate between Au contacts. They find that dipole effects due to the sulfur-gold bond affect the lineup, and the results are very encouraging. Tomfohr et al.⁷⁶ followed up on the Schottky barrier analogy and determined the charge neutrality level of octanedithiol. The CNL is then compared to a self-consistent electronic structure calculation. The self-consistent alignment of the Fermi level is found to agree well with the CNL of the molecule. This gives hope that general concepts that give guidelines may be developed as for Schottky barriers. Clearly more theoretical work is needed to obtain a comprehensive theory for the lineup, and *direct* comparison with experiment is lacking.

In addition to the issue of the alignment of the Fermi level relative to the molecular orbitals, the metal contacts can perturb the molecular states. Clearly, overlap between metallic and molecular states is a prerequisite of electronic coupling, and overlap produces hybridization. This effect is usually small, much less than an eV, which is smaller than effects from polarization and charge transfer at the interface that controls the Fermi-level alignments (which can shift (uniformly) states by an eV or more in energy).⁸⁰ The presence of metals is also important in determining local electric fields (see section 2.3.3). An extreme example of this is resonance Raman enhancements owing to coupling to plasmons in metallic nanoclusters.

Electroactive molecules generally have redox-accessible states that lie within an eV or so of the metal Fermi level, and bonding such molecules to metal electrodes may modulate their conductivity. It is, however, surprising that significant effects are implicated for the *n*-alkane bridges discussed in section 2.3.1, as these are inert molecules with highly localized electronic states. Thus, it appears that contacting these (electrochemically) inert molecules to gold electrodes at both ends may have a profound effect on their conductivity. It could be the case that these metal-induced effects result from a major change in the electronic properties of the system compared to its components. Alternatively, the changes may be caused by constraining the conducting molecule to remain attached to the electrodes, eliminating degrees of freedom available to unconstrained molecules. Whatever the cause, it is clear that metal contacts can play a significant role in the electronic properties of a metal-molecule-metal nanoscale system. These effects will have to be characterized and understood, using such tools as photoelectron spectroscopy (PES) and 2 photon ES,⁸¹ as well as local probe measurements on well characterized assemblies. This is a necessary step in the rational design of nanoscale molecular electronic devices that rely on metal contacts.

2.3.3. Electric Field. A concept related to that discussed in section 2.3.2 is the voltage drop profile of the metal/molecule system under bias and how it affects the I - V characteristics. Mujica et al.³⁴ used a simple tight-binding model to find the voltage profile across a molecular chain. These results are quite informative in that they show that the largest potential drop occurs for atoms near the electrodes. Li et al.⁸² have found similar results for dithiolated alkanes connected to Au, where the largest drop occurs between Au and the end S atoms of the molecule.

A nice model to view this behavior comes from the work of Tian et al.⁸³ They consider the molecular levels as being fixed under bias, while the two chemical potentials E_F^L and E_F^R (for the left and right electrodes) are displaced from each other by eV , where V is the external voltage bias. Electrons that can transfer through the molecule are those within the "energy window" between E_F^L and E_F^R . If the molecule and its contacts are symmetric, E_F^L moves down by $eV/2$ ($E_F^L = E_F - eV/2$) and E_F^R moves up by $eV/2$ ($E_F^R = E_F + eV/2$). This produces a symmetric I - V curve ($-I(-V) = +I(+V)$). At high enough bias, a molecular orbital may enter the energy window between E_F^L and E_F^R to produce a resonance and a rapid increase in current. This rapid turn-on of the current occurs at the same magnitude of bias for either positive or negative bias.

A symmetric situation is not the norm. Even for a symmetric molecule the left and right chemical contacts may not be the same; one contact may be much stronger than the other. Tian et al.⁸³ introduce an asymmetry parameter η which raises or lowers the two-electrode Fermi levels (relative to the molecular levels) at different rates under bias, $E_F^L = E_F - \eta eV$ and $E_F^R = E_F + (1 - \eta)eV$. The difference between E_F^L and E_F^R is eV as required. This asymmetry parameter can produce a very *asymmetric* I - V curve. To see this, suppose we have a molecule with a 3 eV HOMO-LUMO gap, and suppose that the two metal electrodes line up their Fermi levels at E_F , which is +1 eV above the HOMO (or equivalently 2 eV below the LUMO). Consider the extreme case of $\eta = 0$. This means that the Fermi level of the left electrode is "locked" onto the molecular levels, while the right metal electrode Fermi level floats up or down exactly in line with eV . This might model a system with a strong chemical contact with the left electrode and a weak one for the right. If we apply a bias of +1 V, the energy window between E_F^L and E_F^R ranges from 1 to 2 eV above the HOMO (or equivalently 2 eV to 1 eV below the LUMO). The situation changes drastically under reverse bias. Reverse the bias to -1 V. The energy window now ranges from 1 eV to 0 eV above the HOMO (2-3 eV below the LUMO). Since the energy window here has just captured the HOMO, we open up a resonant channel for conduction and the current becomes very large. Instead of the I - V being symmetric, we instead find rectifying-like behavior: a large current (due to resonance with the HOMO) with one bias, and little current (no molecular orbital resonance) for the opposite bias. Such rectifying behavior of an asymmetrically coupled molecule has recently been simulated using the advanced nonequilibrium Green's function technique.⁸⁴

The magnitude of the field in reported I - V measurements is in the range of $10^7 - 10^9$ V/m. (The field used routinely in Stark (electroabsorption) experiments is 10^7-10^8 V/m.) The field used for the I - V measurements is comparable to that common in electron-transfer solution experiments: for a D-B-A assembly in a solvent of dielectric constant D_s , undergoing charge transfer from negatively charged D to neutral A separated by $d_{DA} = 1$ nm, the field across the molecule is

$10^9/D_s$ V/m– 10^7 to 10^9 V/m, depending on the solvent used. As described above, the field need not, and generally will not, be uniform across the molecule, and likely there is a reduced field within the molecule and a significant enhancement of the field at the metal/molecule interfaces.

2.4. Comparison between Electron-Transfer Kinetics and Conductance in Metal–Bridge–Metal (MBM) Junctions.

The kinetics of electron (or hole) transfer between localized molecular donor and acceptor sites, mediated by a molecular bridge or spacer (eq 2.1) or in the related interfacial electron-transfer process (eq 2.9), shares many features with conductance in related metal–bridge–metal (MBM) junctions. Guided by appropriate dynamical models,^{29–33,85,86} it is important to appreciate the similarities as well as significant differences between the two types of charge-transfer process. While a given DBA entity may be common to both processes, many details of the system may differ, including the nature of the initial and final states and the “reservoirs” to which the D and A sites are coupled.^{29,30,86} It has been proposed recently^{31,85} that the Landauer expression (eq 2.11), initially introduced to account for coherent electron tunneling, can be reexpressed and generalized as follows:

$$g = e^2 k_{\text{et}}(E_F) \rho_i(E_F) \quad (2.14)$$

where the electron-transfer rate constant k_{et} , defined by considering steady-state charge transport ($k_{\text{et}} = k_{\text{ss}}$), may include in parallel both coherent tunneling through the bridge (k_{tun}) and incoherent hopping initiated by thermal charge injection onto the bridge (k_{hop}) and where $\rho_i(E_F)$ is the initial electrode density of states (introduced as $\rho_M(E_F)$ in eq 2.9):

$$k_{\text{et}} = k_{\text{tun}} + k_{\text{hop}} \quad (2.15)$$

We consider now the special limit $k_{\text{et}} = k_{\text{tun}}$ which occurs when the energy gaps between resonant initial and final states and an intermediate charge-transfer state involving the bridge are sufficiently large. In this case the bridge-mediated tunneling may be described by superexchange tunneling, as discussed in section 2.1.1.⁸⁷ Dealing first with the DBA system in isolation, we may express the rate constant for electron transfer between D and A, k_{et} , as eq 2.1, and more generally we may write

$$k_{\text{et}} = (4\pi^2/h) |H_{\text{DA}}|^2 \text{DOS} \quad (2.16)$$

where DOS is the effective density of states associated with the standard Golden Rule formulation of the rate constant. For homogeneous electron transfer, DOS corresponds to FCWD, the Franck–Condon weighted density of vibronic states controlling activated electron transfer when D and A sites are coupled to vibronic reservoirs (eq 2.1).^{29,32,33} For electron transfer from a molecular adsorbate to a metal electrode, the FCWD due to the electrolyte phase, as well as the molecular modes of the DBA system, is supplemented by an additional factor γ_M , due to the electronic manifold of the metal^{23,60,62,88} (eq 2.10).

$$\text{DOS} = \gamma_M(\text{FCWD}) \quad (2.17)$$

When $\Delta G^\circ = 0$, Franck–Condon weighted density of states

$$\text{FCWD} = \left[\frac{1}{4\pi\lambda k_B T} \right]^{1/2} \exp \left[-\frac{\lambda}{4k_B T} \right] \quad (2.18)$$

From eq 2.10, with $k_B T = 0.026$ eV (298 K) and $\rho_M(E_F) = 0.3$ eV⁻¹ for a gold electrode,^{52,89} $\gamma_M = 0.024$.

The simple McConnell superexchange model (for nearest-neighbor or tight-binding coupling among D, A, and bridge sites) may be expressed as^{29,30,32,33}

$$H_{\text{DA}} = (H_{\text{D1}})(H_{\text{NA}})G_{1N}(E_D) \quad (2.19)$$

where the D and A sites are coupled, respectively, to the sites 1 and N of the bridge (taken as a linear sequence of N sites) and $G_{1N}(E_D)$ is the Green’s function of the bridge, evaluated at the energy of the donor state E_D . Note that the coupling between D and A is indirect through the bridge, so that there is no direct coupling between the two. Instead, higher order perturbation theory is needed, which is exactly solved by the \mathbf{T} -matrix, $\mathbf{T} = \mathbf{H} + \mathbf{H}\mathbf{G}\mathbf{H}$, leading in the present case to H_{DA} (as in eq 2.19) = $T_{\text{DA}} = H_{\text{D1}}G_{1N}(E_D)H_{\text{NA}}$.⁹⁰

In dealing with the larger context of an MBM junction, one may attempt to maintain the identity of the DBA moiety involved in the electron transfer (eq 2.1 or 2.9), as Nitzan has done,³² but now providing for the coupling of the D and A sites to metal electrodes (i.e., electronic reservoirs; at the same time, the vibronic reservoirs so central to electron-transfer kinetics may be absent or of much less significance^{29,30}). In effect, the model for the isolated DBA systems is broadened to include the additional “donor” and “acceptor” sites provided by the metal electrodes. We thus have an extended Green’s function, $G_{\text{DA}}(E_F)$ which includes the D and A sites as well as the N sites of B:^{29,30,32,33}

$$G_{\text{DA}}(E_F) = \frac{H_{\text{D1}}H_{\text{NA}}\bar{G}_{1N}(E_F)}{(E_F - E_D - \Sigma_D(E_F))(E_F - E_A - \Sigma_A(E_F))} \quad (2.20)$$

If the D and A energies (E_D, E_A) are assumed to be quite close to the metal Fermi energy (E_F) (e.g., as a result of strong contact interactions³²), it is essential to include the so-called “self-energies”, Σ_D and Σ_A (generally complex), which reflect the influence of the metal reservoirs. Discrete levels of the molecular bridge are resonant with the metal continuum of states. The initial molecular δ -function density of states broadens into a continuous local density of states spectrum with peaks and widths described by Σ . The self-energies are also crucial if the bridge sites approach resonance with E_F .^{29,30} The over bars in eq 2.20 allow for the fact that incorporating DBA into the junction may modify the electronic structure,^{31–33,85} although such effects are not included in the treatment below. In terms of G_{DA} , the conductance may be expressed as,^{29,32}

$$g(E_F) = \left(\frac{2e^2}{h} \right) |G_{\text{DA}}(E_F)|^2 \Gamma_D(E_F) \Gamma_A(E_F) \quad (2.21)$$

where the “widths” Γ (the imaginary components of Σ) reflect the strength of the M–D and A–M coupling. Nitzan has pointed out³² that when Σ is dominated by its Γ component (as might be expected for strong chemisorptive coupling), then the following simple relationship between g and k_{et} emerges (subject to various assumptions³²):

$$g \sim \frac{8e^2}{\pi^2 \Gamma_D \Gamma_A} \left(\frac{k_{\text{et}}}{\text{DOS}} \right) \quad (2.22)$$

Making the plausible assumption that $\Gamma_D = \Gamma_A \sim 0.5$ eV yields the order of magnitude relationship

$$g \sim 5 \times 10^{-19} k_{\text{et}} / \text{DOS} \quad (2.23)$$

TABLE 2: Comparison of Experimental $g(\Omega^{-1})$ and k_{et} (s^{-1}) Data for Alkane Chain-Mediated Charge Transfer

alkane bridge ^a ($\text{X}(\text{CH}_2)_{n-2}$)	g (Ω^{-1}) ^b	$5 \times 10^{-19}k_{\text{et}}/\text{DOS}^c$ (eq 2.23)	$8 \times 10^{-21}k_{\text{et}}/\text{DOS}^c$ (eq 2.25)
$n = 8$	$(10.3 \pm 0.5) \times 10^{-10}$	2×10^{-8}	3×10^{-11}
$n = 10$	$(3.5 \pm 0.2) \times 10^{-10}$	$(2 \pm 1) \times 10^{-9}$	$(3 \pm 1) \times 10^{-12}$
$n = 12$	$(1.2 \pm 0.1) \times 10^{-10}$	$(2 \pm 1) \times 10^{-10}$	$(3 \pm 1) \times 10^{-13}$

^a $\text{X} = (\text{CH}_2)_2$ in the conductance measurements^{16,92} and some of the electrochemical k_{et} measurements.⁹¹ In other electrochemical measurements, X is an amide^{62,91} ($\text{C}(\text{O})\text{NH}$) or ester⁶⁰ ($-\text{C}(\text{O})\text{OC}$) moiety. ^b In the conductance measurements^{16,92} D and A thiolate groups are coupled, respectively, to a planar gold electrode surface and a gold nanocluster. ^c In the electrochemical^{60,62,63,91} k_{et} measurements, the D and A groups are, respectively, a thiolate linked to a gold electrode surface and a ferrocene group. The room-temperature FCWD was evaluated on the basis of a classical model using a value of 0.9 eV for the reorganization energy ($\text{FCWD} = \exp(-\lambda/4k_{\text{B}}T)/(4\pi k_{\text{B}}T\lambda)^{1/2} = 2.95 \times 10^{-4} \text{ eV}^{-1}$).^{60,62,91} A value of 42 was used for $1/\gamma_{\text{M}}$ (see eq 2.10).

where the units of g , k_{et} , and DOS are, respectively, reciprocal ohms (Ω^{-1}), seconds (s^{-1}), and electronvolts (eV^{-1}). In eqs 2.22 and 2.23, k_{et} is taken as k_{tun} (see eq 2.15).

As an alternative to the limiting case described above (where Σ is dominated by Γ , due to the near resonance of the D and A levels with the Fermi level) we may adopt a model of conductance in which the explicit presence of D and A sites is dropped and the bridge is taken as being directly coupled to generalized donor and acceptor sites, including the metal electrodes.³¹ If the coupling is characterized by H_{LB} and H_{BR} , and the metal density of states by ρ_{L} and ρ_{R} (where L and R denote the “left” and “right” electrodes), one obtains

$$g = \frac{e^2}{2\pi^2} \left(\frac{k_{\text{et}}}{\text{DOS}} \right) \left(\frac{H_{\text{LB}}^2 H_{\text{BR}}^2}{H_{\text{DB}}^2 H_{\text{BA}}^2} \right) (\rho_{\text{L}} \rho_{\text{R}}) \quad (2.24)$$

(by analogy with the notation in eq 2.21, “widths” Γ_{L} or Γ_{D} may be defined as $\Gamma_{\text{L}} = \rho_{\text{L}} H_{\text{LB}}^2$ and $\Gamma_{\text{R}} = \rho_{\text{R}} H_{\text{BR}}^2$). If the ratio of H s is taken as order of unity and $\rho_{\text{L}}, \rho_{\text{R}} \sim 0.3 \text{ eV}^{-1}$ (as already adopted above for gold following eq 2.18), we obtain

$$g \sim 7 \times 10^{-22} k_{\text{et}}/\text{DOS} \quad (2.25)$$

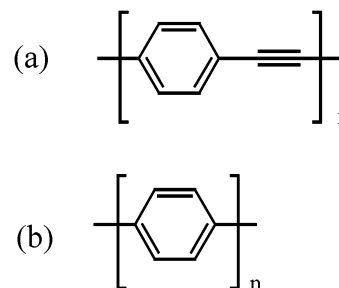
(A related analysis has been discussed in ref 31.)

Equations 2.23 and 2.25 provide a convenient approximate basis for comparing estimates of g and k_{et} involving a common bridge unit. As an example, Table 2 offers experimental conductance and electrochemical kinetics results^{16,60,62,91,92} based on charge transfer through linear chains comprised of N framework atoms ($N = 8, 10, \text{ or } 12$) of types $(\text{CH}_2)_N$, $\text{C}(\text{O})\text{NH}(\text{CH}_2)_{N-2}$, $\text{C}(\text{O})\text{O}(\text{CH}_2)_{N-2}$, all of which have similar lengths (for a given value of N). In the conductance experiments^{16,92} alkane bridges are terminated by thiolate groups linked on one end to a planar gold electrode and on the other to a gold nanocluster through which contact to the conducting atomic force microscope (AFM) tip is made. In the electrochemical k_{et} measurements,^{60,62,91} one end of the bridge is linked to a gold electrode by a thiolate group, and the other end is linked to a ferrocene group. Thus, in all cases, both bridge termini are covalently linked to their outer neighbors.

Table 2 indicates that the limiting theoretical model represented by eq 2.23, i.e., with D and A levels nearly resonant with the Fermi level, accounts for the observed transport data to within about 1 order of magnitude, a result which may be considered quite satisfactory given the assumptions involved in the model and the fact that the various experimentally studied systems, despite their generic similarities, do exhibit chemical differences. The alternative (nonresonant) model given by eq 2.25 yields appreciably smaller predicted g values lying below the experimental values by factors ranging from 30 ($n = 8$) to 400 ($n = 12$).^{16,92} Corresponding to the intriguing fact that the falloff of g with n (1.8 per CH_2 group⁹²) is appreciably more

gradual than observed in the k_{et} data ($\sim 3\text{--}4$ per CH_2 group^{60,62,88}), the calculated ratio of g to k_{et} increases by an order of magnitude over the range $n = 8$ to 12. This difference in falloff rates suggests important sensitivity of the transport rate to details of the contacts between the components of the junctions.^{16,92} The presence of the gold nanoclusters in the conductance studies may also play a role.

Comparisons may also be made for unsaturated bridges. For example, the scaled k_{et} value (eq 2.23) for electron transfer through an oligophenyleneethynylene bridge (a)⁶³ is within an order of magnitude of g for conductance through an oligophenylene bridge (b)⁹³ in a case where the two systems have similar overall metal–metal separations ($\sim 18\text{--}20 \text{ \AA}$, corresponding respectively to two phenyleneethynylene units and three phenylene units).

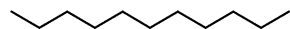
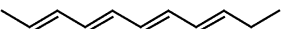
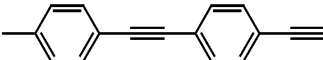


2.5. Calculation of β . Theory and computation are essential to interpretation of electron transport mechanisms. The superexchange description has been widely used for molecular electron-transfer processes in solution.⁴⁰ At the heart of these calculations is the calculation of the molecular Green’s function, also known as the propagator. The quantum mechanical propagator describes the propagation of an electron of a given energy through the molecule.

2.5.1. Calculation of β with a Recursion Relation. A recursion relation has been formulated for the Green’s function for calculating the effective electronic coupling in bridge-assisted electron-transfer systems, within the framework of the tight-binding Hamiltonian.⁹⁴ The recursion expression relates the Green’s function of a chain bridge to that of the bridge that is one unit less. It is applicable regardless of the number of orbitals per unit. This method has been applied to a ferrocenylcarboxy-terminated alkanethiol on the Au(111) surface. At larger numbers of bridge units, the effective coupling strength shows an exponential decay as the number of methylene ($-\text{CH}_2-$) units increases. This sequential formalism shows numerical stability even for a very long chain bridge and, since it uses only small matrices, requires much less computer time for the calculation. Identical bridge units are not a requirement, so the method can be applied to more complicated systems.

2.5.2. Calculation of β with a Complex Bandstructure Approach. A complex bandstructure approach has recently

proven valuable in interpreting the conductances of alkane dithiols bridging a gold electrode and an AFM tip.^{16,92} The complex bandstructure of a periodic system is the conventional bandstructure extended to complex Bloch k vectors. The k vectors with an imaginary part describe spatially decaying wave functions and arise in, for example, the analysis of impurity and surface states. They also represent the quantum tunneling states, which are vehicles of electron transport through a barrier such as a thin oxide layer or a molecule. Plots of the band energy as a function of the distance decay coefficient β are used to determine which bands have sufficiently small values of β to be effective in long-range transfer. For alkane, alkene, and benzene chains the following results were obtained⁷⁶ providing

	$\beta, \text{\AA}^{-1}$	$\beta, \text{ per C}$
	0.79	~ 1
	0.27	0.34
	0.27	

a direct link with experiment. The form of the complex bandstructure clearly elucidates the molecule length dependence of the tunneling current. In formulas such as eqs 2.19 or 2.21, the effect of tunneling manifests itself through the Green's function, which depends on the electron's energy within the HOMO–LUMO gap of the bridge. The Green's function can theoretically be composed of a sum of contributions from Bloch-like wavevectors, with the wavevectors being complex (exponentially damped instead of oscillating). For long molecules, one need only keep the smallest complex wavevector (the smallest β value) to arrive at a simple, yet exact in principle, method to estimate the Green's function. The structure of the complex bandstructure also suggests a scheme to align the Fermi level of the metal with the molecular orbital energies, similar to Schottky barrier alignment in metal semiconductor systems.

2.6. General Issues for the Future. *2.6.1. Methods for Collection of Statistically Significant Data Sets.* Many studies of the conductance of molecules (entry 3 in Table 1) have been carried out one molecule at a time. It is desirable to be able to efficiently collect sets of data for a large number of molecules. Utilization of self-assembled monolayers offers one solution to this problem,^{15,16,95} but other approaches, such as use of patterned electrode arrays onto which the molecules of interest could be adsorbed, need to be in wide use.

2.6.2. Coupled Electron and Ion Motion. Charge transfer in classical chemical systems involves motion of fixed ionic charges, often via a combination of long-range electron transfer and counterion motion. The overall reaction driving force and rate in such systems are greatly affected by the electrostatic interactions of ions with their local environment and with each other. Charge balance is usually simple since no electrons or ions are added from external sources, and one can usually consider the system in isolation. As discussed in section 2.2, electrochemical systems are more complex because charges due to electron transfer may be generated at one electrode while charge-compensating counterions are generated at another electrode that is usually positioned far away. The coupled nature of electron and ion transfer is certain to be important in many other nanoscale systems involving charge transfer. This will include nearly all systems utilizing nanoscale materials in energy

conversion, for example, in battery and fuel-cell electrodes and galvanic photoelectrochemical devices. Energy conversion in such devices nearly always involves creation and/or motion of charges, therefore energy conversion will always be fastest and most efficient when charges can be generated and moved without high energetic cost. This idea is quite general, such that any nanoscale system which transports charge by a site-to-site hopping mechanism should be strongly affected by the energetics of ion generation and motion. The coupled nature of electron and ion hopping is widely recognized for charge transport in bulk materials such as redox polymers,⁹⁶ and the ideas that have evolved to describe charge transport in such systems should translate well to nanoscale systems.

In some nanoscale systems involving charge transfer, the situation is less clear. For example, consider the case of charge transfer between two metal electrodes connected via a single bridging molecule. Charge transfer can occur across such a two-terminal structure in the absence of electrolyte or solvent without ever generating a fixed charge; thus, the energetic cost of generating and moving ions is expected to have relatively little effect on the rate (current). In such a structure, charge transport could also occur by a hopping mechanism involving transient creation of charged sites on the bridge. Three-terminal molecular devices in which a third electrode is brought into close proximity to an electron donor or acceptor in the bridge to achieve control over the charge transfer across the bridge are also of interest, primarily for applications in molecular electronics and information processing. It seems likely that the energy associated with forming and transporting ionic sites could be important in such structures. The question of how one should think about the charge balance in such structures is an open one, since ionic sites are presumably generated but charge-compensating counterions need not be present to transport charge. These systems present an opportunity for improved understanding of charge transport on the nanoscale.

Metal nanoparticles and nanoparticle arrays comprise another nanoscale system in which fixed ionic sites may effect charge transport. Metal nanoparticles can transport charge by a hopping mechanism involving transient charging of the nanoparticle (treating the particle as a nanoscale capacitor)^{97,98} and/or by a metal-like transport mechanism involving significant electron delocalization among the particles.⁹⁹ Particle size and spacing, the dielectric properties of the medium in which the particles are immersed, and the presence of free ions (electrolyte) in the local medium will be crucial to the behavior of such materials. A unified picture of charge transport in such materials has not yet emerged, and the development of such a picture constitutes another significant opportunity in the area of nanoscale charge transfer.

3. Electron Transport at Interfaces

Although there are many manifestations of charge transport at interfaces, the nature of electron transport at the interface of a metal with a single molecule or molecular nanostructure is critically important for understanding a broader array of interfacial phenomena and for many technological issues. For example, the drive toward electronic processing of information into the nm dimensional regime will require a major shift from current silicon-based MOS device structures. Molecular and nanoscale organic materials offer a potential new paradigm, but our understanding of these phenomena is limited. Many of the proposed schemes for a molecule-based nanoelectronic device require making electronic contacts to one or a group of molecules.^{100–108} In this regard, electronic interaction between

a metal electrode and a molecule determines not only contact resistance but also the functional nature of the molecular device. For a small molecule contacted by two metal electrodes, the complete system could be regarded as an interface problem. The transfer of electrons through such interfaces can also directly influence the effectiveness of energy conversion processes important to advanced fuel cell development, solar energy harvesting, or photocatalysis.

From scattering theory, the electrical conductance (g) for a single molecular orbital coupled to two electrodes may be described through the expression (which is equivalent to eq 2.21 in section 2.4)^{29,30}

$$g = g_c \Delta_L \Delta_R G^2 \quad (3.1)$$

where $g_c (= 2e^2/h)$ is the quantum of conductance; Δ_L and Δ_R represent the electronic coupling strength between the molecular orbital and the left and right electrodes, respectively; and G is the Green's function matrix element for the molecular bridge. This approach separates the problem into two parts: the contact problem and the bridge problem. This formalism clearly shows that the contacts are as important as the molecular structure in governing electron transport.^{109,110} In reality of course, the molecular bridge itself can be strongly influenced by and not strictly separable from the contacts.⁷⁹

The conceptual starting point for treating the contact can be the Newns–Anderson chemisorption model,^{111,112} but the one-dimensionality of the metal in this model is a significant limitation. An improvement treats the metal electrode as a semi-infinite continuum, the so-called “jellium” model.¹¹³ More recent treatments employ atomistic models of contacts and reveal the sensitivity of interfacial electron transfer to structural details of the contact, such as surface coordination number, bond distance, symmetry, and chemical identity.^{114,115} These structural factors determine the electronic configurations of the interfaces. A limitation for all of these theoretical approaches is the absence of dynamics, i.e., the time scale for electron transfer and electron–nuclear coupling. An accurate account of dynamic factors will necessitate inclusion of the breakdown of the Born–Oppenheimer approximation.

Here we briefly examine the key issues involved in interfacial electron transfer mainly from an experimental perspective and for metal–molecule and metal–nanoparticle assemblies in the absence of solvent and electrolyte. We illustrate some directions and concepts for elucidating these issues: (1) *Structure* – what atoms are present at the interface and where are they located? (2) *Electronic configuration* – what are the electronic states of the molecules at the interface and how are they coupled to the electronic states of the metal? (3) *Dynamics* – what is the time scale for electron transport and for response of the system to the electron transport?

3.1. Structure at the Metal–Molecule Interface. Molecular systems are strongly influenced by interaction with different phases present at an interface. To the extent that the Born–Oppenheimer approximation is suitable for describing molecular systems, it is critical to know how the atomic species are configured as a first step toward defining the electronic configurations of these species. We also recognize that the local environment, whether gaseous or liquid or solid, does and can influence very strongly the atomic configurations.

The development of scanning probe microscopy (SPM), particularly scanning tunneling microscopy (STM), has revolutionized our capability to determine experimentally molecular configurations at interfaces, and many studies have demonstrated the efficacy of these techniques. As an illustration, Figure 3.1

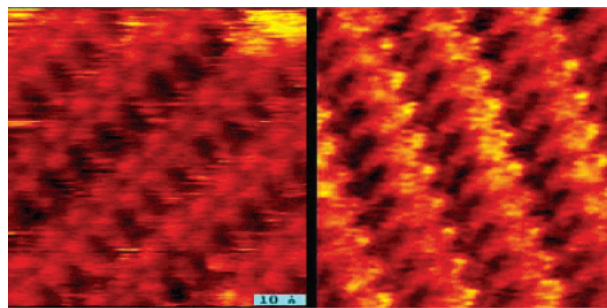


Figure 3.1. Molecular resolution STM images of flat-lying pentacene monolayer (left) and π -stacked multilayer (right) on the Au(111) surface. The scale bar is 10 Å. The molecules are vapor deposited onto the surface in ultrahigh vacuum at a substrate temperature of 25 °C. (J.-H. Kang and X.-Y. Zhu).

shows STM images of pentacene molecules at monolayer and multilayer coverages on the Au(111) surface. The strong molecule–metal interaction leads to the formation of a new molecular lattice structure: π -stacking, as opposed to the herringbone structure observed for the bulk pentacene crystal. Note that these images reveal the density of electronic states with submolecular resolution, but an actual determination of nuclear coordinates and chemical identity is not such an easy task. Recent experiments on inelastic tunneling with STM have allowed the recording of vibrational spectroscopy of single molecules on metal surfaces.¹¹⁶ This development provides a powerful means of structural determination on the single adsorbate level. However, SPM techniques are of limited use when the substrate deviates from a flat, single-crystal surface.

Other bulk-based probes, such as X-ray absorption fine structure, X-ray photoelectron diffraction, and electron diffraction, are also sensitive to interfacial structure, but these techniques provide ensemble averages. Although these techniques are useful and can provide detailed information on molecular configuration at well-defined interfaces, it remains a great challenge to obtain similar levels of understanding for molecular configurations at interfaces useful for nanoscale electron transport, particularly when the interface is buried, such as in a metal–molecule–metal device. The knowledge of molecular configuration in such a “sandwich” is critical to the interpretation of experimental observations in molecular devices, such as the negative differential resistance observed recently.^{102,103} However, we may need to infer this knowledge from model molecule–metal systems until breakthroughs in experimental techniques are found.

3.2. Electronic Configuration at the Metal–Molecule Interface. Given a molecular configuration on a metal surface, we need to understand and describe the electronic structure of the coupled metal–molecule system. In some cases it may suffice to describe the electronic configuration of the molecular system and then to understand the couplings of this system with the metal. In other cases, especially where covalent bonding between the molecule and the metal occurs, this may be insufficient and a complex description is necessary. Key issues include (a) the extent of charge redistribution due to adsorption and the resulting surface dipole; (b) the alignment of molecular orbital (MO) energies to the metal Fermi level; and (c) the strength of electronic coupling (wave function mixing) between discrete molecular orbitals and continuous metal bands. Charge redistribution at the molecule–metal interface produces an electrostatic field. Such an electrostatic potential rectifies interfacial electron transport; this is similar to the rectifying effect of a Schottky barrier. Moreover, at the nanometer scale of concern here, these fields may strongly influence energy

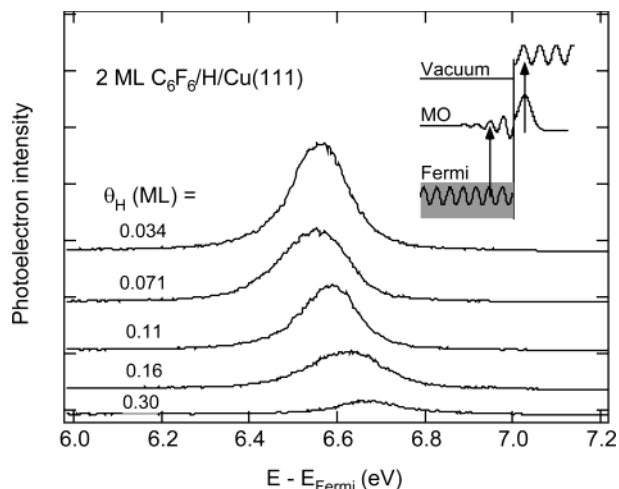


Figure 3.2. 2PPE spectra of bilayer C_6F_6 on $H/Cu(111)$ at the indicated surface hydrogen coverages (0.034–0.30 ML). The inset shows schematically the 2PPE process involving an initial metal state below the Fermi level, an intermediate molecular orbital (MO), and a final free-electron state above the vacuum level. The arrows represent photon absorption

levels within molecular units that are not directly involved in bonding. Experimentally, this kind of interfacial charge redistribution can be probed by surface work function measurements.

The energetic position of molecular orbitals with respect to the Fermi level determines the so-called charge injection energetics in molecule-based electronic or optoelectronic devices. Beyond the immediate contact, a precise knowledge of this energetic alignment is critical to a successful understanding of charge transport mechanisms, including molecular orbital-assisted tunneling, resonant charge hopping, and band-like ballistic transport. Experimentally, energetic positions of occupied and unoccupied molecular orbitals of adsorbates can be determined by photoelectron spectroscopies, including one-photon photoemission, inverse photoemission, and two-photon photoemission spectroscopy. Alternatively, scanning tunneling spectroscopy is capable of determining both occupied and unoccupied MOs on surfaces with spatial resolution on the Å scale.^{117,118}

Perhaps the most important issue regarding interfacial electronic configuration is the electronic coupling (wave function mixing) between a molecule and a metal surface, i.e., the Δ terms in eq 3.1. The extent of electronic coupling determines not only the energetics discussed above but also the dynamics of interfacial electron transfer. Electronic coupling has been traditionally difficult to quantify experimentally, but the recent development of two-photon photoemission (2PPE) spectroscopy has shed light on this issue.⁸¹ The inset in Figure 3.2 illustrates the principle of 2PPE. The interaction between a molecular orbital (MO) and the metal band structure is illustrated by a mixed wave function, with the major part of the wave function localized to the molecule and a minor oscillating tail in the periodic substrate lattice. This tail is a quantitative measure of electronic coupling. The first photon excites an electron from an occupied metal state to the mixed molecular state; this is electron transfer from the metal to the molecular resonance. The second photon ionizes the transient molecular anion for detection. The kinetic energy of the photoemitted electron provides the energetic position of the molecular orbital. The rate of photoemission in this mechanism is proportional to the square of the amplitude of the transition dipole moment (metal-to-molecule electron transfer) or the square of the amplitude of

the oscillating tail of the mixed MO. A weakening in electronic coupling between the molecule and the metal should result in a decrease in amplitude of this tail and, thus, a decrease in photoemission yield. This effect is observed experimentally in a recent 2PPE study of C_6F_6 on hydrogen passivated $Cu(111)$, Figure 3.2.¹¹⁹ With increasing coverage ($\theta = 0$ –0.34 ML) of preadsorbed atomic H, which systematically weakens the electronic interaction between C_6F_6 and $Cu(111)$, the 2PPE yield from the low-energy, unoccupied MO (LUMO) of C_6F_6 decreases by more than 1 order of magnitude. These results demonstrate the critical importance of the chemical state of the interface in governing the electronic coupling strength. Note that with a decrease in electronic coupling strength, we expect the lifetime of the transiently populated LUMO to increase significantly beyond the value of ~ 10 fs on clean $Cu(111)$.⁸¹ These time-resolved experiments are underway.

In addition to the general issues discussed above, the specific system of thiolate–metal contact is of particular interest. Self-assembled monolayers of thiols on metal surfaces have been popular choices for the construction and testing of molecular electronic devices.^{102,103,106–108} The facile reactive formation of the thiolate–gold contact provides an attractive method to connect molecular components to metal electrodes. The effect of covalent linkage and the role of contact resistance have been explored by a number of transport measurements.^{16,28,120,121} An important question is: What is the electronic configuration of the thiolate–metal contact? Recent 2PPE measurements and ab initio calculations on model SAM/ $Cu(111)$ systems¹²² have shown the presence of two σ^* states localized to the C–S–Cu linker. For symmetry reasons, these localized σ^* states introduced by the anchoring bond cannot couple to the delocalized π^* states within a conjugated molecular framework. Thus the thiolate contact can be considered “insulating” for electron transport through a self-assembled monolayer of molecular wires. On the other hand, the model ab initio cluster calculations show that the π HOMO is delocalized between the molecular framework and the metal surface via the –S– bridge. Therefore, in contrast to electron transport, the thiolate contact may be conducting for hole transport. This prediction is supported by a recent experiment using Hg as a contacting electrode.¹²⁰ The model ab initio calculations cannot, of course, yield reliable values of the Fermi energy for the SAM modified system. An example of semiempirical adjustment of such gaps has been given.³⁸ Analogous studies of alkane thiols on silver have been reported.¹²³

From the examples above, we may see that there are now some powerful tools available that can provide information concerning the electronic structure of molecules bound to or near a metal interface. As this type of information becomes more readily available, we can anticipate a much more complete understanding of the coupling of metals to molecules at the metal interface. It also should be noted that techniques such as those described here can be augmented and supported by comparisons with classical electrochemical measurements.

3.3. Dynamics of Charge Transport at the Metal–Molecule Interface. Ultimately we need to understand not only the static aspects of electron transport at molecule–metal interfaces but also the dynamics. Key questions include: what is the time scale for the electron to cross the interface? What is the time scale for localization or delocalization of the charges in response to electron transport? What are the conductance or transmission coefficients? These are indeed challenging problems, and at the present time there is no general methodology for attacking these issues. It is clear that single-molecule

experiments provide the opportunity to examine the dynamics of individual molecules or groups of molecules. It is also clear that photoexcitation provides a valuable means for initiating an electron-transfer event, following which the dynamic response can be measured with femtosecond resolution. Thus we will provide here a few examples to demonstrate some of the capabilities to use photoexcitation and to monitor some of the dynamics of electron transport in some systems.

The two-photon photoemission experiment can be carried out in a time-resolved manner^{124,125} to directly establish the lifetime of the transiently populated MO. In most cases, the measured lifetime is determined by the ultrafast rate of electron transfer from the MO to the metal substrate. Thus, the lifetime provides a quantitative measure of the electronic coupling matrix element for interfacial electron transfer. For the system illustrated in Figure 3.2, pump-probe experiments with C_6F_6 on clean Cu(111) have shown that the lifetime of the transiently populated LUMO increases from ~ 7 fs at 1 ML to ~ 32 fs at 5 ML coverage.¹²⁶ This dependence of the lifetime on coverage suggests that the electronic coupling between the LUMO and the metal surface weakens as film thickness increases. With increasing film thickness, the wave function delocalizes in the z -direction; this leads to an increased distance of the center-of-gravity of the wave function from the surface and a diminishing amplitude of the tail inside the metal.⁸¹

A critical question is: how do we probe the dynamics of electron–nuclear coupling and localization at molecule–metal interfaces? For fast localization dynamics, one approach is time-resolved 2PPE. If the transiently populated MO is delocalized within the molecular layer, i.e., dispersed in the surface plane, the dynamics of localization may be studied by measuring the disappearance of dispersion as a function of time. The feasibility of this approach was demonstrated by Harris and co-workers who showed that image state electrons in the alkane/Ag(111) system can be trapped at the surface of the alkane film, leading to the formation of small polarons.¹¹⁴ The dynamics of image state decay to localized small polarons was directly followed in time- and angle-resolved 2PPE. A second and more general approach may rely on a time-resolved technique with sensitivity to nuclear movements. A promising candidate is time-resolved sum-frequency generation.¹²⁷

Semiconductor nanocrystal luminescence provides a powerful probe of charge transfer dynamics. Brus and co-workers have studied extensively the blinking of the luminescence from individual CdSe nanoparticles near metallic substrates under intense optical excitation.^{18,128} The blinking phenomenon can be explained through the scheme outlined in Figure 3.3. Optical excitation normally creates hole–electron pairs that can recombine emitting luminescence. However, if the electron tunnels through an insulating layer into the metal, then the particle will be left ionized in a nonluminescing state. More recently this hypothesis has been confirmed through electric force microscopy (EFM) studies, which provide a particularly powerful tool for examination of charge transport in these systems.^{129–131} These techniques involve direct imaging of particles through conventional atomic force microscopy as well as mapping of the corresponding charge distribution and dielectric response under various conditions including optical excitation. For example, experiments reported to date show the following. (1) CdSe nanocrystals develop a single positive charge if stored for weeks in room light. (2) These crystals on graphite photoionize with yield of about 10^{-5} per photon. The photoinduced hole is stable for about 1 h. The efficiency depends on surface passivation and distance from surface. (3) The linear intensity or fluence

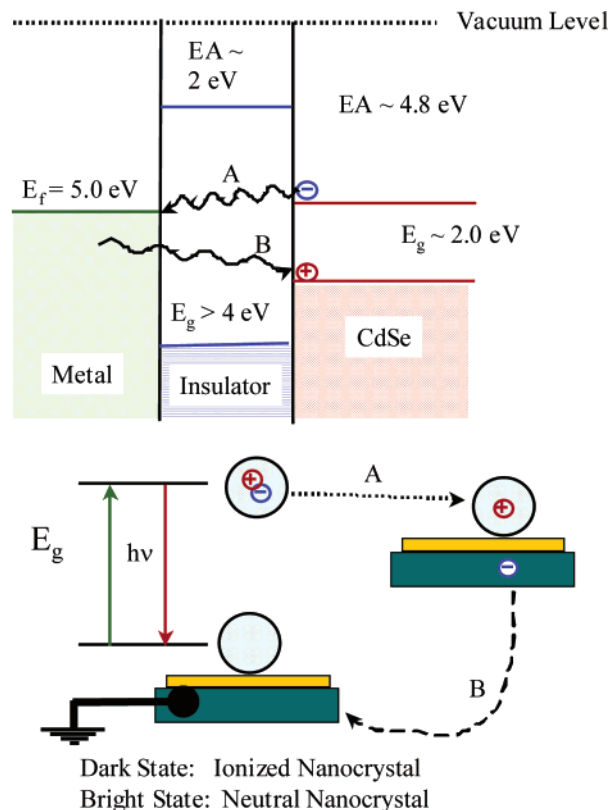


Figure 3.3. Schematic representation for charge transfer in photo-excited CdSe nanoparticles.

dependence implies electron tunneling from the nanocrystal excited state into the graphite. (4) The hole is probably self-trapped on the surface of the nanocrystal creating a large induced dipole moment.

Single-molecule fluorescence combined with near-field optical scanning microscopy can provide very important details of the dynamics of charge transfer in *single molecules* at the interface with conductors and semiconductors. At the heart of molecular level electronics ultimately lies the connection of a molecule to an electrode and the movement of electrons between the two. Thus there is a need for experiments designed to probe the discrete electronic and molecular dynamic fluctuations of single molecules near electrodes in the microsecond and longer time regime. As indicated above, local molecular and surface structural variations may lead to unique local environments for each molecule which can dramatically influence observed rates of electron transfer. Moreover, stochastic fluctuations in time of the oxidation state of a molecule and molecular dynamical processes that influence the electrical behavior are expected to result in a type of “noise” associated with molecular electronics. Research into this behavior of single molecules may eventually lead to new control mechanisms for electron flow in molecular systems. Single-molecule spectroscopy (SMS) has evolved as an important method for the study of the fluorescent behavior of single molecules in ambient environments and has been used to probe motional and excited-state electronic processes of molecules.^{132–135} Monitoring the fluorescence of a single molecule makes possible the elucidation of complex phenomena that are normally obscured in ensemble-averaged measurements. Fluctuations in the fluorescence–time trajectories contain detailed molecular level statistical and dynamical information of the system.

Adams and colleagues have been developing prototype molecular electronic systems and methodology to study

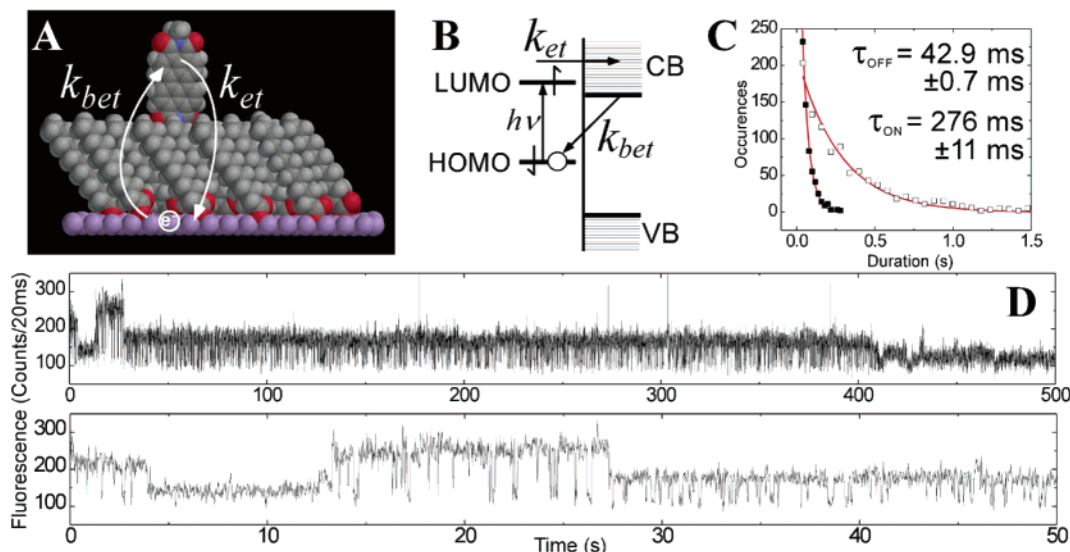


Figure 3.4. Electron transport at pyrene compounds adsorbed onto conducting substrates. (A) Schematic diagram. (B) Energy level diagram. (C) Decay kinetics. (D) Blinking phenomena.

photoinduced interfacial ET between single molecules and electrodes.^{136–138} They have built a combined near-field scanning optical microscope and scanning confocal microscope that allows them to measure the electron-transfer rate, to determine the orientation of a molecular dipole in three dimensions, and to adjust the electron-transfer driving force for by application of an electric field via the metal-coated near-field probe. Through this research it should be possible to relate for a single molecule the kinetics of interfacial electron transfer to distance, molecular structure and dynamics, and energetics.

For example, recent experiments have been directed at measuring the single-molecule electron transfer in a chromophore/linker/electrode system where a perylene chromophore is covalently attached to a modifiable alkyl-carboxylic linker (C_{11} in this case) and self-assembled at low concentration in monolayers onto semiconductive and conductive electrodes such as indium tin oxide and gold, Figure 3.4A.¹³⁷ This is done by repetitively exciting one molecule and determining the distribution of “on” and “off” times. Optical excitation of a single perylene from the ground state (S_0) at a rate (k_{exc}) leads to creation of an excited state (S_1) which decays either radiatively at a rate (k_r) or by charge injection into the conduction band (or trap states) of the electrode (k_{et}), Figure 3.4B. The electron returns to the molecule at a rate for back electron transfer (k_{bet}). The fluorescence of single molecules near electrodes in self-assembled monolayers display blinking behavior with characteristic millisecond off periods (Figure 3.4D). Since the molecule is not fluorescent in the charge transfer state, these off periods may be ascribed to discrete electron-transfer events. The fluorescence blinking is not seen for molecules on polymer-coated glass surfaces since these provide no acceptor states. The electron-transfer rates can thus be obtained from an analysis of the fluorescence time trajectory. k_{bet} is straightforwardly related to the average off time (t_{OFF}), while the average on time (t_{ON}) is related to the excitation rate k_{exc} times the quantum yield for the forward ET process (Φ_{et}) and can be used to estimate k_{et} : $(t_{OFF})^{-1} = k_{bet}$ and $(t_{ON})^{-1} = k_{exc} k_{et}/(k_r + k_{et}) = k_{exc} \Phi_{et}$. For many molecules, single-exponential behavior is observed for both forward and back ET processes. Typical fits of the experimental data for forward and back processes are shown in Figure 3.4C. Also apparent in fluorescence traces are discrete jumps in fluorescence intensity (Figure 3.4D) on a time scale of seconds, which may be the result of molecular reorientation

dynamics where intensity changes arise from increased or decreased absorption of the polarized laser light.

In these experiments, the single molecules at the electrodes serve as probes of how a molecule with discrete energy levels couples to an electrode with a spatially varying continuum of states, an energetically varying density of states, and trap sites. It is not exactly clear whether single exponential behavior should be expected for a single molecule ET. If a molecule can transfer an electron to a continuum of states and possibly different distinct trap sites and with different rates, should the result be single exponential? Can an electron escape into the continuum? Experiments of this sort are currently directed at using near field methods with polarized light to follow molecular orientation and dynamics and using electric fields to modulate the driving force of ET. Eventually it should be possible to use this method to study transistor type molecules in self-assembled monolayers without the need to connect to three electrodes. Application of an electric field could gate the flow of electrons between different legs of a trigonal molecule probed by optical methods.

3.4. Summary and Conclusions. To understand the phenomena relating to charge transport at the interface of a molecule with a metal or semiconductor, it is clearly critical to elucidate the actual nuclear configuration of the molecule at the interface (which can deviate considerably from the molecular configuration in solution or in the gas phase) and to elucidate the corresponding electronic configuration (at least in the Born–Oppenheimer approximation). It is also necessary to understand the coupling of the molecule in its interfacial configuration to the metal or semiconductor. On the basis of this characterization, theory and new experimental techniques can help us develop a detailed understanding for both the static and dynamic behavior of charge transport at the interface. Several experimental tools have been developed to help provide the needed characterization. These include scanning probe techniques such as STM and AFM along with new capabilities such as EFM. They also include new spectroscopies including, for example, photoemission spectroscopy and, in particular, two photon photoemission (2PPE). These spectroscopic techniques have been demonstrated to provide a wealth of static and dynamic information. In addition, single-molecule or single-particle luminescence techniques are proving to be very valuable tools for direct exploration of charge-transfer phenomena. Extension of this exploration to nanoparticle–organic systems of the type discussed in section

5.2 will be important to utilization of assemblies for energy conversion. With our present capabilities it is possible to begin to explore the fundamentals for charge transport at interfaces for selected systems. However, much additional work and new tools will be required to develop a comprehensive understanding for this important field.

4. Toward Functioning Molecular Electronics

Interest in fabricating devices based on active molecular components has been driven by both the fundamental interest in understanding how chemistry can be used to build function at the molecular level and by the looming technological expectation of the end of Moore's law. Can molecules be designed and incorporated into device structures to obtain solid-state analogues of two-terminal diodes and memory devices and three-terminal transistors? By what mechanisms will each of these devices operate? Each device must be stable, providing little shift in turn-on or threshold voltage with operation and time, and from device-to-device the turn-on or threshold voltage must be the same.

4.1. Recent Advances. Some recent advances toward the understanding of the electronic properties of molecules are outlined below.

(1) Scanning tunneling spectroscopy measurements of aromatic thiols incorporated into self-assembled monolayers of alkanethiols on Au(111) show higher conductivity for molecules having aromatic versus aliphatic chains.¹³⁹

(2) Using a revolutionary "break junction" technique, the resistance of 1,4-benzenedithiol was measured to be several $M\Omega$,²⁴ much larger than Landauer's quantum of resistance $h/2e^2 = 12.9 \text{ k}\Omega$,⁷¹ possibly arising from either a mismatch between the Fermi level of Au and the relevant molecular orbital of the molecule, or because of other effects such as Coulomb blockade.

(3) Molecules of 2'-amino-4-ethynylphenyl-4'-ethynylphenyl-2'-nitro-1-benzenthiole self-assembled onto a Au bottom electrode and then topped by low-temperature evaporation of a Au electrode exhibit negative differential resistance in $I-V$ characteristics.¹⁰² The same molecules between Au electrodes exhibit low and high-conductivity states, with an exponential decay of the high-conductivity state of 800 s at 260 K: this has been interpreted as a molecular random access memory cell.¹⁴⁰ While negative differential resistance and changes in conductivity are observed only in nitro-derivatized molecules, stochastic switching in the conductivity of a single to a few molecules of the same ethynylphenylene backbone derivatized with and without nitro and amine substituents have been observed in STM.¹⁰³

(4) The Landauer quantum of resistance, $12.9 \text{ k}\Omega$ ⁷¹ has been measured at room temperature between a single-walled carbon nanotube, glued to a conducting AFM tip, and a pool of liquid Hg.¹⁴¹

(5) Field-effect transistors having carbon nanotubes as the semiconducting channel, fabricated by stretching nanotubes across source and drain electrodes, show p-type conduction with good switching behavior.^{142,143} More recently, n-type semiconducting behavior in single-walled carbon nanotubes was demonstrated by either vacuum annealing or K-doping the nanotube; this enabled p- and n-type regions to be fabricated within a single nanotube and the demonstration of an intramolecular voltage inverter with a gain of 1.6.¹⁴⁴ Single-electron transistor behavior, characterized by Coulomb blockade, was reported in single-walled carbon nanotubes by defining $\sim 20 \text{ nm}$ coherent segments by kinking the tube on either side with an AFM tip.¹⁴⁵

(6) A Langmuir-Blodgett monolayer of a bistable [2] catenane, with a naphthalene group as one "station" and tetrathiafulvalene as the second "station", and a tetracationic catenane hexafluorophosphate salt traveling on it like a "train" on a closed track, were deposited on poly-silicon as one electrode and topped by a 5 nm Ti layer and a 100 nm Al electrode. The current-voltage plot is asymmetric as a function of bias (which moves the train on the track), and a succession of read-write cycles shows that the resistance changes stepwise as the train(s) move from the lower-conductivity station(s) to the higher-conductivity station(s).¹⁴⁶

(7) Unimolecular rectification across a Langmuir-Blodgett monolayer of hexadecylquinolinium tricyanoquinodimethanide was first detected between Mg and Pt electrodes^{147,148} and later observed between Al electrodes,^{100,149,150} most recently even between oxide-free Au electrodes,^{151,152} to be a variant of the Aviram-Ratner mechanism.¹⁵³ The original proposal suggested a $D-B\sigma-A$ molecule connecting an electron donor moiety to an electron acceptor moiety through an insulating saturated "sigma" bridge B_σ ; the mechanism of action involves inelastic tunneling through the molecule from its first electronic excited-state $D^+-B_\sigma-A^-$ to the less polar ground state $D^0-B_\sigma-A^0$.¹⁵³ The first confirmed rectifier was a ground-state zwitterion $D^+-B_\pi-A^-$, connected by a twisted π bridge and used inelastic tunneling from the lower-polarity excited-state $D^0-B_\sigma-A^0$ to the higher-polarity ground state.¹⁵⁴

(8) Most recently, two new monolayer rectifiers have been found when sandwiched between gold electrodes.^{155,156} The first is a pyridinium salt, in which the rectification seems to be due to back-charge transfer from the anion to the pyridinium ion.¹⁵⁷ The second is dimethylaminophenylazafullerene, which has a tremendous rectification ratio (as high as 20,000): here, however, the bulk of the forward current seems to be due to the formation of stalagmites of gold, which do not pierce the monolayer totally, but, once formed, behave ohmically.¹⁵⁶

4.2. An Alternative Approach Using Quantum Cellular Automata. Section 2.3.3 discusses how an electric field influences the distribution of charges within molecules exposed to the field. Field-induced charge movement within a properly designed molecule could be used for transmitting or processing information in a cellular automaton architecture. In the quantum-dot cellular automata (QCA) architecture,¹⁵⁸ bit information is stored in the charge configuration of cells constructed from quantum dots. Charges move within the cells in response to external inputs or the electrostatic influence of neighboring cells. The cell-cell electrostatic interaction means that contacts must only be made at the edges of an array of QCA cells, and that no current need flow through the cells.

QCA has been experimentally demonstrated at 80 mK in nearly a dozen devices,¹⁵⁹ including QCA cells, wires, and logic elements (AND/OR gates), and a clocked memory cell. A power gain of 2.1 was measured for the last device.¹⁶⁰ Recent efforts have focused on implementing QCA at the molecular size scale, in which case each "quantum dot" would consist of a single redox center and the "tunneling junction" would be an organic or inorganic bridging group. Molecular QCA is predicted to function at room temperature, and many mixed-valence molecules would be suitable as QCA cells.¹⁶¹

Recent ab initio calculations¹⁶² show that the electrostatic forces between adjacent molecules are strong enough to cause significant charge transfer to occur. For example, the 1,4-diallyl butane radical cation is a model two-dot QCA cell. It possesses two redox centers (the allyl groups) located 7 Å apart, separated by a butane bridge, and has a single positive charge that can be

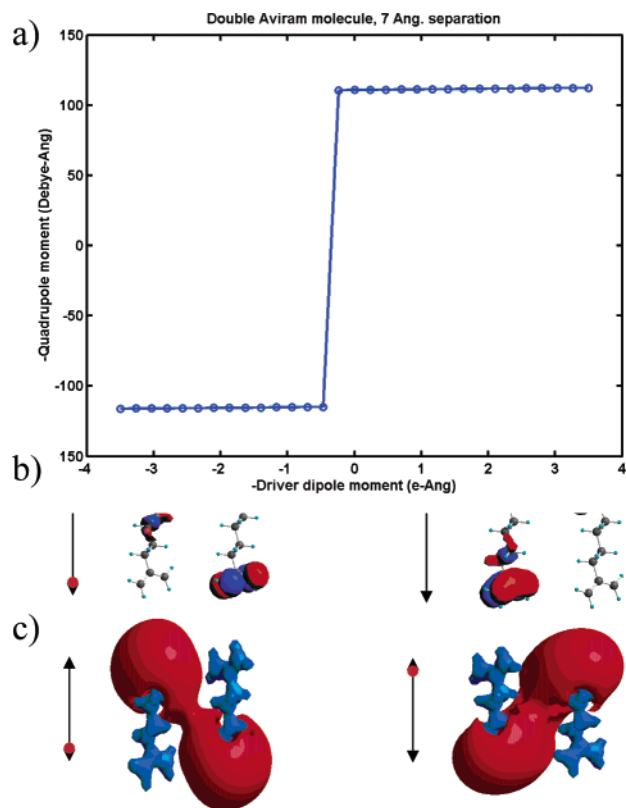


Figure 4.1. Two molecules of 1,4-diallylbutane radical cation, fixed 7 Å apart, and driven by a single positive charge that slides along the path indicated by the black arrow. The driver is at the bottom of its path at left and at the top at right. Gaussian 98 calculation using Hartree–Fock theory and the STO-3G basis set. (a) Quadrupole moment as a function of driver polarization; switching is nonlinear and strongly bistable. (b) Orbital isosurface (LUMO shown) at extremes of driver position. (c) Isopotential surface (red indicates positive charge) at extremes of driver position.

located on either allyl site. Figure 4.1 shows a setup where two of these molecules are fixed adjacent to a single positive charge (the “driver”). When the driver moves over a distance of 7 Å, it causes the positive charge in the neighboring molecule to switch from one allyl group to the other; this perturbation in turn causes the positive charge in the next molecule to switch. Note that the molecule farthest from the driver winds up with its positive charge at the same side of the molecule as the driver, showing that it responds to the electrostatic forces imposed by the intervening molecule

4.3. Issues and Needs. In diodes, it is desirable to obtain a high rectification ratio, with little leakage current, and an accessible and stable turn-on voltage. In memory devices, the issues are switching time, on/off ratio, stability, volatility, and the turn-on/off voltage. In transistors, what is the speed (related both to “effective carrier mobility,” if it can be defined) and the channel length, the current modulation (aka on–off ratio), the threshold voltage, and its stability?

The speed of switching depends on the mechanisms driving the change in the state of the molecule, giving rise to the measured change in resistance. Mechanisms based on mechanical motion, which for example are the mechanistic basis of ring motion in molecules such as rotaxanes and catenanes, are inherently slow. Solution-phase NMR measurements of ring motions in solution are ~ 500 times per second.¹⁶³ These motions may also be constrained by other molecules or interfaces in the solid state. Mechanisms based on molecular diffusion or requiring ionic diffusion should lead to microsecond switching

times typical of diffusion. The larger the molecule/ion and the longer the distances it is required to move will limit the time scale for switching. Moving protons over short distances, ~ 3 Å, has been proposed for switching and may provide the fastest obtainable switching speed for a system based on diffusion.¹⁶⁴ Reduction–oxidation and conformational molecular changes may provide the fastest (\sim picosecond) time scales for switching. If, for example, reduction–oxidation is stabilized by the presence of ions, the time scale for switching will depend on the concentration and diffusion of ions, presumably limiting switching once again to microsecond time scales. There is at present a lively debate about whether each practical molecular device must be as fast as possible (thus necessitating electronic processes for the molecular states involved in the device function) or if slower devices (involving translation or molecular conformation) are acceptable, because, in a massively parallel architecture (Teramac), redundant interconnects with a fault-tolerant algorithm¹⁶⁵ may yield an acceptably fast computer.

As discussed in section 2.3.3, intentional or unintentional incorporation of ions may dramatically change the device behavior. If ions stabilize reduction–oxidation, removing the ions may change both the time scale for switching and the voltage for switching (which may or may not still be accessible). Environmental effects (ions, stray charges within a molecular layer or at an interface) may create electric fields that shift turn-on/threshold voltages in molecular devices.

4.3.1. Intrinsic Limits to Molecular Electronics. The Bohr radius of an electron is 0.1 to 1.0 nm in “insulating” media. Because electrons will tunnel between wires spaced less than a few nm apart, “nanoelectronics” is the limit for circuits with electrons as charge carriers. Since electron tunneling cannot be avoided, we should exploit differential electron tunneling in nanoelectronics. A design for a nanotransistor that exploits this approach could connect source and drain electrodes through an oligophenylene bridge containing ferrocene as a molecular gate. The effective electron tunneling distance depends on the structure of the bridge; it is large for the aromatic unit ($1/\beta = 2.0$ to 2.5 Å) and quite small for saturated (alkane) bridges ($\beta = 0.7$ to 1.1 Å). How rapidly could such a gate switch? If the electronic coupling (and thus level broadening) is limited to the order of kT , the tunneling rate will be of the order $2\pi k_B(300 \text{ K})/h = (25 \text{ fs})^{-1}$. Such a rate would allow 1 THz gates if the circuit capacitances are sufficiently small.

The achievable density of molecular devices in a larger architecture will also be limited at the nanoscale by unavoidable electronic tunneling as it may give rise to crosstalk between discrete devices. While the field is still focused on understanding discrete molecular devices, at some point the need may arise to develop synthetic routes to insulate devices and limit crosstalk and to develop electronic schemes to take advantage of differential conductance and bistability in molecular structures.

4.3.2. Energy Dissipation in Nanostructures. Perhaps the most frequently heard objection to single-molecule electronics is “won’t the current densities roast the molecule.” The objection is based on an extrapolation of macroscale resistance to the nanoscale. This extrapolation is not valid. Once the size of a structure falls below the electron mean-free-path (several hundred Å at room temperature), normal scattering processes no longer play a role. The electron moves from one point to another (taking a semiclassical view) with a velocity given by dE/dk (of course, if there is no delocalization, $dE/dk = 0!$). In this picture there is no scattering and so there is no classical, ohmic resistance and no power dissipation. Resistance (in the

sense that current in a given field is not infinite) arises purely from a transmission coefficient through the nanostructure that is less than unity, i.e., $R = h/2e^2|T|$ (eq 2.11), a form of the well-known Landauer equation. For a metallic nanojunction where the metal atomic states in the junction are degenerate with the bulk, $|T| = 1$ and $R = 12.9 \text{ k}\Omega$. In contrast, in small alkanes, where states are far from the metallic Fermi level, $R \sim 10^9 \Omega$. This does not mean that the power dissipated in the junction is $V^2/10^9 \Omega$! Rather, only one electron in 10^5 gets through the junction. Currents of up to μA have been measured in junctions containing one or a few molecules with no long-term degradation of the junctions. The important factors are the applied bias and the presence of electroactive contamination, both of which lead to irreversible electrochemical degradation of the molecule. An intriguing question remains in the case of a nanoscale system containing redox centers. These trap or donate charge because of coupling to nuclear motions. This is clearly a more complex situation than described by the Landauer approach.

4.3.3. The Right Molecules/Materials. One may imagine an all-organic computer, with molecular electronic devices connected by, for example, a suitable organic conducting polymer “backplane”. However, at present, the lack of enough sturdy and fast molecular electronic devices suggests that for the foreseeable future, inorganic metal contacts will be used to access these devices. To the degree that such contacts remain important, there is a need for improved characterization and understanding of the thermodynamics, kinetics, and electronic properties of the contact (see section 3) and for improved chemical stability. Binding to a metal may simply result from van der Waals forces (as in Langmuir–Blodgett films) or through dative (e.g., NH_3) or covalent bonding. Despite the formation of a strong covalent bond when a thiol binds a gold substrate, the resulting thiolates on Au can be oxidized to sulfoxides with time, creating local Schottky barriers with attendant band bending. In addition, gold atoms are quite mobile, and can move within the monolayer at certain (sufficient?) potentials.¹⁵¹

At present the scientific community has reported examples of molecular “wires”, switches, and rectifiers. The yields of these devices are typically only $\sim 1\%$, and reliable assembly of molecules and deposition of electrodes is required in the near term, to gain understanding of the behavior of molecular devices, and in the long term, for practical application of molecular devices.

Most recent measurements (except for (5) above) have been for two-electrode systems. A crucial stumbling block for molecular electronics is that power gain (i.e., amplification) must be demonstrated in some device before the array of molecular electronic components is considered to be sufficient for serious assembly and circuit design. A great experimental challenge, at present under development by several laboratories simultaneously, is the construction of three- or four-metal electrodes, or points, or shards, which are within 1 to 2 nm of each other. Approaches include complicated break junctions; burning narrow interconnects by bursts of electrical power or by allowing strands of conducting polymers to grow between slightly larger gaps in metal electrodes, or using carbon nanotubes. When such electrode systems become available, then one can hope to think of bridging the gap between them by a novel single molecule whose constituents are such that power gain is obtained from such a device. Fabricating such electrodes and synthesizing the “right” molecule to direct its assembly within the gap are important challenges.

When is a contact ohmic? How does one make an ohmic contact between an inorganic metal and an organic molecule? Making contact to molecules means contacting metal electrodes without damaging the molecule; an interesting new method is the “cold gold” method.^{151,152} At one extreme, if the metal probe is too far, then one has a tunneling gap, not an ohmic contact. At the other extreme, if the metal probe is too close, then the molecules must be compressed, and the energy levels of the molecules will be greatly modified by the contact. When the metal probe is at the “right” distance, then the series resistance between the metal electrode(s) and the molecule may be at a minimum. One might use nanopositioners (piezo drives) to find empirically when the contact resistance is minimized or when the resistance is small and there is no spectroscopic evidence of damage to the molecule. Alternatively, the contact problem can be addressed chemically, by incorporating into the molecule a functional group designed to bind the metal electrode as discussed above.

4.3.4. How Much Potential Can a Monolayer Withstand? The breakdown potential of dry air is about 30 000 V per cm, or $3 \times 10^6 \text{ V/m}$. What is surprising is that potentials much larger than this are experienced by molecules in scanning tunneling microscope experiments ($1 \text{ V}/2 \text{ nm}$) = $5 \times 10^8 \text{ V/m}$. Monolayers sandwiched between electrodes 2.5 nm apart of diameter 0.2 to 0.5 μm^2 can withstand between 2 V¹⁰⁰ and even 5 V,¹⁵¹ which corresponds to a maximum of $2 \times 10^9 \text{ V/m}$. This resistance to breakdown in monolayers is remarkable, but deserves careful further study.

5. Architectures for Energy Conversion

Conversion and storage of solar energy requires efficient photon capture, charge separation and transport, and, finally, efficient utilization or storage by chemical or electrochemical means. The high surface area of nanostructures can immensely enhance light-collection efficiency. Efficiencies of catalytic sequences used for utilization and storage are enhanced by the high surface area, as well. Thus there is the expectation that nanoscale systems can advance solar photoconversion and that advances in the understanding of the relevant charge transfer—and the strongly related energy transfer—process to energy conversion will be central to this progress. As discussed in section 1, the nanostructures include molecular wires, nanoparticles, both of semiconductor and metal, nanotubes, electrodes, and the connectors that attach these objects to create larger structures. Other motifs, such as filled zeolites, aerogels, dendrites, and layered polymers, also offer enormous potential for accomplishment of useful chemical functions. Some simple assemblies are illustrated in Figure 5.1

This section addresses our current utilization and understanding of nanostructures and their complex assemblies in light harvesting (5.1), light-induced charge transport (5.2), and charge storage in advanced conductive aerogels (5.3).

5.1. Nanoscale Energy Transfer, Charge Transfer, and Energy Conversion in Molecular Assemblies. During the past 50 years, much has been learned about the factors that control energy transfer in molecular systems. The primary mechanisms for energy transfer in molecular systems are Förster dipole–dipole coupling¹⁶⁶ and Dexter exchange transfer.¹⁶⁷

More recently the focus has turned to the study of energy transfer processes in supramolecular structures consisting of covalently or noncovalently bound assemblies of two or more individual molecular chromophores (Figure 5.2).¹⁶⁸ Much of this work has been inspired by the natural photosynthetic apparatus in which a large number of individual light-absorbing chro-

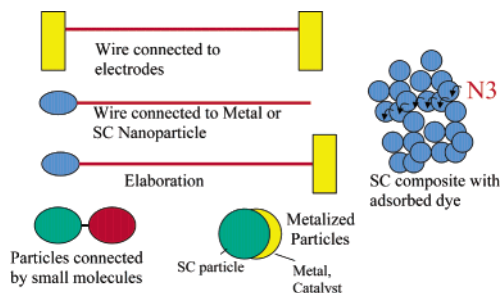


Figure 5.1. Simple assemblies of elementary nanoobjects: A wire connecting two electrodes, a wire connected to a metal or semiconductor (SC) nanoparticle, two particles connected by a molecular connector, metallized semiconductor particles, and a collection of nanoparticles held together by sintering or by van der Waals forces.

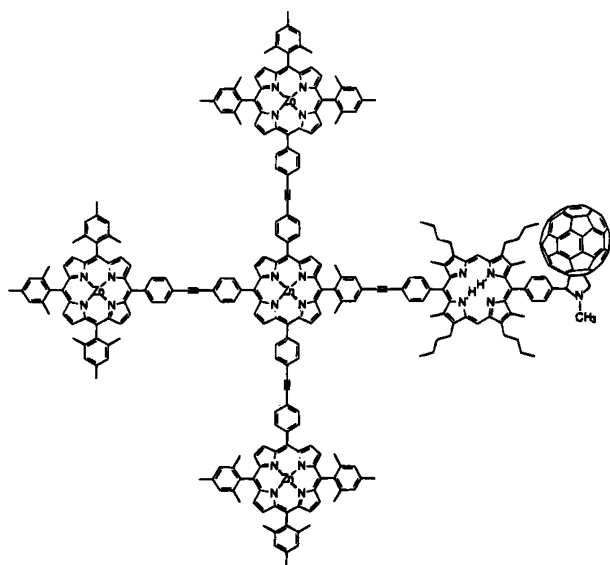


Figure 5.2. A synthetic light-harvesting array. (Reprinted with permission from *J. Am. Chem. Soc.* **1999**, *121*, 8604–8614. Copyright 1999, American Chemical Society.)

mophores that are assembled on a 10–20 nm length scale by a protein scaffold are able to efficiently harvest optical energy and transfer it to a reaction center where the optical energy is stored as electrical potential.^{169,170}

Some of the noteworthy supramolecular assemblies that mimic the light harvesting function of the natural photosynthetic apparatus consist of arrays of porphyrin-type chromophores. Early work in this area utilized assemblies of two or three porphyrins,¹⁷¹ but, more recently, examples have appeared in which structures are well-defined at the molecular level and contain as many as 20 individual porphyrin chromophores (Figure 5.3).^{172,173} These assemblies have dimensions on the 10-nm length scale, and they have been investigated using a number of optical methods to establish the mechanism and pathways for energy transport and migration among the individual chromophoric units.¹⁷⁴

Another approach to construction of supramolecular light harvesting arrays is the synthesis of dendrimers containing many individual chromophores that efficiently transfer their energy to a single low-energy chromophore.^{175–177} The spherical shape of the dendrimers is believed to be optimal for energy transfer; however, the trap site is usually in the core, which may limit its accessibility to engage in chemical processes. Polymers containing pendant chromophores can also serve as light-harvesting arrays that operate with reasonable efficiency.^{178–180}

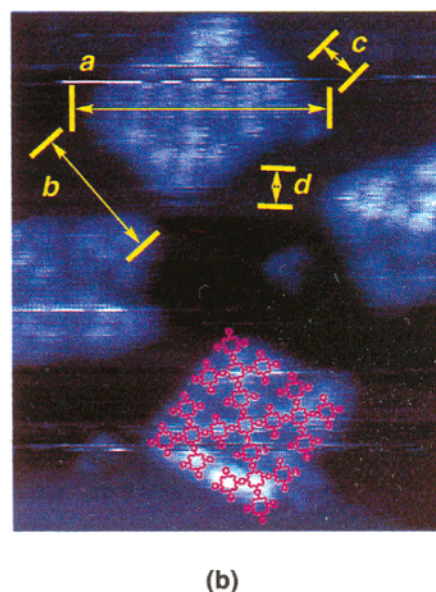
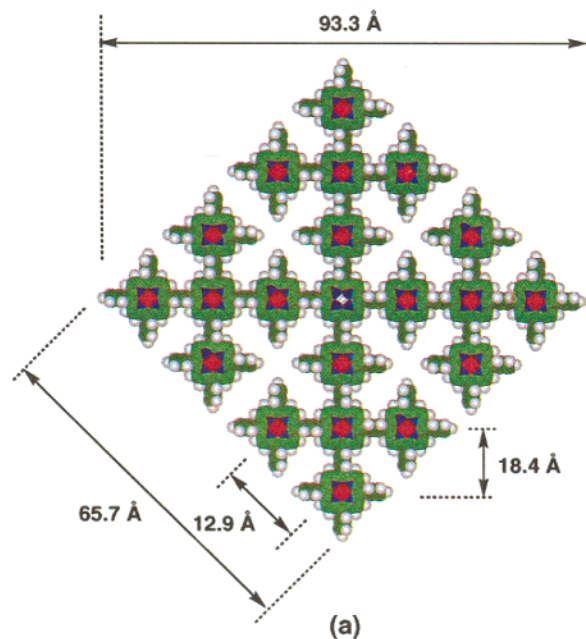


Figure 5.3. Supramolecular assembly consisting of 21 tetraporphyrin units. (a) Space-filling model of molecule. (b) High-resolution STM image of molecules on a Cu(111) surface. (Reprinted from *Chem. Lett.* **1999**, 1193–1194.)

Self-assembly provides another route into nanoscale assemblies that can carry out the energy transfer and conversion. A number of recent examples consist of chromophoric units self-assembled by hydrogen-bond formation or electrostatic and/or solvophobic interactions (Figure 5.4).^{176,181–185}

Conjugated polymers can very efficiently transfer energy over distances as large as 50–100 nm. For example, near-field optical scanning microscopy has been used to demonstrate that singlet excitons can diffuse over length scales as large as 50 nm in thin films consisting of MEH–PPV.¹⁸⁶ A related phenomenon is “amplified quenching” of conjugated polymers.^{187–189} In this process a single electron or energy acceptor quenches the singlet exciton located on an entire conjugated polymer chain comprising more than 1000 individual monomer repeat units. The key step in this process is believed to be ultrafast exciton diffusion along the polymer chain.^{188,189} Although it is possible that the

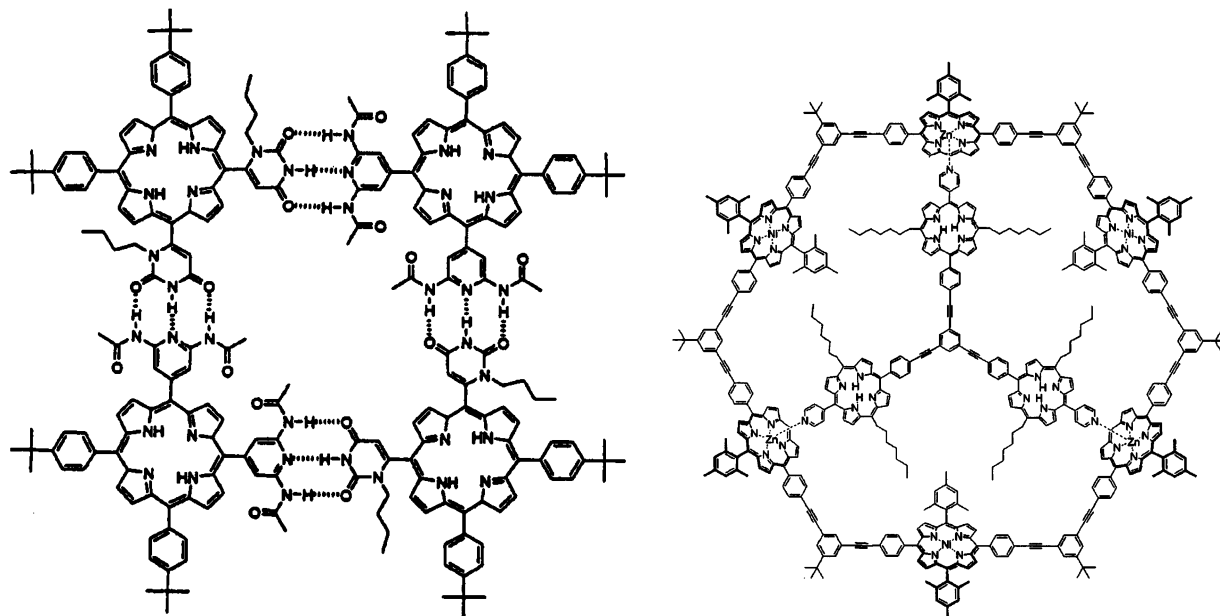


Figure 5.4. Self-assembled light harvesting arrays. (Reprinted with permission from *J. Org. Chem.* **2001**, *66*, 6513–6522 and *J. Org. Chem.* **2001**, *66*, 4973–4988. Copyright 2001, American Chemical Society.)

mechanism involves one or more Förster transfer steps, the details of the process have yet to be worked out.

The process of exciton diffusion in conjugated polymers is closely related to the mechanism of exciton diffusion in dye aggregates, a phenomenon that has been known for many years because of the importance of dye aggregates to silver halide photography.¹⁹⁰ Kuhn and co-workers demonstrated long-range exciton diffusion in J-aggregates formed in Langmuir–Blodgett films containing cyanine dyes.¹⁹¹ Very recently, Whitten and co-workers demonstrated exciton diffusion over 50 nm in J-aggregates formed in polymers containing pendant cyanine dyes.¹⁹² The diffusion lengths are even greater (up to 200 nm) when the dye aggregates are templated on nanoscale colloidal clay particles. Another interesting example of energy transport and transduction over nm length scale is in assemblies of dyes loaded into nanometer-sized zeolite particles. The dyes are constrained so they are unable to form aggregates, yet efficient exciton diffusion occurs over > 300 nm.¹⁹³

Oligomers or polymers that may serve as molecular wires have been created and investigated for use in molecular electronics.^{5,8,12,45,117,194–199} Such wires could also serve as aids to efficient solar energy conversion and storage. Good nanoscale molecular wires must be excellent charge carriers, even at very long lengths, while satisfying the somewhat contradictory requirement that their energetics not change drastically with length. They should be reasonably immune to the effects of stray charges or other impurities; a requirement that will place more stringent demands on molecular design as the wires become longer. For use in energy production they should have energy levels appropriate to accept charges from viable donors, which may be molecules, assemblies of molecules, or semiconductors, or nanoparticles in their ground or excited states. They must be reasonably durable and readily produced. The durability requirement is a substantial hurdle for electronics applications, where, if current devices are used, substantial currents must be maintained for long periods of time. For transferring charges created by sunlight, currents are likely to be low in each wire. It is therefore possible to imagine that molecular wires, first developed for electronics, could find as much or more use in energy conversion.

Low solar fluxes could be imagined to imply little need for very fast charge transport. However fast transport is desirable in order to prevent charge recombination and to prevent high-energy charges from reacting with oxygen or other impurities. There are few measurements of the time scales for charge transport in molecular wires, so this is a research need. One of the major challenges of the next few decades will be to develop tools and methods to extrapolate the fundamental processes of molecular electron and energy transfer into supramolecular assemblies having dimensions >100 nm. An approach to fabricating materials that can transfer and transduce energy on length scales of 100 nm or longer will be to use supramolecular building blocks such as those described above to create nanoscale assemblies. One example of this approach is the fabrication of layer-by-layer films consisting of conjugated polyelectrolytes.²⁰⁰ With this approach it is possible to fabricate films consisting of many individual bilayers. Access to variable band gap conjugated polyelectrolytes will allow the fabrication of films having thickness of >100 nm that contain an energy gradient to drive the excitation to a selected film interface. Nanostructured layered materials of this type can also be fabricated by spin-coating or Langmuir–Blodgett deposition techniques.^{201,202}

One can also envision the design of molecular wires that can rapidly direct energy (or charge) in one direction. For example, construction of a di- or tri-block conjugated polymer consisting of blocks of variable band gap could be used to separate charge at the junction between the blocks (Figure 5.5, top) or to channel excitation energy in one direction (Figure 5.5, bottom). Some examples of block conjugated polymers are already known.^{203–206} Another advantage of using block copolymers is their propensity to self-organize into well-defined nanoscale phase-segregated morphologies in the solid state.^{207,208} Such materials can be used to self-assemble nanoscale composites that contain light harvesting polymers and metal or semiconductor particles which add functionality such as catalysis.^{209,210}

5.2. Nanostructured Photovoltaic Cells. Photoelectrochemical cells based on dye-sensitized nanocrystalline TiO₂ have been known for over a decade.^{211,212} Because of the very high surface area of the nanocrystalline support, relatively thin films of the

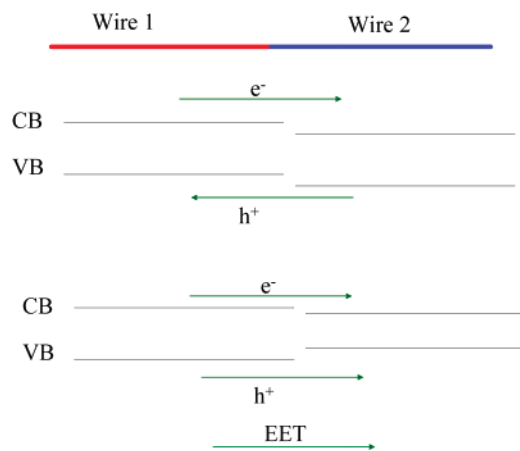


Figure 5.5. Schematic diagram of a diblock copolymer comprising conjugated polymer blocks of different band gap. CB and VB represent, respectively, the energy levels of the conduction and valence bands of the polymers. Arrows indicate the expected drift of photogenerated electrons (e^-) and holes (h^+). EET = electronic energy transfer.

dye sensitizer effectively harvest most of the incident light at wavelengths absorbed by the dyes. Much effort has been expended to optimize the efficiency of these cells and to understand the fundamental mechanisms for their operation.²¹³ Solar-to-electrical energy conversion efficiencies approaching 11% have been achieved. While there has been considerable enthusiasm for this technology, more work is required to increase the efficiency of the dye-sensitized cells before widespread application becomes economical.

There has also been a substantial increase in the efficiency of photovoltaic cells based on organic materials.^{214,215} In most cases, enhanced efficiencies have been achieved by creating nanostructured heterojunctions, which result in interpenetration of the donor and acceptor materials.^{216,217} The nanoscale phase-segregated morphology overcomes a principal problem with the earlier devices based on “flat” heterojunctions, i.e., the large distance that excitons must diffuse to arrive at the donor–acceptor junction. It is likely that further increases in the efficiency of organic photovoltaics will arise from the development of nanostructured materials that control the diffusion of excitons and charge carriers within the active material.

5.2.1. Inorganic–Organic Hybrid Structures for Light Energy Conversion and Storage. Nanoscale materials are important in developing a new generation of electronic and optical nanodevices.^{75,218–222} Of particular interest are the semiconductor and noble metal nanoclusters which display size-dependent optical, electronic, and chemical properties (see for example, refs 18 and 223–231). It is a challenge for chemists to exploit these unique properties in systems that carry out photochemical conversion and storage of light energy. Despite the breakthrough represented by demonstration that nanostructured semiconductor-based photochemical solar cells can operate with power conversion efficiencies of 10–11%,²¹³ barriers remain toward improving the overall photoconversion efficiency. New strategies that exploit the architecture of metal–fluorophore nanoassemblies, as well as metal–semiconductor semiconductor–semiconductor composite structures, have to be designed to achieve efficient charge separation and transport of charge carriers. The key to creation of these hybrid structures is to understand the chemistry at a fundamental level. Elucidation of the excited-state interactions with semiconductor and metal nanoparticles will continue to be a major research topic in the coming years.

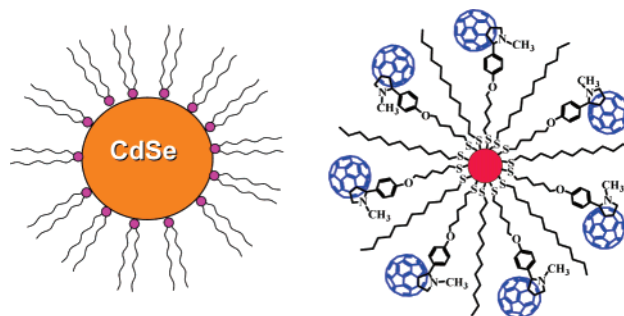
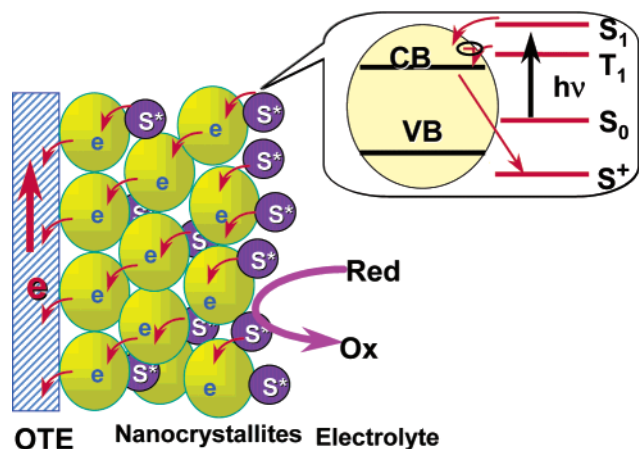


Figure 5.6. Examples of organic-capped semiconductor and metal nanoparticles.

5.2.2. Interaction of Semiconductor and Metal Nanoparticles with Organic Molecules. Assembling nanoparticles as spatially well-defined arrays is crucial in retaining the electronic properties of individual particles. While it is beneficial to obtain robust architectures for light-harvesting applications, close packing of metal and semiconductor nanoparticles will cause aggregation effects. For example, a red shift in the plasmon absorption is seen when metal nanoparticles undergo aggregation.^{232–235} It should be possible to maintain the spatial distance in 3-D assemblies by binding these nanoparticles with suitable organic molecules (e.g., alkane thiols). The distance separating the adjacent nanoparticles would then be determined by the length of the alkyl chain. If, on the other hand, photoactive molecules are chemically bound to the semiconductor or metal surface via a functional end group such as $-SH$ or $-NR_2$, it can serve the dual purpose of spatial distribution as well as absorption of incident photons. A layer-by-layer assembly of functionalized nanoparticles and redox couples can also provide the desired architecture to obtain a 3-D array on an electrode surface. Significant efforts have been made to synthesize quantum dots of semiconductor nanoparticles with narrow size distributions. Steigerwald et al.^{236,237} synthesized nanometer sized CdSe clusters using organometallic reagents in inverse micellar solution followed by chemical modification of the surface of the clusters. Later the trioctylphosphine oxide (TOPO) method²³⁸ was developed to synthesize size-controlled CdSe nanocrystallites of the highest monodispersity (standard deviation less than 5%). Capping CdSe colloids formed at high temperature (300 °C) with TOPO stabilizes the particles against further growth. Capping with a large band gap semiconductor such as ZnS enhances the radiative recombination of photogenerated charge carriers. Although this method has been widely adopted for synthesis of quantum dots having narrow absorption and emission bands in the entire visible range, a simplified method of preparing such colloids under ambient conditions remains to be developed. The organic capping material usually controls the nature of surface states and hence excited-state dynamics. For particles of less than 2 nm, the majority of the atoms are at the surface and so are in contact with the adjacent organic layer.

Although most published reports focus on the synthesis of organic capped gold nanoparticles, limited effort has been made to understand the mode of interaction of metal nanoparticles with organic capping agents and solvents.²³⁹ Nuclear magnetic resonance (NMR)^{240–244} and surface enhanced Raman scattering (SERS),^{245,246} as well as the spectroscopies described in section 3, are useful techniques to probe the surface-induced structural distortion of the molecular geometry and nanoparticle–molecule bonding sites and binding strength. Because of the photocatalytic activity of semiconductor colloids, one has to look into the photostability issues of capping agents.²⁴⁷ A



OTE Nanocrystallites Electrolyte
Figure 5.7. Dye sensitization of semiconductor nanostructures is the primary photochemical event in a photochemical solar cell.

recent study has pointed out the instability of hydrophilic thiol-capped CdSe colloids.²⁴⁸

5.2.3. Photoinduced Charge Separation in Semiconductor–Sensitizer and Metal Particle–Sensitizer Nanoassemblies. The possibility of tailoring semiconductor or metal nanoparticle surfaces with organic molecules has generated overwhelming interest in the design of light harvesting nanoassemblies. Moreover, metal nanoparticles are excellent building blocks for inorganic–organic hybrid structures that can be tailored to carry out multifunctional tasks – from light energy harvesting to charge storage and delivery.

The sensitizing dyes bound to semiconductor nanoparticles participate in interfacial charge transfer under photoexcitation (Figure 5.7). The efficiency of charge separation can be greatly improved by employing surface modifiers, composite systems, and sacrificial donors/acceptors. One collective way to utilize these photoinduced charges in semiconductor nanoclusters is to assemble them on a conducting surface in the form of thin films. The photogenerated charges in these semiconductor nanoclusters can then be utilized collectively to generate photocurrent or carry out selective redox processes.

The scope of ultrafast transient absorption spectroscopy for probing excited-state interactions on semiconductor surfaces needs to be extended to the single-particle level so that we can gain a better understanding of the photosensitization phenomenon at the single particle level. The heterogeneity observed in charge-transfer rate constants needs to be understood based on morphology, particle dispersity, and electronic coupling between the sensitizing dye and the semiconductor.

Earlier studies have shown that photoactive molecules bound to a bulk metal surface are inactive when exposed to light.^{249–252} Both energy-transfer and electron-transfer processes are considered to be the major deactivation pathways for the excited fluorophore on metal surfaces.^{253,254} Although similar quenching of excited states in nanoparticle systems has been noted in a few studies, no major effort has yet been made to elucidate the excited-state deactivation processes of a surface-bound fluorophore in nanostructures. The nature of the charge-transfer interaction of fluorophores with the gold surface dictates the pathways via which the excited state deactivates.^{239,255–258} Exploring ways to utilize these photoactive metal–sensitizer nanoassemblies for light energy conversion offers a challenge for the coming years.

As for molecular electronics applications, photocatalytic processes such as oxidation of the thiol ligands on the surface of nanoparticles and/or passivation of the nanoparticles them-

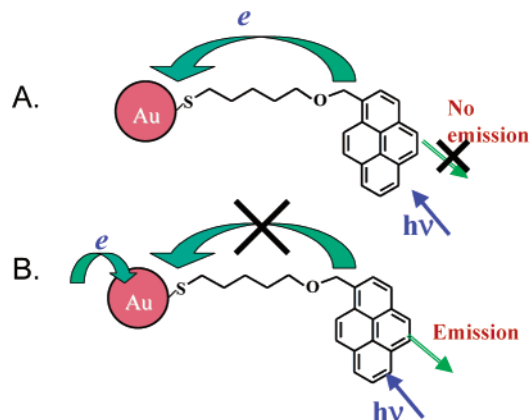


Figure 5.8. Control of charging of gold nanoparticle will enable modulation of fluorophore properties.

selves need to be understood fully before implementing them for long-term applications. Gold nanoparticles capped with organic molecules are able to retain the charge when subjected to an electric field.^{75,259} Control of gold nanoparticle charging thus becomes an important factor if one is interested in modulating the interaction between the gold nanocore and a surface-bound fluorophore (Figure 5.8). Understanding the properties of a surface-bound molecule can provide valuable information concerning the charge transfer interactions as well as the microenvironment near the metal nanocore. If indeed the gold particles act as electron acceptors, it should be possible to modulate the electron transfer quenching of the excited fluorophore by charging the gold nanoparticle at an electrode surface. While the collective charging effects in organic-capped gold nanoparticles can be monitored from the shift of plasmon band to lower energies,²⁶⁰ surface bound fluorophores can provide useful information on the mechanism and kinetics of the charge-transfer events. Furthermore, the newly developed electronic force microscopy (EFM) could be used to monitor charging effects on individual particles.²⁶¹

5.2.4. Semiconductor–Metal Composites. The functional properties of nanomaterials can be greatly improved by capping the semiconductor or metal nanocluster with another layer of compatible material. Such core–shell geometry not only improves the stability of the nanoparticles but also expands the scope of composite nanoclusters in a wide array of applications such as luminescent displays, microelectronics, photochemical solar cells, sensors, and memory devices.^{262–265} Some examples of core–shell type nanomaterials include semiconductor–semiconductor,^{266–270} semiconductor–metal,²⁷¹ metal–semiconductor,^{272–274} metal–metal,^{275–278} and metal–metal oxide^{252,279–281} systems.

One of the major goals behind designing semiconductor–metal composite nanoparticles is to improve the charge rectification and to improve the interfacial charge-transfer kinetics (Figure 5.9). The storing and shuttling of electrons by gold nanoparticles has been demonstrated by monitoring molecule-like charging effects^{75,259} and Fermi-level equilibration with semiconductor nanostructures.^{282–284} A thermally activated electron hopping from one gold particle to another has been proposed as a possible way of conducting charge through nanostructured gold films.²⁸⁵ The mechanism of charge transport at the semiconductor–metal interface as well as charge rectification still remains an intriguing issue and needs to be explored further. Probing the charging effects in composite particles using single-molecule spectroscopy techniques and/or EFM techniques will provide a better understanding of the interfacial events.

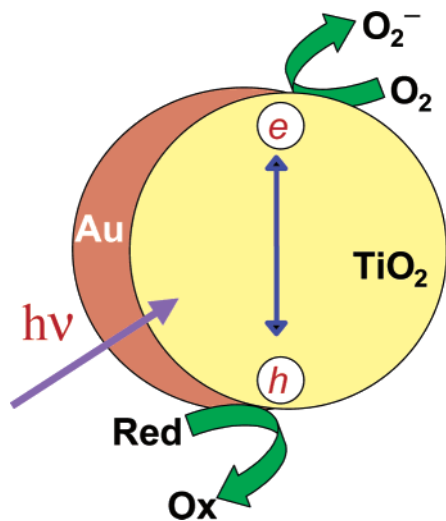


Figure 5.9. Interfacial charge-transfer processes in a metal–semiconductor nanoparticle.

Semiconductor–metal nanocomposite particles have been found useful in improving the efficiency of photocatalytic and photoelectrochemical conversion of light energy (see, for example, ref 284 and references therein). Photogenerated holes in semiconductor materials such as TiO_2 are strong oxidants and are capable of oxidizing metals such as Au at the semiconductor interface. Such oxidation events in composite films will not only disrupt the TiO_2 –metal interface but will also create new electron–hole recombination centers. The contribution of these recombination centers is likely to be counterproductive for photoelectrochemical and photocatalytic operation. Questions remain regarding the identity of oxidized metal ions and their role in altering the energetics of the semiconductor. EXAFS studies can provide insight into the neighboring atoms as well as the oxidation state of the intercalated metal ions. Whereas modification of the semiconductor surface with metal nanoparticles promotes interfacial charge transfer, it is important to tackle the problems associated with metal oxidation at the semiconductor–metal interface.

5.2.5. Light Harvesting Nanoassemblies. Exploring ways to improve photoinduced charge separation in donor–acceptor type dyads and triads by binding them to metal nanostructures and/or semiconductor composites will aid in mimicking artificial photosynthesis with improved efficiency. Fundamental understanding of the dynamics and kinetics of the electron-transfer process will allow us to optimize design strategies for such units. The basic role of the gold nanoparticle will be to promote charge separation and shuttle photogenerated electrons from a fluorophore or from a donor–acceptor dyad assembly to a collecting surface. Based on a similar concept, efforts have recently been made to fabricate devices using a fluorescein photoreceptor on an Au/ TiO_2 /Ti multilayer structure.²⁸⁶

By anchoring a redox moiety along with the fluorophore molecule, it should be possible to achieve photoinduced charge separation in these molecular–metal nanoparticle assemblies (Figure 5.10). Anchoring a donor–acceptor dyad (e.g., C_{60} –aniline dyad or $\text{Ru}(\text{bpy})_3^{2+}$ –viologen dyad with a –SH functional group) on the gold surface can further advance the concept of achieving charge separation in these photoactive nanoassemblies. The fullerene–aniline dyad in Figure 5.10 illustrates the principle of this concept. This dyad has been shown to undergo efficient charge separation and to produce photocurrent in a photoelectrochemical cell.²⁸⁷ By choosing a proper linker group it should be possible to systematically

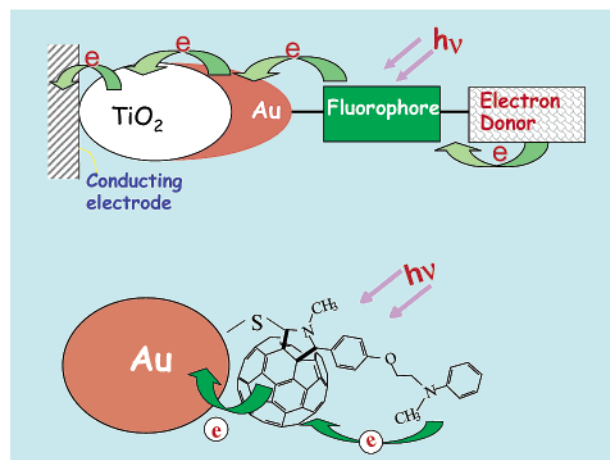


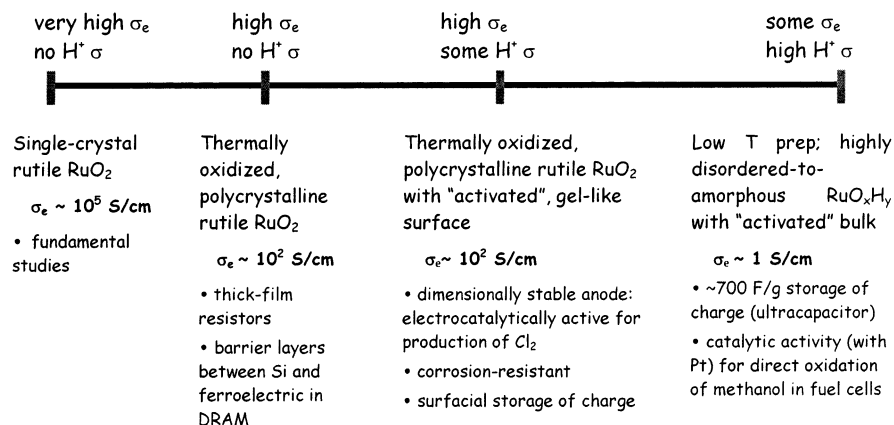
Figure 5.10. Assembling nanoparticles and molecules for light harvesting applications. Au–fullerene–aniline dyad assembly (bottom) illustrates the principle of photoinduced electron transfer and collection of electrons at gold nanocore.

investigate the distance dependent electron/energy transfer processes between the metal nanoparticle and fluorophore.

5.3. Designing Three-Dimensional Pore–Solid Architectures as Advanced Electrochemical Materials for Charge Storage and Energy Conversion. Disordered and amorphous materials are critical components in numerous technologies of societal and military importance. Examples of such materials, in which charge transport is required for the technological end use, include amorphous semiconductors (for photovoltaics or electrophotographic imaging); superconducting cuprates and magnetoresistive manganates whose properties derive from localized defects (for motors and ferroelectrics, respectively); and insertion solids such as carbon and metal oxides or –hydrides (for electrochemical power storage).²⁸⁸ In particular, it has recently been recognized that nanoscale, poorly crystalline, charge-insertion solids function as high-performance materials in power sources²⁸⁹ such as lithium-ion batteries,^{290–295} direct methanol fuel cells (DMFCs),²⁹⁶ and reformate-fed fuel cells.^{297–299} The difficulty of analytical and physicochemical characterization of disordered-to-amorphous materials is further compounded when the materials and phases are nanoscopic.

5.3.1. Importance of Irregular/Nonperiodic Architectures. As an example of the pervasiveness of the disordered realm, surfaces are actually nanoscale, often highly disordered, domains that differ from the underlying bulk and dictate many of the technologically most relevant catalytic, optical, or electrical properties of the solid. In that the electrified interface mediates the properties and performance of all electrochemical power sources, understanding the nature of the surface, dependently and independently of bulk properties, has been a long-pursued goal of electrochemical surface science.³⁰⁰ Because our experimental bias lies toward synthesizing and characterizing ordered materials, the physical and chemical nature of the most technologically relevant states are often poorly understood, especially when they are present only at a surface, under as-used conditions, or as nanoscale nonorder amidst ordered bulk.^{288,301}

Conventional X-ray diffraction, and other traditional techniques used to determine the structure of materials, may be the place to start when characterizing any new material, but it is not the place to finish when working with charge-insertion nanomaterials of interest in batteries, supercapacitors, ultracapacitors, electrochromics, photovoltaics, fuel cells, and electrocatalysis. Even with averaging spectroscopic techniques,

SCHEME 1: Ruthenium Dioxide—An Example of the Spectrum of Properties for One Metal Oxide as Disorder Creeps into Order

which are thought to provide reliable information on nanomaterials because such materials and objects have a large surface-to-volume ratio (a 2-nm Au particle has 63% of its atoms on the surface), evidence is accumulating that interior vs. interface/surface still matters for nanomaterials.^{302–304}

As an example of the need to understand heterogeneity and disorder even in nanometer-scale solids, Scheme 1 illustrates a spectrum of properties for RuO_2 as disorder creeps into order. Single-crystal RuO_2 is a metallic conductor with a conductivity approaching 10^5 S/cm.³⁰⁵ The anhydrous, polycrystalline form retains good electronic conductivity ($\sim 10^2$ S/cm) and finds use in thick-film resistors and as thin-film barrier layers to prevent oxygen diffusion between silicon and the ferroelectric oxide in DRAM capacitors.^{306,307} When the surface of RuO_2 polycrystalline films is made defective and becomes hydrous, the electronic properties remain dominated by the polycrystalline bulk, but the surface becomes catalytically active and can store electron and proton charge in the damaged surface layer.³⁰⁸ Low temperature, sol-gel preparations produce bulk, highly disordered hydrous ruthenium oxide ($RuO_2 \cdot xH_2O$ or RuO_xH_y), which stores electron and proton charge as a (nonlinear) function of the amount of structural water; an optimal storage of 720 F/g (F, capacitance) occurs for $RuO_2 \cdot 0.5 H_2O$ (high-surface-area carbon supercapacitors store < 100 F/g³⁰⁹). When platinized, RuO_xH_y has recently been shown to be a more active catalytic state for direct methanol oxidation than the current best DMFC catalyst PtRu bimetallic alloy.^{296,310}

As Scheme 1 indicates, when charge transport in a metal oxide is predominantly electronic (i.e., the charge carrier is an electron) rather than electrical in nature (i.e., mixed electron plus ion or ion-only transport), the critical structure-property predictor is crystalline structure—and the absence of disorder. For RuO_2 , catalytic and charge/energy storage properties are enhanced when proton conductivity arises and the physicochemical disorder at the surface or in the bulk increases. Metallic conductivity in hydrous ruthenium oxide persists even when long-range order, as determined by conventional X-ray diffraction, is absent (even to compositions of $RuO_2 \cdot xH_2O$, where $x \geq 2$). When high-surface area $RuO_2 \cdot \sim 2H_2O$ (> 50 m²/g) is dehydrated by heating in air, diffraction lines characteristic of the rutile habit only appear once the mole fraction of H_2O drops to $x \sim 0.3$, at which point the charge-storage capacity of the solid drops from 720 F/g ($x = 0.5$) to 530 F/g.³¹¹

The local structure of $RuO_2 \cdot xH_2O$, as determined by EXAFS (extended X-ray absorption fine structure), indicates that the bond distances in the RuO_6 octahedra of $RuO_2 \cdot \sim 2H_2O$ are highly distorted from those that characterize the rutile structure

(see Figure 5.11a).³¹² But EXAFS is an averaging structural technique, which can mask the true nature of this and other charge-transport materials, even on the nanoscale. When a medium-range structural analysis is performed on this family of materials, using atomic-pair density functional analysis of high energy X-ray diffraction patterns, the reason for retention of metallic conductivity (even in $RuO_2 \cdot \sim 2H_2O$) becomes apparent: nanocrystalline RuO_2 persists at a volume fraction sufficient for a percolation path for electrons.^{313,314} In essence, $RuO_2 \cdot xH_2O$ innately forms a bifunctional nanocomposite (Figure 5.11b) in which the types of carriers that transport charge are determined by the composition of the nanocomposite: an electron nanocrystalline wire (which becomes the majority volume fraction as $RuO_2 \cdot xH_2O$ is dehydrated) is always present, while protons are transported only in the disordered hydrous phase. With the structure-property insight made possible by determining the medium-range structure of $RuO_2 \cdot xH_2O$, the nature of mixed conduction in this technologically important charge-insertion oxide, and perhaps other charge-insertion oxides and materials, offers a new design strategy to optimize the properties of materials that are functionally, physically, and chemically heterogeneous, rather than compositionally and structurally uniform.

Determining medium-range structure is critical to understanding properties of disordered materials, disordered components within ordered materials, and disordered interfaces, but the current state-of-the-art requires intensive instrumentation: (1) variable coherence or fluctuation microscopy;^{315,316} (2) pulsed, inelastic, wide or small angle, anomalous diffraction and scattering techniques that use X-ray or neutron sources;^{317–320} and (3) high-field magnetic resonance spectroscopy.^{318,321} Pragmatic drawbacks to these approaches as routine structure determinants (unlike the manner in which conventional XRD is widely available and routine) include the likely prerequisite of a regional instrumentation facility; high-energy (> 20 keV synchrotron-derived) X-rays; nonthermal neutrons; high-voltage electron microscopes or high-field resonance spectrometers; the amount or form of sample necessary for the analysis (grams worth of nanoparticles for some of the scattering and diffraction approaches; transmissive films or powders for electron microscopy); high vacuum for the microscopy approaches (which may not serve to establish the innate nature of the nanomaterial); and the difficulty of data analysis because the structural assignments are coupled to intricate modeling.

If disorder or amorphousness is a desired state for a functional material (or phase within it) in applications requiring charge transport, the challenge then becomes how to maintain the

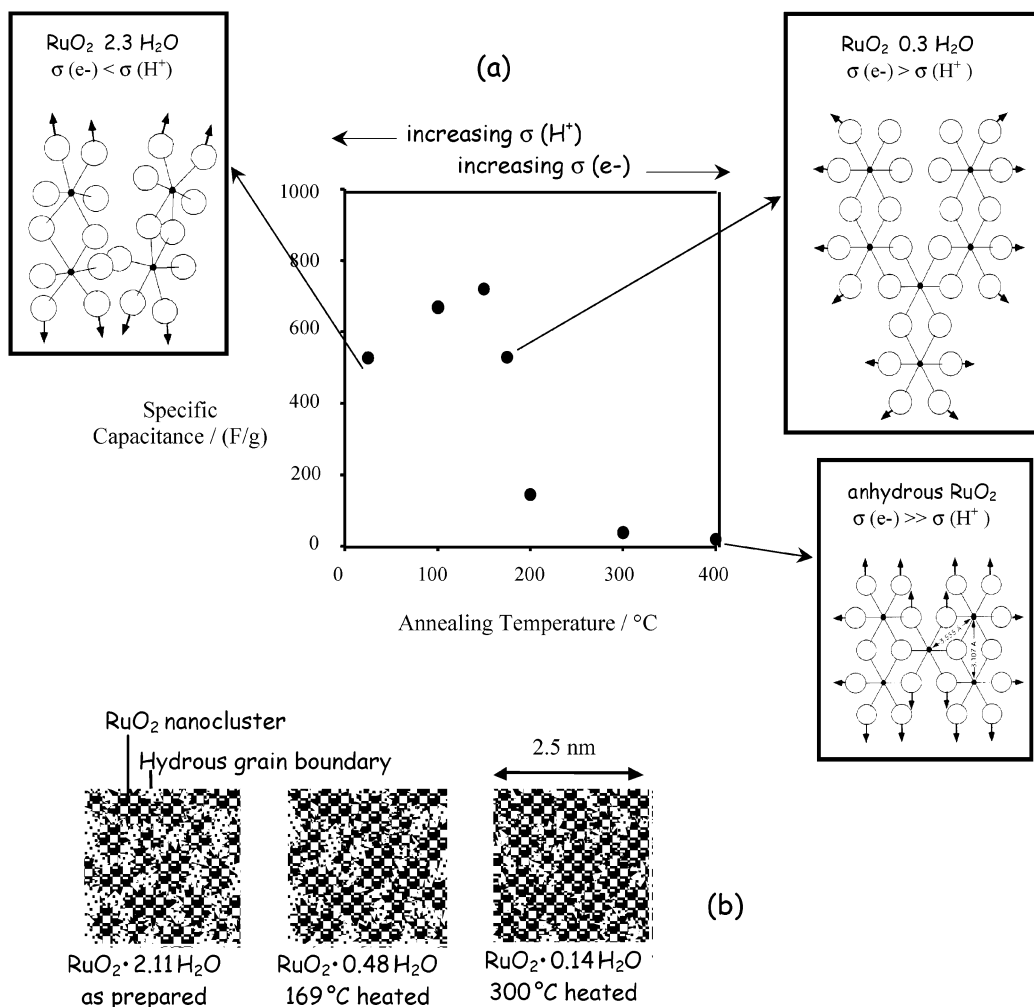


Figure 5.11. Structure and charge-transport properties of high-surface-area RuO₂ and the magnitude of charge stored in the oxide (pseudocapacitance) are all correlated, but the structure modeled for RuO₂·xH₂O once long-range order is lost depends on whether the spectroscopy is sensitive to averaged local structure (a) or medium-range structure (b).

desired local structure in the face of thermodynamic forces inherent to the application. In technologies dependent on charge transport, such driving forces would include the operating temperatures of a fuel cell; electron-volts (eV) of stored (and cycled) energy in a battery; and harvesting several eV of photonic energy in a solar cell. Conversely, the functional material may exhibit greater performance tolerance under operating conditions because highly disordered materials have a manifold of physically possible but energetically similar structures, rather than a unique structure.³²²

5.3.2. Importance of Nothing in Nanoarchitectures. Nothing—free volume—is important in many charge-transfer situations because reacting species or solvating molecules or mobile ions (or all three) must be transported to and from the reaction site, whether that site is another molecule or an electrified interface or a fabricated nanoscopic feature. As the rules of charge transport on the nanoscale are explored and discerned, optimized charge-transport performance on the nanoscale will be realized by fabricating supramolecular hierarchies, nanostructured materials, or nanoarchitectures for specific applications. A case is being made that the performance and rate of electrochemical processes improve when the “nothing” (i.e., porosity) is incorporated at the design stage in order to integrate effective paths for mass transport to (and away from) the nanostructured electroactive material.^{295,323,324} Examples of such preplanned pore—solid architectural design of electrochemical materials

include membrane-templated materials,³²⁵ aerogels,^{290,295} and lyotropically templated metals and metal oxides.³²⁶ Schematic representations of these architectures, which contain nanostructured solid and 2-, 3-, or 1-dimensional nanostructured porosity, respectively, are shown in Figure 5.12.

When disorder and nanoarchitecture intersect, recent literature indicates that charge-insertion stoichiometries, rates of charge—discharge, and electrochromic efficiencies are greater than those obtained for the crystalline, dense materials.³²⁷ The Li-to-V₂O₅ stoichiometry increases to >4 for sol—gel-derived V₂O₅·xH₂O, as processed to yield minimal collapse of the pore network (thereby forming an aerogel or ambigel), while dense, polycrystalline V₂O₅ stores at most one Li per V₂O₅.^{291,292} The mechanism(s) by which the ultraporous V₂O₅·xH₂O nanoarchitectures store the extra charge are under discussion,^{290,295} but the number density and nature of the defects may play a critical role in the increased charge storage available with V₂O₅ aerogels.

Recent evidence supports the role of lattice defects on Li-ion capacity in even micrometer-sized crystallites of V₂O₅. Deliberate atmosphere/temperature treatments to induce anion defects lowered the Li ion capacity (relative to the as-received V₂O₅ powder), while treatment to induce proton-stabilized cation defects increased the Li-ion capacity by 23%.³²⁸ Changes in the long-range order of either the anion-defective or the proton-stabilized, cation-defective V₂O₅ were not apparent by conven-

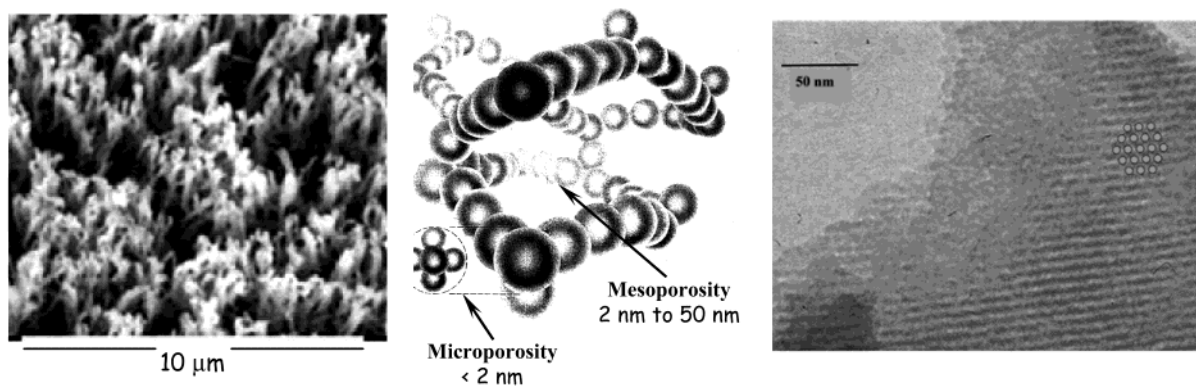


Figure 5.12. Representations of three types of pore–solid architectures providing improved electron turnover (charge–discharge rates in batteries or moles of fuels oxidized per gram of electrocatalyst in fuel-cell electrodes). Left-to-right: membrane-templated lithium-ion insertion electrodes [adapted from <http://www.chem.ufl.edu/~crmartin/>]; metal oxide aerogels or electron-wired composite aerogels [adapted from ref 295]; and lyotropically templated porous metals [Ni-coated silica; adapted from ref 326].

tional XRD;³²⁸ medium-range structural analysis should offer some insight into these systems as well. Approaches to nanomaterials that invoke soft chemistry, control of disorder, and deliberate design of pore–solid architectures offer exciting new ways to improve the performance of charge-transporting materials of technological importance. Along the way, new insights into charge transfer on the nanoscale are inevitable.

As the examples above indicate, the physicochemical database and intuition that we bring to the study of charge-transporting nanomaterials, from our historical understanding of macroscopic (or ordered or homogeneous) materials, often needs realignment on the nanometer scale. Recent computational and calorimetric studies of nanoscale oxides and oxyhydroxides indicate that energy differences between polymorphs are small on the nanoscale and that a polymorph or phase transition characteristic on the macroscale is not necessarily the dominant form or process on the nanoscale.^{329–331} Expecting quantum dots or nanowires to retain the stability inherent to the constituent compounds or metal (even noble metals) can thwart the effort invested to fabricate such nanostructured materials. Practical stability usually requires environmental “hardening” (such as using capping ligands or passive layers) to avoid surface chemistry dominated by reactions with water or oxygen that prove deleterious to the desired properties of the nanostructured material. When stability in air and water is necessary for charge transport, wiring a nanoarchitecture with an electron- or mixed conducting metal oxide provides one means to do so, as seen for a silica aerogel internally wired with 4-nm-wide laths of crystalline RuO₂; this 3-D nanowire provides electronic conductivity, even in water, and without sacrificing internal surface area or porosity.³³²

The following areas will need to make advances singly and in concert to improve our understanding and optimized use of disordered materials: (1) computational and combinatorial exploration with respect to how disordered chemical composition and physical structure may be stabilized (or pinned); (2) soft, low-temperature chemical approaches (*chimie douce*) that synthesize disorder to match (or prod) theory and modeling; and (3) greater imagination in how our experimental tools are used to characterize partial disorder to total amorphousness in the solid state. An honored philosophy of glass science (and glass is perhaps the ultimate in technologically important disordered materials) states that to stabilize a composition chemically, add more ingredients.³³² With that philosophy in mind, the need is apparent for a combinatorial/computational approach in order to direct the choice of compositional phase

space to explore as new nanomaterials are designed and synthesized and new nanoarchitectures are fabricated.

6. Summary and General Needs

The breadth of assemblies of nanosized objects that have been and can be created is remarkable and their potential impact for basic science and for applications is very great. There will be needs, and therefore challenges. Prominent will be connections and structure. For many of the assemblies discussed here, chemical and physical connectors are needed to guide objects into alignment and then hold them together. Some connectors, like the gold–thiol bond, are widely used yet still far from well understood. Many other connectors are needed but not yet invented and are therefore wholly unknown. Research into connectors will be important and essential.

Nanoscience will also demand new developments in techniques for determination of structure. A strength of nanostructures is their capacity for elaboration and complexity, but a consequence is the need for new way to characterize them. The challenges are very great when disorder is intentionally introduced. Chemistry can progress in an Edisonian manner, but certainly the greatest and most satisfying advances have come through knowledge of molecular structure and insights from principles based on that knowledge. Nanoscience is developing with a host of new techniques in microscopy. These and more will be needed to know the structures of the amazing objects sure to be created.

Acknowledgment. This is the report of the Workshop “Charge Transfer on the Nanoscale”, held in January 2002 in Santa Fe, New Mexico, sponsored by the Council on Chemical Sciences of the United States Department of Energy, Office of Basic Energy Sciences, Chemical Sciences, Geosciences and Biosciences Division. The authors thank the Council on Chemical Sciences of the United States Department of Energy for making possible this workshop and the Department of Energy for its sponsorship. We particularly thank Mary E. Gress of the Chemical Sciences, Geosciences and Biosciences Division, Office of Basic Energy Sciences and George W. Flynn, on behalf of the Council, for their assistance in and encouragement in organization of this workshop. In addition, the authors are indebted to the agencies responsible for funding of their individual research efforts, without which this work would not have been possible. Insightful discussions with N. Sutin, S. Feldberg, J. Smalley, and T. J. Meyer are also gratefully acknowledged.

Appendix A. Notation and Conversions

k_{et}	first-order electron-transfer rate constant, s^{-1}
H_{DA}	electronic coupling between the donor and acceptor sites
λ	nuclear reorganization parameter
h	Planck's constant, $3.91 \times 10^{-15} \text{ eV}\cdot\text{s}/\text{molecule}$, $6.26 \times 10^{-34} \text{ J}\cdot\text{s}/\text{mol}$
k_{B}	Boltzmann constant, $1.43 \times 10^{-25} \text{ eV}/\text{K}\text{--molecule}$
ΔG°	standard free-energy change for the electron transfer
β	attenuation factor for electronic coupling with distance
ρ_{M}	effective density of electronic states in a metal electrode at the Fermi level
E_{app}	applied potential ($E_{\text{F}} = -E_{\text{app}}e$)
E°	reduction potential of the redox species
ϵ	energy of a particular electrode level relative to the Fermi level of the electrode
E_{F}	energy of the Fermi level
e	elementary charge $1.60 \times 10^{-19} \text{ C}/\text{proton}$; $-1.60 \times 10^{-19} \text{ C}/\text{electron}$
energy conversions	$1 \text{ eV} = 1.60 \times 10^{-19} \text{ J}$
F	Faraday, $9.65 \times 10^4 \text{ C}/\text{mol}$
C	Coulomb, one ampere \cdot s, $\text{A}\cdot\text{s}$; $6.24 \times 10^{18} \text{ electrons}/\text{C}$
$f(\epsilon)$	Fermi–Dirac distribution of occupied states in the metal $f(\epsilon) = 1/[1 + \exp(\epsilon/k_{\text{B}}T)]$
g	conductance, reciprocal of resistance Ω^{-1} , $(\text{C}^2/\text{J}\cdot\text{s})$; quantum per mode is $2e^2/h = (12.8 \text{ k } \Omega)^{-1}$
T	electron transmission coefficient
\mathbf{T}	transfer matrix
Landauer formula	$g = (2e^2/h)T(E_{\text{F}})$; relates the linear conductance g of a contact-(molecular bridge)-contact system to the electron transmission coefficient T
I	current
R	resistance
Ω	ohm
S	Siemens, unit of conductance, Ω^{-1}
Ohmic behavior	behavior described by Ohm's law: $V = IR$, typically exhibited by metals, but also observable for molecular contacts provided the voltage range probed is sufficiently small
FCWD	Franck–Condon-weighted density of states
NDR	negative differential resistance R , where $1/R = dI/dV$ becomes negative for some restricted range of V
STM	scanning tunneling microscopy
AFM	atomic force microscopy
EFM	electronic force microscopy
SPM	scanning probe microscopy (general term)
D–B–A	donor–bridge–acceptor assembly
QCA	quantum dot cellular automata
F	Farad, unit of capacitance

References and Notes

- Barbara, P. F.; Meyer, T. J.; Ratner, M. A. *J. Phys. Chem.* **1996**, *100*, 13148–13168.
- Holstein, T. *Ann. Phys.* **1959**, *8*, 343–389.
- Jortner, J.; Bixon, M. *Adv. Chem. Phys.* **1999**, *106*, 1–734.
- Marcus, R. A.; Sutin, N. *Biochim. Biophys. Acta* **1985**, *811*, 265–322.
- Ratner, M. A.; Jortner, J. In *Molecular Electronics*; Ratner, M. A., Jortner, J., Eds.; Blackwell: Oxford, UK, 1997; pp 5–72 and references therein.
- Ratner, M. A.; Davis, B.; Kemp, M.; Mujica, V.; Roitberg, A.; Yaliraki, S. *Ann. N.Y. Acad. Sci.* **1998**, *852*, 22–37.
- Datta, S. *Electronic Transport in Mesoscopic Systems*; Cambridge University Press: Cambridge, 1995.
- Jortner, J., Ratner, M., Eds. *Molecular Electronics*; Blackwell Science: Cambridge, MA, 1997.
- Aviram, A., Ratner, M., Eds. *Molecular Electronics: Science and Technology (Annals of the New York Academy of Sciences)*; The New York Academy of Sciences: New York, NY, 1998; Vol. 852.
- Templeton, A. C.; Wuelfing, W. P.; Murray, R. W. *Acc. Chem. Res.* **2000**, *33*, 27–36.
- Bumm, L. A.; Arnold, J. J.; Dunbar, T. D.; Allara, D. L.; Weiss, P. S. *J. Phys. Chem. B* **1999**, *103*, 8122–8127.
- Cygan, M. T.; Dunbar, T. D.; Arnold, J. J.; Bumm, L. A.; Shedlock, N. F.; Burgin, T. P.; Jones, L., II; Allara, D. L.; Tour, J. M.; Weiss, P. S. *J. Am. Chem. Soc.* **1998**, *120*, 2721–2732.
- Claypool, C. L.; Francesco Faglioni, W. A. G., III; Gray, H. B.; Lewis, N. S.; Marcus, R. A. *J. Phys. Chem. B* **1997**, *101*, 5978–5995.
- Giancarlo, L. C.; Flynn, G. W. *Annu. Rev. Phys. Chem.* **1998**, *49*, 297–336.
- Dorogi, M.; Gomez, J.; Osifchin, R.; Andres, R. P.; Reifenberger, R. *Phys. Rev. B* **1995**, *52*, 9071–9077.
- Cui, X. D.; Primak, A.; Zarate, X.; Tomfohr, J.; Sankey, O. F.; Moore, A. L.; Moore, T. A.; Gust, D.; Harris, G.; Lindsay, S. M. *Science* **2001**, *294*, 571–574.
- Haram, S. K.; Quinn, B. M.; Bard, A. J. *J. Am. Chem. Soc.* **2001**, *123*, 8860–8861.
- Nirmal, M.; Dabbousi, B. O.; Bawendi, M. G.; Macklin, J. J.; Trautman, J. K.; Harris, T. D.; Brus, L. E. *Nature* **1996**, *383*, 802–804.
- Hicks, J. F.; Templeton, A. C.; Chen, S.; Sheran, K. M.; Jasti, R.; Murray, R. W.; Debord, J.; Schaaff, T. G.; Whetten, R. L. *Anal. Chem.* **1999**, *71*, 3703–3711.
- (a) Stuchebrukhov, A. A. *Adv. Chem. Phys.* **2001**, *118*, 1–44. (b) Stuchebrukhov, A. A.; Marcus, R. A. *J. Phys. Chem.* **1995**, *99*, 7581–7590.
- Winkler, J. R.; Gray, H. B. *Chem. Rev.* **1992**, *93*, 369–379.
- Langen, R.; Chang, I.-J.; Germanas, J. P.; Richards, J. H.; Winkler, J. R.; Gray, H. B. *Science* **1995**, *269*, 1733–1735.
- Chidsey, C. E. D. *Science* **1991**, *251*, 919–922.
- Reed, M. A.; Zhou, C.; Muller, C. J.; Burgin, T. P.; Tour, J. M. *Science* **1997**, *278*, 252–254.
- Slowinski, K.; Fong, H. K. Y.; Majda, M. *J. Am. Chem. Soc.* **1999**, *121*, 7257–7261.
- Bezryadin, A.; Dekker, C. *J. Vac. Sci. Technol. B* **1997**, *15*, 793–799.
- Holmlin, R. E.; Haag, R.; Chabiny, M. L.; Ismagilov, R. F.; Cohen, A. E.; Terfort, A.; Rampi, M. A.; Whitesides, G. M. *J. Am. Chem. Soc.* **2001**, *123*, 5075–5085.
- Wold, D. J.; Frisbie, C. D. *J. Am. Chem. Soc.* **2000**, *122*, 2970.
- Mujica, V.; Kemp, M.; Ratner, M. A. *J. Chem. Phys.* **1994**, *101*, 6849.
- Mujica, V.; Kemp, M.; Ratner, M. A. *J. Chem. Phys.* **1994**, *101*, 6856.
- Segal, D.; Nitzan, A.; Ratner, M.; Davis, W. B. *J. Phys. Chem. B* **2000**, *104*, 2790–2793.
- Nitzan, A. *J. Phys. Chem. B* **2001**, *105*, 2677–2679.
- Nitzan, A. *Annu. Rev. Phys. Chem.* **2002**, *52*, 681–750.
- Mujica, V.; Roitberg, A. E.; Ratner, M. *J. Chem. Phys.* **2000**, *112*, 6834–6839.
- Sutin, N. *Prog. Inorg. Chem.* **1983**, *30*, 441–498.
- Newton, M. D. *Chem. Rev.* **1991**, *91*, 767–792.
- Davis, W. B.; Wasielewski, M. R.; Ratner, M. A.; Mujica, V.; Nitzan, A. *J. Phys. Chem. A* **1997**, *101*, 6158–6164.
- Siddarth, P.; Marcus, R. A. *J. Phys. Chem.* **1990**, *94*, 2985–2989.
- McConnell, H. M. *J. Chem. Phys.* **1961**, *35*, 508.
- Newton, M. D.; Cave, R. J. In *Molecular Electronics*; Ratner, M. A., Jortner, J., Eds.; Blackwell: Oxford, UK, 1997; pp 73–118.
- Brunschwig, B. S.; Ehrenson, S.; Sutin, N. *J. Am. Chem. Soc.* **1984**, *106*, 6858–6859.
- Yu, Z. G.; Song, X. *Phys. Rev. Lett.* **2001**, *86*, 6018–6021.
- Renger, T.; Marcus, R. A., to be submitted.
- Woitellier, S.; Launay, J. P.; Spangler, C. W. *Inorg. Chem.* **1989**, *28*, 273.
- Reimers, J. R.; Hush, N. S. In *Electron Ion Transfer Condens. Media: Theor. Phys. React. Kinet., Proc. Conf.*; Kornyshev, A. A., Ed.; World Scientific: Singapore, 1997; pp 326–346.
- Closs, G. L.; Johnson, M. D.; Miller, J. R.; Piotrowiak, P. *J. Am. Chem. Soc.* **1989**, *111*, 3751–3753.
- Shephard, M. J.; Paddon-Row, M. N.; Jordan, K. D. *Chem. Phys.* **1993**, *176*.
- Yonemoto, E. H.; Saupe, G. B.; Schmehl, R. H.; Hubig, S. M.; Riley, R. L.; Iverson, B. L.; Mallouk, T. E. *J. Am. Chem. Soc.* **1994**, *116*, 4786–4795.
- Tong, G. S. M.; Kurnikov, I. V.; Beratan, D. N. *J. Phys. Chem. B* **2002**, *106*, 2381–2392.
- Murphy, C. J.; Arkin, M. R.; Jenkins, Y.; Ghatlia, N. D.; Bossmann, S. H.; Turro, N. J.; Barton, J. K. *Science* **1993**, *262*, 1025–1029.

- (51) Fukui, K.; Tanaka, K. *Angew. Chem., Int. Ed. Engl.* **1998**, *37*, 158–161.
- (52) Jortner, J.; Bixon, M.; Langenbacher, T.; Beyerle, M. E.; Langenbacher, T.; Beyerle, M. E. *Proc. Nat. Acad. Sci.* **1998**, *95*, 12759.
- (53) Jortner, J.; Bixon, M.; Langenbacher, T.; Beyerle, M. E. *Proc. Natl. Acad. Sci.* **1998**, *95*, 12759.
- (54) Giese, B.; Amaudrut, J.; Köhler, A.-K.; Spormann, M.; Wessely, S. *Nature* **2001**, *412*, 318–320.
- (55) Davis, W. B.; Svec, W. A.; Ratner, M. A.; Wasielewski, M. R. *Nature* **1997**, *396*, 60.
- (56) Davis, W. B.; Hess, S.; Naydenova, I.; Haselsberger, R.; Ogronnik, A.; Newton, M. D.; Michel-Beyerle, M. E. *J. Am. Chem. Soc.* **2002**, *124*, 2422–2423.
- (57) Levich, V. G. In *Advances in Electrochemistry and Electrochemical Engineering*; Delahay, P., Tobias, C. W., Eds.; Interscience: New York, 1966; Vol. 4.
- (58) Royea, W. J.; Fajardo, A. M.; Lewis, N. S. *J. Phys. Chem. B* **1997**, *105*, 11152–11159.
- (59) Gosavi, S.; Marcus, R. A. *J. Phys. Chem. B* **2000**, *104*, 2067–2072.
- (60) Smalley, J. F.; Feldberg, S. W.; Chidsey, C. E. D.; Linford, M. R.; Newton, M. D.; Liu, Y.-P. *J. Phys. Chem.* **1995**, *99*, 13141.
- (61) Gosavi, S.; Qin Gao, Y.; Marcus, R. A. *J. Electroanal. Chem.* **2001**, *500*, 71–77.
- (62) Weber, K.; Hockett, L.; Creager, S. *J. Phys. Chem. B* **1997**, *101*, 8286.
- (63) Sachs, S. B.; Dudeck, S. P.; Hsung, R. P.; Sita, S. R.; Smalley, J. F.; Newton, M. D.; Feldberg, S. W.; Chidsey, C. E. D. *J. Am. Chem. Soc.* **1997**, *119*, 10563–10564.
- (64) Sikes, H. D.; Smalley, J. F.; Dudeck, S. P.; Cook, A. R.; Newton, M. D.; Chidsey, C. E. D.; Feldberg, S. W. *Science* **2001**, *291*, 1519–1523.
- (65) Creager, S.; Yu, C. J.; Bamdad, C.; O'Connor, S.; MacLean, T.; Lam, E.; Chong, Y.; Olsen, G. T.; Luo, J.; Gozin, M.; Kayyem, J. F. *J. Am. Chem. Soc.* **1999**, *121*, 1059–1064.
- (66) Smith, C. P.; White, H. S. *Anal. Chem.* **1992**, *64*, 2398–2405.
- (67) Fawcett, W. R. *J. Electroanal. Chem.* **1994**, *378*, 117–124.
- (68) (a) Vakarin, E. V.; Holovko, M. F.; Piotrowiak, P. *Chem. Phys. Lett.* **2002**, *363*, 7–12. (b) Sumner, J. J.; Creager, S. E. *J. Phys. Chem. B* **2001**, *105*, 8739–8745.
- (69) Marcus, R. A. *J. Phys. Chem. B* **1998**, *102*, 10071–10077.
- (70) Barnett, R. N.; Cleveland, C. L.; Joy, A.; Landman, U.; Schuster, G. B. *Science* **2001**, *294*, 567–571.
- (71) Landauer, R. *IBM J. Res. Dev.* **1957**, *1*, 223–231.
- (72) Kerkeris, C.; Bourgoin, J.-P.; Palacin, S.; Esteve, D.; Urbina, C.; Magoga, M.; Joachim, C. *Phys. Rev. B* **1999**, *59*, 12505–12513.
- (73) Selzer, Y.; Salomon, A.; Cahen, D. *J. Am. Chem. Soc.* **2002**, *124*, 2886–2887.
- (74) Brown, L. O.; Hutchison, J. E. *J. Am. Chem. Soc.* **1997**, *119*, 9, 12384–12385.
- (75) Chen, S.; Ingram, R. S.; Hostetler, M. J.; Pietron, J. J.; Murray, R. W.; Schaff, T. G.; Khoury, J. T.; Alvarez, M. M.; Whetten, R. L. *Science* **1998**, *280*, 2098–2101.
- (76) Tomfohr, J. K.; Sankey, O. F. *Phys. Rev. B* **2002**, *65*, 245105–245112.
- (77) Monch, W. *On the physics of metal-semiconductor interfaces, Reports on Progress in Physics* **1990**, *53*, 221–278.
- (78) Tersoff, J. *Phys. Rev. Lett.* **1984**, *52*, 465–468.
- (79) Xue, Y.; Datta, S.; Ratner, M. A. *J. Chem. Phys.* **2001**, *115*, 4292–4299.
- (80) Shen, C.; Kahn, A.; Hill, I. G. In *Conjugated Polymer and Molecular Interfaces*; Salaneck, W. R., Seki, K., Kahn, A., Pireaux, J. J., Eds.; Marcel Dekker: New York, 2001; pp 351–400.
- (81) Zhu, X. Y. *Annu. Rev. Phys. Chem.* **2002**, *53*, 221–247.
- (82) Li, J.; Tomfohr, J. K.; Sankey, O. F. to be published.
- (83) Tian, W.; Datta, S.; Hong, S.; Reifenberger, R.; Henderson, J. I.; Kubiak, C. P. *J. Chem. Phys.* **1998**, *109*, 2874–2882.
- (84) Taylor, J.; Brandbyge, M.; Stokbro, K. *Phys. Rev. Lett.* **2002**, *89*, 138301–138301, 138304.
- (85) Segal, D.; Nitzan, A.; Davis, W. B.; Wasielewski, M. R.; Ratner, M. A. *J. Phys. Chem. B* **2000**, *104*, 3817–3829.
- (86) Yaliraki, S. N.; Roitberg, A. F.; Gonzalez, C.; Mujica, V.; Ratner, M. A. *J. Chem. Phys.* **1999**, *111*, 6997.
- (87) McConnell, H. M. *J. Chem. Phys.* **508**, 35, 508.
- (88) Sumner, J. J.; Creager, S. E. *J. Am. Chem. Soc.* **2000**, *122*, 11914–11920.
- (89) Lewis, N. S. *J. Phys. Chem. B* **1998**, *102*, 4843–4855.
- (90) Economou, E. N. *Green's Functions in Quantum Physics*; Springer-Verlag: Berlin, 1983; Chapter 4.
- (91) Sumner, J. J.; Weber, K. S.; Hockett, L. A.; Creager, S. E. *J. Phys. Chem. B* **2000**, *104*, 7449.
- (92) Cui, X. D.; Primak, A.; Zarate, X.; Tomfohr, J.; Sankey, O. F.; Moore, A. L.; Moore, T. A.; Gust, D.; Nagahara, L. A.; Lindsay, S. M. *J. Phys. Chem.* **2002**, *106*, 8609–8614.
- (93) Wold, D. J.; Haag, R.; Rampi, M. A.; Frisbie, C. D. *J. Phys. Chem. B* **2002**, *106*, 2813–2816.
- (94) Hsu, C.-P.; Marcus, R. A. *J. Chem. Phys.* **1997**, *106*, 584–598.
- (95) Fan, F.-R. F.; Yang, J.; Dirk, S. M.; Price, D. W.; Kosynkin, D.; Tour, J. M.; Bard, A. J. *J. Am. Chem. Soc.* **2001**, *123*, 2454–2455.
- (96) Murray, R. W., Ed. *Molecular Design of Electrode Surfaces; Techniques of Chemistry Series*; John Wiley & Sons: New York, 1992; Vol. 22.
- (97) Hicks, J. F.; Zamborini, F. P.; Osisek, A.; Murray, R. W. *J. Am. Chem. Soc.* **2001**, *123*, 7048–7053.
- (98) Feldheim, D. L.; Keating, C. D. *Chem. Soc. Rev.* **1998**, *27*, 1–12.
- (99) Sampaio, J. F.; Beverly, K. C.; Heath, J. R. *J. Phys. Chem. B* **2001**, *105*, 8797–8800.
- (100) Metzger, R. M.; Chen, B.; Hopfner, U.; Lakshminathan, M. V.; Vuillaume, D.; Kawai, T.; Wu, X.; Tachibana, H.; Hughes, T. V.; Sakurai, H.; Baldwin, J. W.; Hosch, C.; Cava, M. P.; Brehmer, L.; Ashwell, G. J. *J. Am. Chem. Soc.* **1997**, *119*, 10455–10466.
- (101) Collier, C. P.; Wong, E. W.; Belohradský, M.; Raymo, F. M.; Stoddart, J. F.; Kuekes, P. J.; Williams, R. S.; Heath, J. R. *Science* **1999**, *285*, 391–394.
- (102) Chen, J.; Reed, M. A.; Rawlett, A. M.; Tour, J. M. *Science* **1999**, *286*, 1550–1552.
- (103) Donhauser, Z. J.; Mantooh, B. A.; Kelly, K. F.; Bumm, L. A.; Monnell, J. D.; Stapleton, J. J.; Price, D. W., Jr.; Rawlett, A. M.; Allara, D. L.; Tour, J. M.; Weiss, P. S. *Science* **2001**, *292*, 2303–2307.
- (104) Service, R. F. *Science* **2001**, *294*, 2442–2443.
- (105) Pease, A. R.; Jeppesen, J. O.; Stoddart, J. F.; Luo, Y.; Collier, C. P.; Heath, J. R. *Acc. Chem. Res.* **2001**, *34*, 433–444.
- (106) Kagan, C. R.; Afzali, A.; Martel, R.; Gignac, L. M.; Solomon, P. M.; Schrott, A. G.; Ek, B. *Nano Lett.* **2003**, *3*, 119–124.
- (107) Lee, J.-O.; Lientschnig, G.; Wiertz, F.; Martin Struijk, R. A. J. J.; Egberink, R.; Reinhoudt, D. N.; Hadley, P.; Dekker, C. *Nano Lett.* **2003**, *3*, 113–117.
- (108) Schön, J. H.; Meng, H.; Bao, Z. *Nature* **2003**, *422*, 92.
- (109) Yaliraki, S. N.; Ratner, M. A. *J. Chem. Phys.* **1998**, *109*, 5036.
- (110) Yaliraki, S. N.; Kemp, M.; Ratner, M. A. *J. Am. Chem. Soc.* **1999**, *121*, 3428.
- (111) News, D. M. *Phys. Rev. Lett.* **1969**, *178*, 1123.
- (112) Anderson, P. W. *Phys. Rev. Lett.* **1961**, *124*, 41.
- (113) Lang, N. D. *Phys. Rev. B* **1995**, *52*, 5335.
- (114) Seminario, J. M.; Zacarias, A. G.; Tour, J. M. *J. Am. Chem. Soc.* **1999**, *121*, 411.
- (115) Magoga, M.; Joachim, C. *Phys. Rev. B* **1997**, *56*, 4722.
- (116) Stipe, B. C.; Rezaei, M. A.; Ho, W. *Science* **1998**, *280*, 1732.
- (117) Hu, J.; Odom, T. W.; Lieber, C. M. *Acc. Chem. Res.* **1999**, *32*, 435.
- (118) Avouris, Ph. *J. Phys. Chem.* **1990**, *94*, 2246.
- (119) Dutton, G.; Zhu, X.-Y. *J. Phys. Chem. B* **2001**, *105*, 10912.
- (120) Selzer, Y.; Salomon, A.; Cahen, D. *J. Am. Chem. Soc.* **2002**, *123*.
- (121) Son, K. A.; Kim, H. I.; Houston, J. E. *Phys. Rev. Lett.* **2001**, *86*, 5357.
- (122) Vondrak, T. W. H.; Winget, P.; Cramer, C. J.; Zhu, X.-Y. *J. Am. Chem. Soc.* **2000**, *122*, 4700–4707.
- (123) Miller, A. D.; Gaffney, K. J.; Liu, S. H.; Szymanski, P.; Garrett-Roe, S.; Wong, C. M.; Harris, C. B. *J. Phys. Chem. A* **2002**, *106*, 7636–7638.
- (124) Petek, H.; Ogawa, S. *Prog. Surf. Sci.* **1998**, *56*, 239.
- (125) Harris, C. B.; Ge, N.-H.; Lingle, R. L.; McNeill, J. D.; Wong, C. M. *Annu. Rev. Phys. Chem.* **1997**, *48*, 711.
- (126) Gahl, C.; Ishioka, K.; Zhong, Q.; Hotzel, A.; Wolf, M. *Faraday Discuss.* **2000**, *117*, 191.
- (127) Bonn, M.; Hess, C.; Wolf, M. *J. Chem. Phys.* **2001**, *115*, 7725.
- (128) Nirmal, M.; Brus, L. E. *Acc. Chem. Res.* **1999**, *32*, 407.
- (129) Krauss, T. D.; Brus, L. E. *Phys. Rev. Lett.* **1999**, *83*, 4840.
- (130) Krauss, T. D.; O'Brien, S.; Brus, L. E. *J. Phys. Chem. B* **2001**, *105*, 1725–1733.
- (131) Cherniavskaya, O.; Chen, L.; Islam, M. A.; Brus, L. *Nano Lett.* **2003**, *3*, 497–501.
- (132) Xie, X. S.; Trautman, J. K. *Annu. Rev. Phys. Chem.* **1998**, *49*, 441–480.
- (133) Van-Hulst, N. F.; Veerman, J. A.; Garcia-Parajo, M. F.; Kuipers, L. *J. Chem. Phys.* **2000**, *112*, 7799–7810.
- (134) Nie, S. M.; Zare, R. N. *Ann. Rev. Biophys. Biomol. Struct.* **1997**, *26*, 567–596.
- (135) Moerner, W. E. *J. Phys. Chem. B* **2002**, *106*, 910–927.
- (136) Zang, L.; Liu, R.; Holman, M. W.; Nguyen, K. T.; Adams, D. M. *J. Am. Chem. Soc.* **2002**, *124*, 10640–10641.
- (137) Holman, M. W.; Liu, R.; Zang, L.; Adams, D. M. *J. Am. Chem. Soc.*, submitted.
- (138) Liu, R.; Holman, M. W.; Zang, L.; Adams, D. M. *J. Phys. Chem. A*, submitted.

- (139) Bumm, L. A.; Arnold, J. J.; Cygan, M. T.; Dunbar, T. D.; Burgin, T. P.; Jones, L., II; Allara, D. L.; Tour, J. M.; Weiss, P. S. *Science* **1996**, *271*, 1705–1707.
- (140) Reed, M. A.; Chen, J.; Rawlett, A. M.; Price, D. W.; Tour, J. M. *Appl. Phys. Lett.* **2001**, *78*, 3735–3737.
- (141) Frank, S.; Poncharal, P.; Wang, Z. L.; de Heer, W. A. *Science* **1999**, *280*, 1744–1746.
- (142) Tans, S. J.; Verschueren, R. M.; Dekker, C. *Nature* **1998**, *393*, 49.
- (143) Martel, R.; Schmidt, T.; Shea, H. R.; Hertel, T.; Avouris, Ph. *Appl. Phys. Lett.* **1998**, *73*, 2447.
- (144) Derycke, V.; Martel, R.; Appenzeller, J.; Avouris, Ph. *Nano Lett.* **2001**, *1*, 453–456.
- (145) Postma, H. W. C.; Teepen, T.; Yao, Z.; Grifoni, M.; Dekker, C. *Science* **2001**, *293*, 76–79.
- (146) Collier, C. P.; Mattersteig, G.; Wong, E. W.; Beverly, K.; Sampaio, J.; Raymo, F. M.; Stoddart, J. F.; Heath, J. R. *Science* **2000**, *289*, 1172–1175.
- (147) Ashwell, G. J.; Sambles, J. R.; Martin, A. S.; Parker, W. G.; Szablewski, M. *J. Chem. Soc., Chem. Commun.* **1990**, 1374–1376.
- (148) Martin, A. S.; Sambles, J. R.; Ashwell, G. J. *Phys. Rev. Lett.* **1993**, *70*, 218–221.
- (149) Chen, B.; Metzger, R. M. *J. Phys. Chem. B* **1999**, *103*, 4447–4451.
- (150) Vuillaume, D.; Chen, B.; Metzger, R. M. *Langmuir* **1999**, *15*, 4011–4017.
- (151) Metzger, R. M.; Xu, T.; Peterson, I. R. *J. Phys. Chem. B* **2001**, *105*, 7280–7290.
- (152) Xu, T.; Peterson, I. R.; Lakshminantham, M. V.; Metzger, R. M. *Angew. Chem., Int. Ed.* **2001**, *40*, 1749–1752.
- (153) Aviram, A.; Ratner, M. A. *Chem. Phys. Lett.* **1974**, *29*, 277–283.
- (154) Baldwin, J. W.; Chen, B.; Street, S. C.; Konovalov, V. V.; Sakurai, H.; Hughes, T. V.; Simpson, C. S.; Lakshminantham, M. V.; Cava, M. P.; Kispert, L. D.; Metzger, R. M. *J. Phys. Chem. B* **1999**, *103*, 4269–4277.
- (155) Baldwin, J. W.; Amaresh, R. R.; Peterson, I. R.; Shumate, W. J.; Cava, M. P.; Amiri, M. A.; Hamilton, R.; Ashwell, G. J.; Metzger, R. M. *J. Phys. Chem. B* **2002**, *106*, 12158–12164.
- (156) Metzger, R. M.; Baldwin, J. W.; Shumate, W. J.; Peterson, I. R.; Mani, P.; Mankey, G. J.; Morris, T.; Szulcowski, G.; Bosi, S.; Prato, M.; Comito, A.; Rubin, Y. *J. Phys. Chem. B* **2003**, *107*, 1021–1027.
- (157) Baldwin, J. W.; Amaresh, R. R.; Peterson, I. R.; Shumate, W. J.; Cava, M. P.; Amiri, M. A.; Hamilton, R.; Ashwell, G. J.; Metzger, R. M. *J. Phys. Chem. B* **2002**, *106*, 12158–12164.
- (158) Lent, C. S.; Tougaw, P. D. *Proc. IEEE* **1997**, *85*, 541–557.
- (159) Amlani, I.; Orlov, A.; Toth, G.; Bernstein, G. H.; Lent, C. S.; Snider, G. L. *Science* **1999**, *284*, 289–291.
- (160) Kummamuru, R.; Timler, J.; Toth, G.; Lent, C. S.; Ramasubramanian, R.; Orlov, A. O.; Bernstein, G. H.; Snider, G. L. *App. Phys. Lett.* **2002**, *81*, 1332–1334.
- (161) Lieberman, M.; Chellamma, S.; Varughese, B.; Wang, Y.; Lent, C. S.; Bernstein, G. H.; Snider, G. L.; Peiris, F. C. *Ann. N.Y. Acad. Sci.* **2002**, *960*, 225–239.
- (162) Lent, C. S.; Isaksen, B.; Lieberman, M. *J. Am. Chem. Soc.* **2003**, *125*, 1056–1063.
- (163) Balzani, V.; Gomex-Lopez, M.; Stoddart, J. F. *Acc. Chem. Res.* **1998**, *31*, 405–414.
- (164) Aviram, A.; Seiden, P. E.; Ratner, M. A. In *Molecular Electronic Devices*; Carter, F. L., Ed.; Marcel Dekker: New York, 1982; p 5.
- (165) Heath, J. R.; Kuekes, P. J.; Snider, G. S.; Williams, R. S. *Science* **1998**, *280*, 1716–1721.
- (166) Förster, T. *Faraday Discuss.* **1959**, *27*, 7–17.
- (167) Dexter, D. L. *J. Chem. Phys.* **1953**, *21*, 836–850.
- (168) Gust, D.; Moore, T. A.; Moore, A. L. *Acc. Chem. Res.* **2001**, *34*, 40–48.
- (169) McDermott, G.; Prince, S. M.; Freer, A. A.; Hawthornthwait-Elawless, A. M.; Papiz, M. Z.; Cogdell, R. J.; Isaacs, N. W. *Nature* **1995**, *374*, 517–521.
- (170) Yang, M.; Agarwal, R.; Fleming, G. R. *J. Photochem. Photobiol., A* **2001**, *142*, 107–119.
- (171) Wasielewski, M. R. *Chem. Rev.* **1992**, *92*, 435–461.
- (172) Sugiura, K.; Tanaka, H.; Matsumoto, T.; Kawai, T.; Sakata, Y. *Chem. Lett.* **1999**, 1193–1194.
- (173) Kuciauskas, D.; Liddell, P. A.; Lin, S.; Johnson, T. E.; Weghorn, S. J.; Lindsey, J. S.; Moore, A. L.; Moore, T. A.; Gust, D. *J. Am. Chem. Soc.* **1999**, *121*, 8604–8614.
- (174) Lammi, R. K.; Ambrose, A.; Balasubramanian, T.; Wagner, R. W.; Bocian, D. F.; Holtan, D.; Lindsey, J. S. *J. Am. Chem. Soc.* **2000**, *122*, 7579–7591.
- (175) Devadoss, C.; Bharathi, P.; Moore, J. S. *J. Am. Chem. Soc.* **1996**, *118*, 9635–9644.
- (176) Yeow, E. K. L.; Ghiggino, K. P.; Reek, J. N. H.; Crossley, M. J.; Bosman, A. W.; Schenning, A. P. H. J.; Meijer, E. W. *J. Phys. Chem. B* **2000**, *104*, 2596–2606.
- (177) Adronov, A.; Frechet, J. M. J. *Chem. Commun.* **2000**, 1701–1710.
- (178) Webber, S. E. *Chem. Rev.* **1990**, *90*, 1469–1482.
- (179) Fox, M. A. *Acc. Chem. Res.* **1999**, *32*, 201–207.
- (180) Fleming, C. N.; Maxwell, K. A.; DeSimone, J. M.; Meyer, T. J.; Papanikolas, J. M. *J. Am. Chem. Soc.* **2001**, *123*, 10336–10347.
- (181) Deng, Y. Q.; Roberts, J. A.; Peng, S. M.; Chang, C. K.; Nocera, D. G. *Angew. Chem., Int. Ed. Engl.* **1997**, *36*, 2124–2127.
- (182) Sessler, J. L.; Sathiosatham, M.; Brown, C. T.; Rhodes, T. A.; Wiederrecht, G. *J. Am. Chem. Soc.* **2001**, *123*, 3655–3660.
- (183) Lahiri, S.; Thompson, J. L.; Moore, J. S. *J. Am. Chem. Soc.* **2000**, *122*, 11315–11319.
- (184) Shi, X. X.; Barkigia, K. M.; Fajer, J.; Drain, C. M. *J. Org. Chem.* **2001**, *66*, 6513–6522.
- (185) Rucareanu, S.; Mongin, O.; Schuwey, A.; Hoyler, N.; Gossauer, A.; Amrein, W.; Hediger, H. U. *J. Org. Chem.* **2001**, *66*, 4973–4988.
- (186) Nguyen, T. Q.; Schwartz, B. J.; Schaller, R. D.; Johnson, J. C.; Lee, L. F.; Haber, L. H.; Saykally, R. J. *J. Phys. Chem. B* **2001**, *105*, 5153–5160.
- (187) Zhou, Q.; Swager, T. M. *J. Am. Chem. Soc.* **1995**, *117*, 12593–12602.
- (188) Chen, L.; McBranch, D. W.; Wang, H.-L.; Helgeson, R.; Wudl, F.; Whitten, D. G. *Proc. Natl. Acad. Sci. U.S.A.* **1999**, *96*, 12287–12292.
- (189) Harrison, B. S.; Ramey, M. B.; Reynolds, J. R.; Schanze, K. S. *J. Am. Chem. Soc.* **2000**, *122*, 8561–8562.
- (190) Higgins, D. A.; Reid, P. J.; Barbara, P. F. *J. Phys. Chem.* **1996**, *100*, 1174–1180.
- (191) Kuhn, H.; Möbius, D. *Angew. Chem., Int. Ed. Engl.* **1971**, *10*, 620–637.
- (192) Jones, R. M.; Lu, L. D.; Helgeson, R.; Bergstedt, T. S.; McBranch, D. W.; Whitten, D. G. *Proc. Natl. Acad. Sci. U.S.A.* **2001**, *98*, 14769–14772.
- (193) Calzaferri, G.; Pauchard, M.; Maas, H.; Huber, S.; Khatyr, A.; Schaafsma, T. *J. Mater. Chem.* **2002**, *12*, 1–13.
- (194) Tour, J. M. *Chem. Rev.* **1996**, *96*, 537–553.
- (195) Harriman, A.; Ziessel, R. *Coord. Chem. Rev.* **1998**, *171*, 331–339.
- (196) Dekker, C.; Tans, S. J.; Geerligs, L. J.; Bezryadin, A.; Wu, J.; Wegner, G. *NATO ASI Ser., Ser. E* **1997**, *341*, 129–138.
- (197) Jiang, B.; Yang, S. W.; Bailey, S. L.; Hermans, L. G.; Niver, R. A.; Bolcar, M. A.; Jones, J.; Wayne, E. *Coord. Chem. Rev.* **1998**, *171*, 365–386.
- (198) Jestin, I.; Frere, P.; Blanchard, P.; Roncali, J. *Angew. Chem., Int. Ed.* **1998**, *37*, 942–945.
- (199) Swager, T. M. *Acc. Chem. Res.* **1998**, *31*, 201–207.
- (200) Decher, G. *Science* **1997**, *277*, 1232–1237.
- (201) Kim, J.; McQuade, D. T.; Rose, A.; Zhu, Z.; Swager, T. M. *J. Am. Chem. Soc.* **2001**, *123*, 11488–11489.
- (202) Levitsky, I. A.; Kim, J.; Swager, T. M. *J. Am. Chem. Soc.* **1999**, *121*, 1466–1472.
- (203) Bazan, G. C.; Miao, Y. J.; Renak, M. L.; Sun, B. J. *J. Am. Chem. Soc.* **1996**, *118*, 2618–2624.
- (204) Francke, V.; Rader, H. J.; Geerts, Y.; Mullen, K. *Macromol. Rapid Commun.* **1998**, *19*, 275–281.
- (205) Kukula, H.; Ziener, U.; Schops, M.; Godt, A. *Macromolecules* **1998**, *31*, 5160–5163.
- (206) Li, W.; Wang, H.; Yu, L.; Morkved, T. L.; Jaeger, H. M. *Macromolecules* **1999**, *32*, 3034–3044.
- (207) Fasaloka, M. J.; Banerjee, P.; Mayes, A. M.; Pickett, G.; Balazs, A. C. *Macromolecules* **2000**, *33*, 5702–5712.
- (208) Leclere, P.; Parente, V.; Bredas, J. L.; Francois, B.; Lazzaroni, R. *Chem. Mater.* **1998**, *10*, 4010–4014.
- (209) Balazs, A. C.; Ginzburg, V. V.; Qiu, F.; Peng, G. W.; Jasnow, D. *J. Phys. Chem. B* **2000**, *104*, 3411–3412.
- (210) Fogg, D. E.; Radzilowski, L. H.; Blanski, R.; Schrock, R. R.; Thomas, E. L. *Macromolecules* **1997**, *30*, 417–426.
- (211) O'Regan, B.; Grätzel, M. *Nature* **1991**, *353*, 737–740.
- (212) Hagfeldt, A.; Grätzel, M. *Acc. Chem. Res.* **2000**, *33*, 269–277.
- (213) Grätzel, M. *Nature* **2001**, *414*, 338–344.
- (214) Peumans, P.; Forrest, S. R. *Appl. Phys. Lett.* **2001**, *79*, 126–128.
- (215) Brabec, C. J.; Sariciftci, N. S.; Hummelen, J. C. *Adv. Funct. Mater.* **2001**, *11*, 15–26.
- (216) Yu, G.; Gao, J.; Hummelen, J. C.; Wudl, F.; Heeger, A. J. *Science* **1995**, 1789–1791.
- (217) Granstrom, M.; Petritsch, K.; Arias, A. C.; Lux, A.; Andersson, M. R.; Friend, R. H. *Nature* **1998**, *395*, 257–260.
- (218) Hickman, J. J.; Ofer, D.; Laibinis, P. E.; Whitesides, G. M.; Wrighton, M. S. *Science* **1991**, *252*, 688–691.
- (219) Elghanian, R.; Storhoff, J. J.; Mucic, R. C.; Letsinger, R. L.; Mirkin, C. A. *Science* **1997**, *277*, 1078–1081.

- (220) Markovich, G.; Collier, C. P.; Henrichs, S. E.; Remacle, F.; Levine, R. D.; Heath, J. R. *Acc. Chem. Res.* **1999**, *32*, 415–423.
- (221) Willner, I.; Willner, B. *Pure Appl. Chem.* **2001**, *73*, 535–542.
- (222) Gomez-Romero, P. *Adv. Mater.* **2001**, *13*, 163–174.
- (223) Henglein, A. *Ber. Bunsen-Ges. Phys. Chem.* **1995**, *99*, 903–913.
- (224) Wang, Y.; Herron, N. *Science* **1996**, *273*, 632–634.
- (225) Kamat, P. V. *Prog. Inorg. Chem.* **1997**, *44*, 273–343.
- (226) Alivisatos, A. P. *J. Phys. Chem.* **1996**, *100*, 13226–13239.
- (227) Pileni, M. P. *New J. Chem.* **1998**, 693–702.
- (228) Henglein, A. *Langmuir* **1998**, *14*, 6738–6744.
- (229) Link, S.; El-Sayed, M. A. *J. Phys. Chem. B* **1998**, *103*, 4212–4217.
- (230) Kim, S.-H.; Medeiros-Ribeiro, G.; Ohlberg, D. A. A.; Williams, R. S.; Heath, J. R. *J. Phys. Chem. B* **1999**, *103*, 10341–10347.
- (231) El-Sayed, M. A. *Acc. Chem. Res.* **2001**, *34*, 257–264.
- (232) Fujiwara, H.; Yanagida, S.; Kamat, P. V. *J. Phys. Chem. B* **1999**, *103*, 2589–2591.
- (233) Porter, L. A.; Ji, D.; Westcott, S. L.; Graupe, M.; Czernuszewicz, R. S.; Halas, N. J. *Langmuir* **1998**, *14*, 7378–7386.
- (234) Westcott, S. L.; Oldenburg, S. J.; Lee, T. R.; Halas, N. J. *Chem. Phys. Lett.* **1999**, *300*, 651–655.
- (235) Brust, M.; Kiely, C. J.; Bethell, D.; Schiffrin, D. J. *J. Am. Chem. Soc.* **1998**, *120*, 12367–12368.
- (236) Steigerwald, M. L.; Alivisatos, A. P.; Gibson, J. M.; Harris, T. D.; Kortan, R.; Muller, A. J.; Thayer, A. M.; Duncan, T. M.; Douglass, D. C.; Brus, L. E. *J. Am. Chem. Soc.* **1988**, *110*, 3046–3050.
- (237) Steigerwald, M. L.; Brus, L. E. *Acc. Chem. Res.* **1990**, *23*, 183–188.
- (238) Murray, C.; Norris, D.; Bawendi, M. J. *Am. Chem. Soc.* **1993**, *115*, 8706–8715.
- (239) Kamat, P. V. *J. Phys. Chem. B* **2002**, *106*, 7729–7744.
- (240) Badia, A.; Demers, L.; Dickinson, L.; Morin, F. G.; Lennox, R. B.; Reven, L. *J. Am. Chem. Soc.* **1997**, *119*, 11104–11105.
- (241) Badia, A.; Cuccia, L.; Demers, L.; Morin, F. G.; Lennox, R. B. *J. Am. Chem. Soc.* **2000**, *122*, 2682–2692.
- (242) Hostetler, M. J.; Templeton, A. C.; Murray, R. W. *Langmuir* **1998**, *15*, 3782–3789.
- (243) Kohlmann, O.; Steinmetz, W. E.; Mao, X.-A.; Wuelfing, W. P.; Templeton, A. C.; Murray, R. W.; Johnson, C. S. *J. Phys. Chem. B* **2001**, *105*, 8801–8809.
- (244) Thomas, K. G.; Zajicek, J.; Kamat, P. V. *Langmuir* **2002**, *18*, 3722–3727.
- (245) Chen, M. C.; Tsai, S. D.; Chen, M. R.; Ou, S. Y.; Li, W. H.; Lee, K. C. *Phys. Rev. B* **1995**, *51*, 4507–4515.
- (246) Keating, C. D.; Kovaleski, K. K.; Natan, M. J. *J. Phys. Chem. B* **1998**, *102*, 9414–9425.
- (247) Kamat, P. V. *Chem. Rev.* **1993**, *93*, 267–300.
- (248) Aldana, J.; Wang, Y. A.; Peng, X. G. *J. Am. Chem. Soc.* **2001**, *123*, 8844–8850.
- (249) Avouris, Ph.; Persson, B. N. J. *J. Phys. Chem.* **1984**, *88*, 837–848.
- (250) Saito, K. *J. Phys. Chem. B* **1999**, *103*, 6579–6583.
- (251) Pagnot, T.; Barchiesi, D.; Tribillon, G. *Appl. Phys. Lett.* **1999**, *75*, 4207–4209.
- (252) Makarova, O. V.; Ostafin, A. E.; Miyoshi, H.; Norris, J. R.; Meisel, D. *J. Phys. Chem. B* **1999**, *103*, 9080–9084.
- (253) Dulkeith, E.; Morteani, A. C.; Niedereichholz, T.; Klar, T. A.; Feldmann, J.; Levi, S. A.; van Veggel, F. C. J. M.; Reinhoudt, D. N.; Moller, M.; Gittins, D. I. *Phys. Rev. Lett.* **2002**, *89*, art. no. 203002.
- (254) Maier, S. A.; Brongersma, M. L.; Kik, P. G.; Atwater, H. A. *Phys. Rev. B* **2002**, *65*, art. no. 193408.
- (255) George Thomas, K.; Kamat, P. V. *J. Am. Chem. Soc.* **2000**, *122*, 2655–2656.
- (256) Ipe, B. I.; George Thomas, K.; Barazzouk, S.; Hotchandani, S.; Kamat, P. V. *J. Phys. Chem. B* **2002**, *106*, 18–21.
- (257) Lakowicz, J. R. *Anal. Biochem.* **2001**, *298*, 1–24.
- (258) Geddes, C. D.; Lakowicz, J. R. *J. Fluorescence* **2002**, *12*, 121–129.
- (259) Chen, S.; Murray, R. W. *J. Phys. Chem. B* **1999**, *103*, 9996–10000.
- (260) Templeton, A. C.; Pietron, J. J.; Murray, R. W.; Mulvaney, P. J. *Phys. Chem. B* **2000**, *104*, 564–570.
- (261) Jiang, J.; Krauss, T. D.; Brus, L. E. *J. Phys. Chem. B* **2000**, *104*, 11936–11941.
- (262) Bechinger, C.; Ferrere, S.; Zaban, A.; Sprague, J.; Gregg, B. A. *Nature* **1996**, *383*, 608–610.
- (263) Klein, D. L.; Roth, R.; Lim, A. K. L.; Alivisatos, A. P.; McEuen, P. L. *Nature* **1997**, *389*, 699–701.
- (264) Sotomayor, J.; Will, G.; Fitzmaurice, D. *J. Mater. Chem.* **2000**, *10*, 685–692.
- (265) Hagfeldt, A.; Grätzel, M. *Chem. Rev.* **1995**, *95*, 49–68.
- (266) Haesselbarth, A.; Eychmueller, A.; Eichberger, R.; Giersig, M.; Mews, A.; Weller, H. *J. Phys. Chem.* **1993**, *97*, 5333–5340.
- (267) Bedja, I.; Kamat, P. V. *J. Phys. Chem.* **1995**, *99*, 9182–9188.
- (268) Kamalov, V. F.; Little, R.; Logunov, S. L.; El-Sayed, M. A. *J. Phys. Chem.* **1996**, *100*, 6381–6384.
- (269) Mews, A.; Kadavanich, A. V.; Banin, U.; Alivisatos, A. P. *Phys. Rev. B* **1996**, *53*, 13242–13245.
- (270) Kamat, P. V. In *Semiconductor Nanoclusters – Physical, Chemical and Catalytic Aspects*; Meisel, D., Ed.; Elsevier Science: Amsterdam, 1997; pp 237–259.
- (271) Kraeutler, B.; Bard, A. J. *J. Am. Chem. Soc.* **1978**, *100*, 4317–4318.
- (272) Shanghavi, B.; Kamat, P. V. *J. Phys. Chem. B* **1997**, *101*, 7675–7679.
- (273) Pastoriza-Santos, I.; Koktysh, D. S.; Mamedov, A. A.; Giersig, M.; Kotov, N. A.; Liz-Marzán, L. M. *Langmuir* **2000**, *16*, 2731–2735.
- (274) Schreder, B.; Schmidt, T.; Ptatschek, V.; Winkler, U.; Materny, A.; Umbach, E.; Lerch, M.; G. Müller, G.; Kiefer, W. W.; Spanhel, L. *J. Phys. Chem. B* **2000**, *104*, 1677–1685.
- (275) Marignier, J. L.; Belloni, J.; Delcourt, M. O.; Chevalier, J. P. *Nature* **1985**, *317*, 344–345.
- (276) Freeman, R. G.; Hommer, M. B.; Grabar, K. C.; Jackson, M. A.; Natan, M. J. *J. Phys. Chem.* **1996**, *100*, 718–724.
- (277) Mulvaney, P.; Giersig, M.; Henglein, A. *J. Phys. Chem.* **1993**, *97*, 7061–7064.
- (278) Henglein, A. *J. Phys. Chem. B* **2000**, *104*, 6683–6685.
- (279) Lawless, D.; Kapoor, S.; Kennepohl, P.; Meisel, D.; Serpone, N. *J. Phys. Chem.* **1994**, *98*, 9619–9625.
- (280) Liz-Marzán, L. M.; Giersig, M.; Mulvaney, P. *Langmuir* **1996**, *12*, 4329–4335.
- (281) Hardikar, V.; Matijevic, E. *J. Colloid Interface Sci.* **2000**, *221*, 133–136.
- (282) Wood, A.; Giersig, M.; Mulvaney, P. *J. Phys. Chem. B* **2001**, *105*, 8810–8815.
- (283) Chandrasekharan, N.; Kamat, P. V. *J. Phys. Chem. B* **2000**, *104*, 10851–10857.
- (284) Subramanian, V.; Wolf, E.; Kamat, P. V. *J. Phys. Chem. B* **2001**, *105*, 11439–11446.
- (285) Bethell, D.; Brust, M.; Schiffrin, D. J.; Kiely, C. J. *Electroanal. Chem.* **1996**, *409*, 137–143.
- (286) McFarland, E. W.; Tang, J. *Nature* **2003**, *421*, 616–618.
- (287) Sudeep, P. K.; Ipe, B. I.; George Thomas, K.; George, M. V.; Barazzouk, S.; Hotchandani, S.; Kamat, P. V. *Nano Lett.* **2002**, *2*, 29–35.
- (288) Eckert, J.; Stucky, G. D.; Cheetham, A. K. *Mater. Res. Bull.* **1999**, *24*, 31–41.
- (289) Carlin, R. T.; Swider-Lyons, K. E. *AMPTIAC Quarterly* (free download at: <http://amptiac.iitri.org/amp/jsp/journal/ampjournal.jsp>) **2002**, *6*, 25–30.
- (290) Owens, B. B.; Passerini, S.; Smyrl, W. H. *Electrochim. Acta* **1999**, *45*, 215–224.
- (291) Harreld, J. H.; Dong, W.; Dunn, B. *Mater. Res. Bull.* **1998**, *33*, 561–567.
- (292) Dong, W.; Rolison, D. R.; Dunn, B. *Electrochem. Solid-State Lett.* **2000**, *3*, 457–459.
- (293) Kim, J.; Manthiram, A. *Nature* **1997**, *390*, 265–267.
- (294) Manthiram, A. K. *J. Chem. Mater.* **1998**, *10*, 2895–2909.
- (295) Rolison, D. R.; Dunn, B. *J. Mater. Chem.* **2001**, *11*, 963–980.
- (296) Long, J. W.; Stroud, R. M.; Swider-Lyons, K. E.; Rolison, D. R. *J. Phys. Chem. B* **2000**, *104*, 9772–9776.
- (297) Mukerjee, S.; Lee, S. J.; Ticianelli, E. A.; McBreen, J.; Grgur, B. N.; Markovic, N. M.; Ross, P. N.; Giallombardo, J. R.; De Castro, E. S. *Electrochem. Solid State Lett.* **1999**, *2*, 12–15.
- (298) Camara, G. A.; Ticianelli, E. A.; Mukerjee, S.; Lee, S. J.; McBreen, J. *J. Electrochem. Soc.* **2002**, *149*, A748–A753.
- (299) Zhang, H. Q.; Wang, Y.; Fachini, E. R.; Cabrera, C. R. *Electrochem. Solid-State Lett.* **1999**, *2*, 437–439.
- (300) Kolb, D. M. *Angew. Chem., Int. Ed.* **2001**, *40*, 1162–1181.
- (301) Rolison, D. R.; Bessel, C. A.; Senaratne, C.; Baker, M. D.; Zhang, J. *J. Phys. Chem. B* **1996**, *100*, 8610–8611.
- (302) Kaatz, F. H.; Harris, V. G.; Rolison, D. R.; Kurihara, L.; Edelstein, A. S. *Appl. Phys. Lett.* **1996**, *67*, 3807–3809.
- (303) Stroud, R. M.; Long, J. W.; Swider-Lyons, K. E.; Rolison, D. R. *Microsc. Microanal.* **2002**, *8*, 50–57.
- (304) Zach, M. P.; Ng, K. H.; Penner, R. M. *Science* **2000**, *290*, 2120–2123.
- (305) Schäfer, H.; Schneiderreit, G.; Gerhardt, W. *Z. Anorg. Allg. Chem.* **1962**, *319*, 327–336.
- (306) Green, M. L.; Gross, M. E.; Papa, L. E.; Schnoes, K. J.; Brasen, D. *J. Electrochem. Soc.* **1985**, *132*, 2677–2685.
- (307) Kim, S. H.; Hong, J. G.; Streiffer, S. K.; Kingon, A. I. *J. Mater. Res.* **1999**, *14*, 1018–1025.
- (308) Trasatti, S. *Electrochim. Acta* **1991**, *36*, 225–241.
- (309) Conway, B. E. *Electrochemical Supercapacitors-Scientific Fundamentals and Technological Applications*; Kluwer Academic: New York, 1999.

- (310) Swider-Lyons, K. E.; Love, C. T.; Rolison, D. R. In *Direct Methanol Fuel Cells*; Narayanan, S. T., Zawodzinski, T., Gottesfeld, S., Eds.; Electrochemical Society: Pennington, NJ, 2001; pp 42–49.
- (311) Zheng, J. P.; Cygan, P. J.; Jow, T. R. *J. Electrochem. Soc.* **1995**, *142*, 2699–2703.
- (312) McKeown, D. A.; Hagans, P. L.; Carette, L. P. L.; Russell, A. E.; Swider, K. E.; Rolison, D. R. *J. Phys. Chem. B* **1999**, *103*, 4825–4832.
- (313) Swider-Lyons, K. E.; Bussmann, K. M.; Griscom, D. L.; Love, C. T.; Rolison, D. R.; Dmowski, W.; Egami, T. In *Solid State Ionic Devices II—Ceramic Sensors*; Wachsmann, E. D., Weppner, W., Eds.; Electrochemical Society: Pennington, NJ, 2000; Vol. PV2000–32, pp 148–156.
- (314) Dmowski, W.; Egami, T.; Swider-Lyons, K. E.; Love, C. T.; Rolison, D. R. *J. Phys. Chem. B* **2002**, *106*, 12677–12683.
- (315) Treacy, M. M. J.; Gibson, J. M. *Acta Crystallogr.* **1996**, *A52*, 212–220.
- (316) Voyles, P. M.; Gibson, J. M.; Treacy, M. M. J. *J. Electron Microsc.* **2000**, *49*, 259–266.
- (317) Mamontov, E.; Egami, T.; Brezny, R.; Koranne, M.; Tyagi, S. *J. Phys. Chem. B* **2000**, *104*, 11110–11116.
- (318) Meneau, F.; Greaves, G. N.; Winter, R.; Vaills, Y. *J. Non-Cryst. Solids* **2001**, *293*, 693–699.
- (319) Mao, G.; Saboungi, M. L.; Price, D. L.; Armand, M. B.; Howells, W. S. *Phys. Rev. Lett.* **2000**, *84*, 5536–5539.
- (320) Lamparter, P.; Steeb, S. *J. Non-Cryst. Solids* **1988**, *106*, 137–146.
- (321) Kordas, G. J. *Non-Cryst. Solids* **2001**, *281*, 133–138.
- (322) Huff, N. T.; Demiralp, E.; Cagin, T.; Goddard, W. A. *J. Non-Cryst. Solids* **1999**, *253*, 133–142.
- (323) Martin, C. R.; Mitchell, D. T. In *Electroanal. Chem.*; Bard, A. J., Ed.; Marcel Dekker: New York, 1999; Vol. 21, pp 1–74.
- (324) (a) Anderson, M. L.; Stroud, R. M.; Rolison, D. R. *Nano Lett.* **2002**, *2*, 235–240. (b) Rolison, D. R. *Science* **2003**, *299*, 1698–1701.
- (325) Patrissi, C. J.; Martin, C. R. *J. Electrochem. Soc.* **2001**, *148*, A1247–A1253.
- (326) Nelson, P. A.; Elliott, J. M.; Attard, G. S.; Owen, J. R. *Chem. Mater.* **2002**, *14*, 524–529.
- (327) Long, J. W.; Qadir, L. R.; Stroud, R. M.; Rolison, D. R. *J. Phys. Chem. B* **2001**, *105*, 8712–8717.
- (328) Swider-Lyons, K. E.; Love, C. T.; Rolison, D. R. *Solid State Ionics* **2002**, *152–153*, 99–104.
- (329) Blonski, S.; Garofalini, S. H. *Surf. Sci.* **1993**, *295*, 263–274.
- (330) McHale, J. M.; Auroux, A.; Perrotta, A. J.; Navrotsky, A. *Science* **1997**, *142*, 788–791.
- (331) Zhang, H. Z.; Banfield, J. F. *J. Phys. Chem. B* **2000**, *104*, 3481–3487.
- (332) Ryan, J. V.; Berry, A. D.; Anderson, M. L.; Long, J. W.; Stroud, R. M.; Cepak, V. M.; Browning, V. M.; Merzbacher, C. I.; Rolison, D. R. *Nature* **2000**, *406*, 169–172.